Summer 2002

Catalytic reduction of nitric oxide by solid carbonaceous material under lean condition

Shan Xiao
New Jersey Institute of Technology

ABSTRACT

CATALYTIC REDUCTION OF NITRIC OXIDE BY SOLID CARBONACEOUS MATERIAL UNDER LEAN CONDITION

Shan Xiao

The reactions of O_2, NO_x and soot from Diesel exhaust over Cu containing catalysts can significantly reduce soot and NO_x emissions while producing N_2 and CO_2. The author has evaluated the performance of Cu ion exchanged ZSM-5 and Cu adsorbed on Granulated Activated Carbon (Cu-GAC) using GAC as a surrogate for soot in a packed bed reactor. CO, formed primarily by the oxidation of GAC with O_2, appears to be a stable intermediate in the reduction of NO. With experimental parameters chosen to simulate Diesel exhaust conditions, Cu-GAC is much more effective than GAC mixed with Cu-ZSM-5, converting six times more NO_x to N_2 at 500°C at the representative gas hourly space velocity of 50,000. Both catalysts are poisoned by H_2O and SO_2. A mechanism is presented that is consistent with the experimental results.

Catalytic reduction of nitric oxide (NO) with solid carbonaceous materials to N_2 was also investigated over palladium based catalysts. Catalysts consisting of 4 wt.% Palladium on CeO_2, Al_2O_3 and TiO_2, prepared by the impregnation method, were evaluated as lean NO_x control catalysts with granular activated carbon (GAC) as the reductant. The performance of these catalysts was measured with a gas containing 590 ppm NO, 10% O_2, and the balance He at gaseous hourly volumetric space velocities of 50,000 and 80,000 and at temperatures in the range of 200-600°C. All catalysts exhibited

high activity for NO reduction with GAC. The PdO/Al_2O_3 showed the highest activity among the tested catalysts with maximum conversion over 80% at GHSV of 50,000. The PdO/CeO_2 had the lowest light-off temperature of 450°C with a maximum conversion of 80% at GHSV of 50,000.

The effects of SO_2 and water on the catalysts were also investigated by including 20 ppm SO_2 and 10% water into the gas feed mixture. The results indicated that the palladium catalysts outperform fresh copper exchanged ZSM-5, and are much more slowly poisoned by sulfur compounds and water while promoting NO reduction with GAC to N_2.

The purpose of this study was to develop a novel catalyst that can be used in a rotating fluidized bed reactor (RFBR) containing an attrition resistant high surface area catalytic powder to filter soot and promote the reaction between soot and NO at elevated temperatures and at high space velocities. Consequently, this system is self-cleaning i.e., the soot layer is oxidized by $NO_x + O_2$ and removed as CO_2, while the NO_x is removed as N_2. The RFBR provides good contact between the catalyst and reactants, and a lower relative pressure drop compared to particulate traps and other existing particulate control devices.

CATALYTIC REDUCTION OF NITRIC OXIDE BY SOLID CARBONACEOUS MATERIAL UNDER LEAN CONDITION

by
Shan Xiao

A Dissertation
Submitted to the Faculty of
New Jersey Institute of Technology
In Partial Fulfillment of the Requirements for the Degree of
Doctor of Philosophy in Chemistry

Department of Chemistry and Environmental Science

August 2002

APPROVAL PAGE

CATALYTIC REDUCTION OF NITRIC OXIDE BY SOLID CARBONACEOUS MATERIAL UNDER LEAN CONDITION

Shan Xiao

Dr. Robert Pfeffer, Dissertation Advisor — Date
Distinguished Professor of Chemical Engineering, NJIT

Dr. Henry Shaw, Dissertation Advisor — Date
Professor of Chemical Engineering and Environmental Science, NJIT

Dr. John G. Stevens, Committee Member — Date
Professor of Mathematical Science, Montclair State University

Dr. Barbara Kebbekus, Committee Member — Date
Professor of Chemistry and Environmental Science, NJIT

Dr. Daniel Watts, Committee Member — Date
Professor of Sustainability, Executive Director of YCEES Center, NJIT

Dr. Laurent Simon, Committee Member — Date
Professor of Chemical Engineering, NJIT

BIOGRAPHICAL SKETCH

Author: Shan Xiao

Degree: Doctor of Philosophy

Date: August, 2002

Undergraduate and Graduate Education:

- Doctor of Philosophy in Chemistry,
  New Jersey Institute of Technology, Newark, NJ, 2002

- Master of Science in Applied Chemistry,
  New Jersey Institute of Technology, Newark, NJ, 1999

- Bachelor of Science in Chemistry,
  Sichuan University, Chengdu, Sichuan, P.R.China, 1990

Major: Chemistry

Publications and Presentations:

S. Xiao, K. Ma, H. Shaw, R. Pfeffer, J. G. Stevens,
"The lean catalytic reduction of nitric oxide by solid carbonaceous material", Applied Catalysis B: Environmental 32 (2001) 107 –122.

S. Xiao, I. W. Burdick, H. Shaw, R. Pfeffer, J. G. Stevens,
"Catalytic Reduction of Nitric Oxide with Solid Carbonaceous material over palladium catalysts under lean condition", Applied Catalysis B: Environmental.

S. Xiao, H. Shaw, R. Pfeffer, J. G. Stevens,
"FTIR study of the lean NO reduction with catalyzed carbonaceous material", Proceeding.

S. Xiao, D. J. Watts, D. G. Wei,
"Preparation and characterization of highly dispersed palladium metal catalyst", Proceeding.

S. Xiao, I. Bagyi, H. Shaw, R. Pfeffer, J. G. Stevens,
"The Studies of Catalytic reduction of NO_x Under Lean Condition", Ninth annual Uni-Tech Conference on science and technology, Apirl 28, 2000, Newark, NJ.

S. Xiao, I. Bagyi, H. Shaw, R. Pfeffer, J. G. Stevens,
"The Lean Catalytic Reduction of Nitric Oxide By Solid Carbonaceous Materials", Catalyst Society of Metropolitan New York 2000 spring symposium, March 22, 2000, Lehigh University, Bethlehem, PA.

S. Xiao, I. Bagyi, H. Shaw, R. Pfeffer, J. G. Stevens,
"The Lean Reduction of Nitric Oxide with Solid Carbonaceous material over palladium catalysts", Catalyst Society of Metropolitan New York 2000 spring symposium, March 22, 2000, Lehigh University, Bethlehem, PA.

S. Xiao, I. Bagyi, H. Shaw, R. Pfeffer, J. G. Stevens,
"Development Catalyst for Catalytic Reduction of NO with Solid Reducing Material Under lean Condition", 48th CPI Exposition Nov16-18, 1999, New York City.

S. Xiao, I. Bagyi, H. Shaw, R. Pfeffer, J. G. Stevens,
"Catalytic Reduction of NO with Solid Reducing Material from Diesel Engine Using Rotating Fluidized bed Reactor (RFBR)", AIChE 1999 annual meeting, Oct 31- Nov 5, Dallas, TX.

S. Xiao, I. Bagyi, H. Shaw, R. Pfeffer, J. G. Stevens,
"Catalytic Reduction of NO with Solid Carbonaceous Material", AIChE 1998 annual meeting, Nov15-20, Miami, FL.

This dissertation is dedicated to my beloved family

ACKNOWLEDGEMENT

I would like to express my deepest appreciation to Dr. Robert Pfeffer, Dr Henry Shaw, and Dr John G. Stevens, who not only served as my research advisors, providing valuable and countless resources, insight, and intuition, but also gave me support, encouragement, and reassurance. Special thanks are given to Dr. Barbara Kebbekus and Dr. Daniel Watts for actively participating in my committee. This work was supported by the National Science Foundation under grant # CTS - 9612483 and the EPA Exploratory Research Center on Airborne Organics under grant # R824970.

Many thanks to Dr. Donguang Wei for his timely and valuable assistance in instrument installation and analytical techniques. Many of my fellow graduate students: Kaiwen Ma, Guihua Qian, Ian W. Burdick, and Tian Sang, are deserving of recognition for their help and support. I also wish to thank Dr. Isvan Bagyi for his assistance during the years he was working on the project as a post-doctoral research associate.

TABLE OF CONTENTS

TABLE OF CONTENTS
(Continued)

Chapter **Page**

TABLE OF CONTENTS
(Continued)

Chapter **Page**

TABLE OF CONTENTS
(Continued)

Chapter **Page**

LIST OF FIGURES

LIST OF FIGURES
(Continued)

LIST OF FIGURES
(Continued)

LIST OF FIGURES
(Continued)

Figure **Page**

LIST OF TABLES

CHAPTER 1

INTRODUCTION

1.1 Background

Diesel engines are widely used in transportation and for small power applications. They operate by compressing the diesel fuel and air mixture to very high pressures, raising the gas temperature to the point of combustion. As a consequence of their overall lean operation and higher compression ratio, they tend to emit less CO and unburned hydrocarbons per mile and have higher thermal efficiency than internal combustion gasoline engines.

The design of the combustion process, however, promotes the production of significant quantities of particulate matter (soot) and NO_X. There is evidence that particulates from diesel engines are biologically more active than those from spark ignition engines. They are suspected carcinogens [1](Russell-Jones, 1987). Therefore, diesel emission control is being addressed worldwide. More stringent standards have been proposed and promulgated to limit the emissions of particulates from diesel engines in many parts of the world [2-4] (Heck and Farrauto, 1995, Burgler et al., 1992, Needham et al., 1991).

Controlling diesel emissions is more complex than those from gasoline engines. Since HC and CO emissions are relatively low, the main problem is to reduce the particulate and NO_X [2]. Diesel engine manufacturers are trying to develop improved diesel engines, which will produce less soot and NO_X. Nevertheless, an "after-treatment" technology will be needed to meet the projected stringent emission standards.

1.2 "After-Treatment" Technology for Diesel Engine Exhaust

1.2.1 Diesel Oxidation Catalysts

Unlike those of gasoline engines, diesel gaseous HC and CO emissions are relatively low, and their reduction is not necessary to meet the 1994 U.S. truck standards. Thus, the problem is to reduce particulates. Dry carbon engine emissions can be reduced by engine modification, but this causes an increase in the soluble organic fraction (SOF) [2] (Heck, Farrauto 1995). One approach to meet emission requirements has been to have the catalyst oxidize the SOF, (which represents up to about 65 percent of the particulates), thereby greatly reducing the total particulates emitted. The engine particulate sulfate emissions have been reduced by decreasing the fuel sulfur content from the pre-1994 value of 0.2-0.3 percent to the 1994 value of 0.05 percent. This alone accounts for a drop from 0.05 g/bhp-h to 0.01 g/bhp-h of particulates as sulfate. A combination of reduced fuel sulfur, the presence of a catalyst to reduce the SOF, and engine modification to decrease the dry carbon emitted would bring US trucks into compliance with standards promulgated for 1994, provided suitable catalysts could be developed [2] (Farrauto, 1995).

1.2.2 Monolith Particulate Trap

A monolith is a ceramic or metallic support having the structure of a honeycomb with numerous small parallel channels for gas flow. In catalytic applications, the surfaces of these channels are covered by a wash coat containing the active catalyst. It offers a number of advantages over a packed bed of catalyst pellets, especially a lower pressure drop. Monoliths have been widely used as supports in environmental applications.

In the mid-1980s, many engine manufacturers considered using a device to physically filter or trap the particulates on the wall of a wall-flow honeycomb [5-6] (Farrauto, et al., 1992, Murtagh, et al., 1994). The gases were forced to flow through the monolith wall and exit the adjoining channel. The particulates, having larger particle size than the pore size of the monolith wall, were trapped. Since this device had limited capacity before pressure drop became excessive, it was necessary to periodically regenerate it by combustion. The dry carbon particles of the particulates require at least 400-450°C for ignition. However, the engine exhaust does not reliably reach these temperatures. It was hoped that a heterogeneous catalyst would reduce the light-off temperature of the particulates. This approach has met with limited success. Generally, a burner system to periodically and reliably elevate the temperature of the exhaust to the ignition point of the particulates is required. The best designs required an expensive and elaborate control system, which was not considered economical for most applications.

Although ceramic monolith filter development has proceeded straightforwardly, regeneration systems are problematic and costly. Therefore, these development efforts led to disappointing results. The use of catalytic fuel additives to promote regeneration in a trap through lowering the incineration temperature of the collected soot has now been developed by PSA in France. Both Johnson Mathey and Engelhard in the US have commercialized filters which employ an oxidation step to convert NO to NO_2 and then utilize the reaction: $NO_2 + C \rightarrow CO + NO$ to oxidize soot at low temperatures. Desirable improvements to these technologies would be enhanced durability, reduced probability of plugging, reactor tolerance and greater conversion of the NO_2 to N_2.

An alternate approach under evaluation is to add certain metallo-organic compounds containing either Cu, Fe, or Ce to the diesel fuel which, when reacted with the trapped particulates, can reduce the temperature for light-off. Due to the potential for emissions of these metal oxides into the atmosphere as fine particulates, it is unlikely that this approach will find broad acceptance. Testing, however, is still proceeding [2] (Farrauto, 1995).

1.2.3 Lean NO_x Reduction Catalysts

The most often used technology involves lean NO_x catalysts. Given the relatively cooler operating conditions of diesel engines, there will be demand for catalysts to enhance low temperature particulate oxidation to avoid channel plugging under extended idle operation. Furthermore, improved light-off activity for hydrocarbons with minimum use of expensive precious metals will continue to be important for future HC+NO_x applications. More active, selective, and durable catalysts will have to be developed to be compatible with improved exhaust system designs. Close coupling of the catalyst to the combustion chamber, hydrocarbon trapping, electrically heated monoliths, particulate traps and so on are under consideration by diesel engine manufacturers to further improve the quality of the diesel exhaust [2] (Farrauto, 1995).

Lean NO_x catalysts offer another approach by catalytically reducing NO_x with soot and added hydrocarbons to nitrogen. Today's diesel oxidation catalysts do not eliminate NO_x as do their Otto cycle counterparts. Spark ignition engines use an oxygen sensor to operate near stoichiometric conditions. They oxidize CO and HC and reduce NOx as exhaust oxygen swings between lean and rich operation. Diesels operate lean and have too much excess oxygen in their exhausts, so only oxidation occurs. As now envisioned,

a NOx reduction catalyst would foster reactions between NOx and reducing agents in the exhaust, i.e., HC and CO. Some zeolites hold promise here because they are able to capture HC for these reactions. Research must find a way for them to work over the range of temperatures found in diesel engines and with the variety of hydrocarbons present. The creation of lean NOx catalysts must be coupled to engine design so the exhaust has the proper temperature and spectrum of HCs. Another concern that must be addressed is how sensitive these catalysts are to sulfur and water poisoning.

Right now, many research studies are being carried out for using alternative fuel in diesel engines. Alternative fuels will grow in importance through the early part of the 21st century as a way to control diesel emissions [2] (Heck and Farrauto, 1995). Engines using CNG, LPG, methanol, ethanol, or other fuels may offer the best long-term way to meet exhaust restrictions of emissions because they produce fewer particulates and can be run lean or stoichiometric. Therefore they may be able to meet CO, HC and NO_x standards. The initial commercial fuels in this area are now emerging for buses, e.g., CNG and methanol engines are currently being certified by the EPA. Both engines use a DOC to lower HC and CO. However, if alternate fuels are to emerge as a viable alternative, such issues as fuel cost and availability must be overcome.

1.3 Health and Environmental Effects of PM and NO_x

Particulate matter (PM) is the general term used for a mixture of solid particles and liquid droplets found in the air. Some particles are large or dark enough to be seen as soot or smoke. Others are so small they can be detected only with an electron microscope. These particles are defined by regulations defining fine particles at less than 2.5 micrometers in

diameter and coarser-size particles at larger than 2.5 micrometers. These particles originate from many different stationary and mobile sources as well as from natural sources. Fine particles (PM-2.5) result from fuel combustion from motor vehicles, power generation, and industrial facilities, as well as from residential fireplaces and wood stoves. Coarse particles (PM-10) are generally emitted from sources, such as vehicles traveling on unpaved roads, materials handling, crushing and grinding operations, as well as windblown dust. Some particles are emitted directly from their sources, such as smokestacks and cars. In other cases, gases such as SO_2, NO_x, and VOC interact with other compounds in the air to form fine particles. Their chemical and physical compositions vary depending on location, time of year, and weather.

Respirable PM includes both fine and coarse particles. These particles can accumulate in the respiratory system and are associated with numerous health effects. Exposure to coarse particles is primarily associated with the aggravation of respiratory conditions, such as asthma. Fine particles are most closely associated with such health effects as increased hospital admissions and emergency room visits for heart and lung disease, increased respiratory symptoms and disease, decreased lung function, and even premature death [7] (F. C. Liu, 1996). Sensitive groups that appear to be at greatest risk to such effects include the elderly, individuals with cardiopulmonary disease, such as asthma, and children. In addition to health problems, PM is the major cause of reduced visibility in many parts of the world. Airborne particles also can cause damage to paints and building materials.

In 1997, EPA added two new PM-2.5 standards, set at 15 micrograms per cubic meter ($\mu g/m^3$) and 65 $\mu g/m^3$, respectively, for the annual and 24-hour standards. In

addition, the form of the 24-hour standard for PM-10 was changed. EPA is beginning to collect data on PM-2.5 concentrations. Beginning in 2002, based on 3 years of monitoring data, EPA will designate areas as nonattainment that do not meet the new PM-2.5 standards.

Nitrogen dioxide (NO_2) is a reddish brown, highly reactive gas that is formed in the ambient air through the oxidation of nitric oxide (NO). Nitrogen oxides (NO_x), the term used to describe the sum of NO, NO_2 and other oxides of nitrogen, play a major role in the formation of tropospheric ozone. The major sources of man-made NO_x emissions are high-temperature combustion processes, such as those occurring in automobiles and power plants. Home heaters and gas stoves also produce substantial amounts of NO_2 in indoor settings.

Short-term exposures (e.g., less than 3 hours) to current nitrogen dioxide (NO_2) concentrations may lead to changes in airway responsiveness and lung function in individuals with pre-existing respiratory illnesses and increases in respiratory illnesses in children (5-12 years old) [7] (F. C. Liu, 1996). Long-term exposures to NO_2 may lead to increased susceptibility to respiratory infection and may cause lung alterations. Atmospheric transformation of NO_x can lead to the formation of ozone and nitrogen-bearing particles (most notably in some western urban areas) which are associated with adverse health effects.

Nitrogen oxides also contribute to the formation of acid rain. Nitrogen oxides contribute to a wide range of environmental effects, including potential changes in the composition and competition of some species of vegetation in wetland and terrestrial systems, visibility impairment, acidification of freshwater bodies, eutrophication (i.e.,

explosive algae growth leading to a depletion of oxygen in the water) of estuary and coastal waters (e.g., Chesapeake Bay), and increases in levels of toxins harmful to fish and other aquatic life.

The 1999 National Air Quality: Status and Trend, published by the EPA Office of Air and Radiation, shows that between 1986 and 1998, national SO_2 concentrations decreased 37 percent and SO_2 emissions decreased 18 percent. Between 1997 and 1998, national SO_2 concentrations decreased 17 percent and SO_2 emissions decreased 13 percent. While national SO_2 air quality levels have improved, the EPA remains concerned about NO_x emission control. In the last 10 years, NO_x emissions levels have remained relatively constant. Between 1988 and 1997, NO_x emissions declined 1 percent, while they increased slightly (by 1 percent) between 1996 and 1997. So, the development of a catalytic aftertreatment system for diesel engines for NO_x and particulates reduction is very important to improve air quality.

1.4 Objectives

The aim of this study is to conduct fundamental research needed to develop a novel air pollution control system for diesel engines. The system will consist of a rotating fluidized bed reactor (RFBR) that will collect soot during diesel engine operation, and react the collected soot with NO_x when the temperature is sufficiently elevated. A key aspect of this research is the proper choice of a catalyst or high surface area material that acts as both the filter medium and a promoter of the lean NO_x reduction. It is important to gain a fundamental understanding of a mechanism that explains how a carbonaceous solid, soot, can be catalytically oxidized with concomitant reduction of NO_x to molecular nitrogen in

the presence of oxygen. This information is needed to develop equipment for controlling the most problematic pollutants NO_x and soot from stationary and mobile diesel engines. The five major objectives of this dissertation are presented below.

1. The first objective is a study of lean NO reduction with gaseous reductant over a commercial catalyst, Cu-ZSM-5 in our laboratory catalyst test unit. This will include measurements of catalyst activity of NO reduction with propane and carbon monoxide, and the effect of SO_2 and H_2O on the catalyst. The Cu-ZSM-5 will be used as a reference for our test unit.
2. The second objective is to study lean NO reduction with solid carbonaceous materials over Cu based catalysts. This will include NO reduction over mixtures of Cu-ZSM-5 with granular activated carbon (GAC), and Cu impregnated GAC. The effect of SO_2 and H_2O effects on these catalysts will also be studied..
3. The third objective is to study the mechanism of lean NO reduction with carbonaceous materials, to elucidate the interaction between NO with GAC, and possible intermediates.
4. The fourth objective is to investigate the performance of palladium based catalyst as a novel lean NO reduction catalyst. The investigation focuses on NO reduction to N_2 with solid carbonaceous materials to simulate soot, over palladium catalysts. The effect of SO_2 and H_2O on this catalytic reduction will also be studied.
5. The fifth objective is to investigate the catalytic NO reduction with soot by using a rotating fluidized bed reactor in an actual diesel engine bench, to examine whether the RFB concept is applicable to diesel engine exhaust control processes.

CHAPTER 2

DESCRIPTION OF APPARATUS AND EXPERIMENTAL DATA STATISTICS

2.1 Packed Bed Reactor and Fixed Fluidized Bed Reactor

The packed bed reactor, shown in Figure 2.1a, is made from a quartz tube 2.5 cm in diameter and 59.5cm long. A porous quartz disk is fused approximately 40 cm from the top. The catalyst or catalyst/GAC mixture is placed on this disk. The reactor is placed in the middle zone of a three-zone furnace that is used to control its initial temperature. The mixture of reactant gases enters the reactor from the top and is discharged from the bottom, i.e., this reactor is operated in downflow mode.

A second reactor, which we designate as the fixed fluidized bed reactor, is depicted in Figure 2.1b. It is fabricated from a quartz tube 2.5 cm in diameter and 55 cm long with the bottom having a 45° taper. The reactant gases mixture enters the reactor from the bottom through a stainless steel tube 54 cm long, 0.32 cm in diameter, which extends down from the top (see figure). The gas then travels back up the reactor, causing the catalyst or catalyst/GAC mixture particle to fluidize, and is discharged from the exit on the top cap.

2.2 Rotating Fluidized Bed

A rotating fluidized bed as shown in Figure 2.2, is a cylinder with a porous wall that rotates around its axis of symmetry either vertically or horizontally, allowing gases to enter and preventing filter media from leaving. The granular material is introduced into the cylinder and is forced to the wall due to the large centrifugal forces produced by the

rotation. The drag force of the gas, which flows radially inward through the porous wall, opposes the centrifugal force. At minimum fluidization, the drag force is balanced by the centrifugal force caused by the rotation of the bed. Therefore, the minimum fluidization velocity is much higher than that found in conventional fluidized beds, in which the drag force balances the force of gravity on the bed media. RFBs can be used by rotating the cylindrical bed either around a vertical or a horizontal axis. However, when treating diesel engine exhaust from vehicles, the bed needs to be rotated at relatively high RPM to maintain proper fluidization conditions, resulting in a centrifugal acceleration typically more than 100 times that due to gravity. Therefore, the force of gravity is negligible relative to the centrifugal force and the position of the bed (vertical or horizontal) is unimportant. Since it is much more convenient to configure the bed horizontally in a vehicle, our RFBR was rotated along the horizontal axis.

The gas velocity going through an RFB is a function of radius, r, and decreases with increasing r, resulting in a reduction in fluid drag. In contrast, the centrifugal force increases with increasing r. Consequently, fluidization occurs layer by layer, starting with the inner surface of the bed and progressing outward as the superficial air velocity increases (Chen, 1986). We define the superficial gas velocity, U_g, to be based on the outer radius, r_0, of the bed of particles. The inner surface minimum fluidization velocity, U_{mfi}, is the superficial gas velocity at which the inner surface of the bed is first fluidized. The critical minimum fluidization velocity, U_{mfc}, is the superficial gas velocity at which the entire bed is fluidized.

2.3 Distributor

The perforated cylinder distributor, used in all bench experiments, was made of stainless steel in which 460 holes, 10 mm in diameter were drilled, resulting in a 52% open area. The cylinder wall was covered on the inside with two layers of 250 mesh (60 μm) stainless steel screen. A layer of 10 mesh stainless steel screen was put inside these 250 mesh screens in order to keep them tight against the wall of the distributor and to provide the necessary mechanical strength.

2.4 Experimental Data Statistics

In all experiments described in this dissertation, each experimental data point measurement was repeated four to five times. The average value of these repeated measurements is presented in the figures and tables for each data point, except for the online experimental results generated by FTIR. In the fast scan mode this instrument generates more than 3000 points in 45 minutes. The average and relative standard deviation (%RSD) of the experimental data were calculated to ensure data acceptability. If the RSD of the experimental data was above 5%, the data was rejected, and the experiments redone. As an example, the statistics of the data presented in Figure 3.4 are shown in Table 2.1.

%RSD is calculated as: $\%RSD = (\sum(Xi - X_a)^2/n-1)^{1/2}/X_a * 100$, X_a: average value.

Since the %RSD of the experimental data for each point is less than 5%, the data were accepted, the average values were then presented in the figure.

CHAPTER 3

THE LEAN CATALYTIC REDUCTION OF NITRIC OXIDE BY SOLID CARBONACEOUS MATERIALS

3.1 Introduction

Diesel powered vehicles, because of their high thermal efficiency, tend to emit less carbon monoxide and unburned hydrocarbons than gasoline fueled vehicles, but emit significant quantities of NO_x and soot. Nitrogen oxides are gaseous pollutants that contribute to respiratory problems in humans, acid rain formation, photochemical smog, and depletion of the stratospheric ozone layer. Soot is a suspected carcinogen. It is essential to develop improved pollution control equipment that addresses the NO_x/soot emissions problem from diesel engines.

One promising process to mitigate the emissions of NO_x and soot particulate from diesel exhausts involves the catalytic reduction of NO_x by soot under lean conditions. Soot itself is a high surface area material that is known to promote NO reduction under appropriate conditions. The presence of oxygen above a minimum threshold significantly increases the rate of the C+NO reaction. One theory, according to Suzuki et al. [8], postulates that the formation of surface oxygen complexes by the $C+O_2$ reaction is essential for the C+NO reduction.

Tsutsumi et al. [9, 10] using a rotating fluidized bed to treat diesel engine exhaust gases, reported considerably higher NO conversion to N_2 over Cu-ZSM-5 catalyst than reported elsewhere in the literature, e.g., Iwamoto et al. [11, 12]; Sato et al. [13]; Zhang et al. [14]. They found conversion of NO at 420°C as high as 95% at a low superficial velocity of 15 cm/s, but conversion decreased rapidly to 5% as the superficial velocity

was increased to 55 cm/s. They also found a significant decrease in conversion as the temperature of the gas was decreased to 350°C.

Transition metal ion-exchanged zeolites have been found to be very active for decomposing NO to N_2. Among these, Cu-ZSM-5 is believed to be the most active. Zhang et al. [14], with no reducing agent or O_2 present, found a maximum NO decomposition using 80% Mg or Cu modified ZSM-5 between 450-500°C. However, the rate of this reaction decreased significantly in the presence of 5% O_2 in the same temperature range. Iwamoto et al. [11] and Held et al. [15] also indicated that Cu-ZSM-5 is a relatively active catalyst for the decomposition reaction. It should be noted that this mode of operation is not suitable for diesel engines because efficiency and economics dictate that excess air be used.

The factors that govern the overall performance of zeolite catalysts include metal ion type, oxidation state, extent of metal loading, gaseous hourly space velocity (GHSV), oxygen concentration, temperature, and the poisoning effect of water vapor and SO_2.

The C+NO reaction catalyzed by metal loaded charcoal, both in the presence and in the absence of oxygen, was studied by Yamashita et al. [16]. They found that the C+NO reaction is promoted by the presence of oxygen at temperatures as low as 300 °C. The ratio of the activity for NO_x decomposition to that of carbon oxidation in the presence of oxygen varies with the type of metal catalyst used. Catalytic activity decreases for the lean C+NO reaction in the order of Cu>Ca>Ni>none.

Yamashita et al. [17] reported that the reaction of NO with Cu-impregnated charcoal was remarkably enhanced by the presence of O_2. They investigated the formation of reactive surface intermediates consisting of oxygen atoms adsorbed on

carbon and stable carbon-oxygen complexes by the combination of transient kinetics and temperature programmed desorption techniques. They also found that the presence of both O_2 and Cu containing catalysts increased concentration of reactive adsorbed oxygen. Suzuki et al. [8] similarly reported that the formation of surface oxygen complexes by the $C+O_2$ reaction is essential for the C+NO reduction to N_2 to occur.

Walker [18] has summarized four potential mechanisms proposed for the reduction of NO_x by hydrocarbons over Cu-ZSM-5 under lean conditions. The first mechanism follows the NO decomposition pathway, with the role of the hydrocarbon being to reduce Cu^{II} back to the active Cu^{I} state. The second is that some partially oxidized hydrocarbon compounds react preferentially with the NO. The third proposes that an organonitrogen intermediate forms on the Cu sites and subsequently decomposes to give N_2, CO_2, and H_2O. The fourth mechanism involves bifunctional catalysis, with the hydrocarbon being activated by the Cu sites.

The use of soluble metallic compounds as fuel additives in diesel engines followed by a particle trap to reduce soot emissions is discussed in a number of publications [19 - 21]. In general, these publications report that metallic additives containing Cu and Fe achieved substantial reduction in particles due to the trap and additive. Rao et al. [19] studied the effectiveness of catalyzed traps, plain traps, trap regeneration using copper octoate as a fuel additive, and fuel sulfur content on reducing particulate emissions. Zeller et al. [20] reported on the evaluation of two Fe-based diesel fuel combustion additives in a 5.6-L 6-cylinder test engine. Ferric picrate had no measurable effect on exhaust emissions, while a ferrocene-based additive reduced diesel particulate matter by 4-45%, depending on engine operating conditions. Soot reduction

was attributed to the catalytic oxidation properties of a Fe_2O_3 coating inside the combustion chamber. However, they found an increase in NO_x emission (by about 12%) that was considered the only adverse effect of the additive.

Harvey et al. [21] reported on research to quantify the effects of a copper fuel additive on NO_x, hydrocarbons and total particulate matter (TPM) from a diesel engine using a low sulfur fuel. The engine was operated at two steady-state modes and five additive levels (0, 15, 30, 60 and 100 ppm Cu by mass) with and without a ceramic trap. The fuel additive had little effect on baseline emissions without the trap. The trap reduced TPM from 72 to 93% compared to baseline, had no effect on NO_x, and reduced HC about 30%. Collection of copper by the trap was greater than 95%. The additive reduced the trap regeneration temperature from 510°C to about 375°C and reduced the regeneration time from about 90 minutes with no additive to about 1 minute with 30 ppm and greater additive concentrations. Trap ash analyses showed that approximately 89.5% of the material was CuO, 2.5% was Cu_2O, and 8% was $CuSO_4$. Shaw [22] showed that mass concentrations of up to 0.5% transition metal additives to jet fuels can significantly reduce soot and reduce NO_x by as much as 30%. This study involved very lean combustion as is required for gas turbines. The metal additives that were most effective were Fe and Cu.

Some authors have considered NO_2 to be an intermediate in the decomposition of NO. Jelles et al. [23] studied the influence of NO on the oxidation of certain metals such as cerium, copper, and iron on activated soot. The rate-limiting step in the oxidation with oxygen was suggested to be the decomposition of surface oxygen complexes. In the presence of NO, the oxidation rate of soot mixed with a supported platinum catalyst is

increased significantly, especially for cerium-activated soot. This increase in reaction rate in the presence of NO and a platinum catalyst is explained by a cycle of two catalytic reactions. Platinum catalyzed the oxidation of NO to NO_2, which subsequently oxidizes soot using cerium as a catalyst, forming NO, which can participate in the reaction numerous times. This soot oxidation mechanism can be put into practice by combining a platinum-catalyzed particulate trap with a combination of platinum and cerium fuel additives.

The objective of this study is to enhance our understanding of the catalytic process that promotes the oxidation of soot with the concomitant reduction of NO_x to molecular nitrogen. This information is needed to develop equipment for controlling the most problematic pollutants, NO_x and soot, from stationary and mobile Diesel engines. This paper is part of a project to demonstrate the use of a rotating fluidized bed reactor (RFBR) containing an attrition resistant high surface area catalytic powder to promote the reaction of soot with NO_x. As part of this project, we are developing other catalysts that enhance the beneficial properties of copper exchanged ZSM-5 zeolite while minimizing the poisoning effect of sulfur compounds and water. In addition to catalyst research, the research group is conducting experimental and theoretical studies on the mechanism and competitive kinetics of soot reactions with the two oxidants, NO and O_2. The researchers are working under the hypothesis that the observed soot oxidation/NOx reduction involves a stable intermediate rather than the soot itself. This intermediate, possibly CO produced by the oxidation of soot, can then reduce NO_x on the catalyst.

3.2 Experimental

The experimental flow schematic is shown in Figure 3.1. This system consists of a 2.5 cm inside diameter by 55 cm long quartz tubular reactor residing in a vertical three-zone temperature-controlled furnace. The catalyst is placed on a coarse fritted quartz disk in the middle zone of the furnace. The temperature profile is flat with a variability of less than ± 1°C at 500°C. The reactant gases enter the reactor from the top and are discharged from the bottom (downflow). The flow rate of each gas is measured by calibrated rotameters.

The catalyst temperature is continuously monitored by a calibrated 0.16 cm Chromel-Alumel (K-type) thermocouple. The catalyst or catalyst physically mixed with granulated activated carbon (GAC) is taken from a dessicator, weighed, and placed on the fritted disk inside the reactor and heated to 150°C for about an hour with He at a flow rate of about 200 cm^3/min in order to purge the reactor and catalytic materials of oxygen and residual water. The experiments are started by feeding the desired gaseous mixture after blending the component gases from cylinders supplied by Matheson Gas Products. The feed gas mixture is prepared during the He purge of the reactor and the composition verified by gas chromatography (GC). The outlet gas composition from the reactor is also analyzed by GC at the same operating conditions that are used for the feed gas. Experiments are conducted over the temperature range of 200°C to 600°C, with GC analyses conducted each 50°C.

Each experiment is started by loading a weighed fresh sample from the same batch that was prepared by mixing catalyst and GAC in the desired proportions. A fresh sample is used for each constant temperature experiment. The fresh catalyst/GAC

mixture inside the reactor is purged with He for 30 minutes to drive out any residual air. The desired gasous reactant mixture, without O_2, is then introduced and the desired steady state temperature is achieved after 5 to 10 minutes. Then the 10% oxygen component is introduced into the gas mixture. The minimum inlet gas temperature required to cause the rapid oxidation of GAC is a function of catalyst content and gasous hourly space velocity (GHSV). At GSHV of 50,000, this temperature is 300°C for both 20% Cu-GAC and 10% Cu-GAC, and 400°C for 1% Cu-GAC. The rapid oxidation of GAC results in a temperature increase to approximately 650 to 750°C. After the GAC is consumed, the temperature reverts back to the inlet gas temperature in about 5 minutes. Thus, the total time of the temperature excursion is 9 to 10 minutes, consisting of 4 to 5 minutes during which the GAC is oxidized, followed by a 5 minute cooling down period to the pre-set inlet gas temperature.

The results are presented as plots of conversion of NO to N_2 as a function of inlet gas temperature. As soon as the observed temperature passes through a maximum, the gas flowing through the sampling loop of the six-point sampling valve is injected into the GC in the TCD mode. The effluent gas from the catalyst bed travels through the lower section of the reactor below the fritted disc (36.5 cm length, 2.5 cm diameter) and then through polypropylene tubing (4.5 m length, 3.2 mm diameter) to the sampling loop (2 cm^3). At a GHSV of 50,000, the time delay for injection into the GC is approximately 8.9 s in the bottom of the reactor, 1.7 s in the tubing and 0.1 s in the sampling loop for a total of 10.7 s. The average N_2 conversion from the reduction of NO thus obtained is very reproducible.

GHSV is calculated by dividing the total gas flow rate (cm^3/h) at the temperature and pressure of the experiment by the total solid sample volume (cm^3). NO conversion to N_2 is calculated by $2[N_2]_{out} / [NO]_{in}$. The author monitored N_2O by FTIR and found that less than 5 ppm N_2O is produced at low temperatures, and negligible quantities of N_2O are observed at elevated temperatures.

3.3 Analytical

A Nicolet 520 FTIR equipped with a 2 m gas cell became available toward the end of the research reported here, allowing continuous analyses of NO, NO_2, N_2O, CO, CO_2, and H_2O. The instrument was calibrated with certified gaseous mixtures in which He was the balance gas. At least three different mixtures in the range of interest were used to obtain the overall calibration. The FTIR is used in a scanning mode of 30 scans per sample. The inlet and effluent streams from the catalytic reactor are analyzed with this instrument. In addition, the effluent stream for the FTIR passes through a 2 cm^3 sampling loop of a six-point gas-sampling valve before it is injected into an on-line GC. The GC uses both a thermal conductivity detector (TCD) and a flame ionization detector (FID) to analyze the gaseous mixture. The TCD is used to measure the concentration of NO, NO_2, N_2 and O_2. The FID is used to determine CO and CO_2 concentrations after separating these gases over a Porapak Q column and converting them to methane over a Ni catalyst. A different GC column is used with each detector. The column that is connected to the TCD is 0.32 cm in diameter by 9.14 m long stainless steel column packed with 100/120 mesh HayeSep DB. The column that is connected to the FID is a 0.32 cm in diameter by 2 m long stainless steel tube packed with 80/100 mesh Porapak Q.

The results of the two analytical methods agree to within 10%. N_2 and O_2, which cannot be measured by FTIR, were measured by GC.

3.4 Catalysts

Mobil Oil Co. provided us with attrition resistant fluid cracking catalyst consisting of 50 wt% Cu-ZSM-5 and 50 wt% SiO_2/Al_2O_3. Hereafter, this catalyst is referred to simply as Cu-ZSM-5. No other Cu-ZSM-5 was used for this research. The Cu-ZSM-5 is prepared by ion exchanging 100% of the H^+ with Cu^{2+} and contains 2.4 wt% Cu. The Cu-impregnated GAC used in this research is prepared in our laboratory. The GAC used is obtained from J. T. Baker Chemical Co., Philipsburg, NJ, who prepared it from charcoal. The surface area of this material, as received, is 428.8 ± 1.9 m^2/g.

The impregnation method (incipient wetness) consists of completely incorporating a solution of cupric nitrate, which is made by dissolving the salt in deionized water to the desired concentration to obtain the desired metal weight percentage. After drying at 150°C, the support material is soaked overnight with the exact water pore volume of cupric nitrate solution. The resulting slurry is dried at 100°C for four hours, followed by calcination in flowing N_2 at 550°C to convert the salt to the metal oxide. Calcination of GAC supported catalyst is performed in the fixed bed quartz reactor with flowing N_2.

A physical mixture of 5 wt% GAC with 95 wt% Cu-ZSM-5 was made as a surrogate for soot-covered Cu-ZSM-5. Cu impregnated GAC was prepared at 20%, 10%, and 1% of Cu by weight. The amount of GAC mixed with Cu-ZSM-5 was increased to 50 wt% in order to avoid carbon depletion due to oxidation at elevated temperatures.

Table 3.1 summarizes all compositions of Cu containing catalysts used in this study. All combinations of GAC and catalyst were physically mixed in a ceramic mortar and pestle for about 5 to 10 minutes. The carbon/copper mole ratios for each catalyst used are summarized in Table 3.2.

TGA experiments, designed to measure the amount of unreacted GAC exposed to temperatures above 400°C, showed no weight loss up to 800°C in an O_2 atmosphere indicating that no unreacted GAC was present. In order to investigate the reactivity of GAC for NO reduction to N_2, each experiment was conducted with a fresh charge of catalyst and GAC which had been blended in sufficient quantities for a complete set of experiments. No data point presented in this paper was obtained using the same catalyst and GAC charge for more than one temperature and space velocity.

3.5 Results and Discussion

3.5.1 Reduction of NO with GAC

Figure 3.2 shows that the reduction of NO with predried GAC (without a catalytic metal present) in the presence of 10% oxygen begins between 500 and 550°C for GHSV of 2,000 to 40,000. Conversion rate at 600°C decreases from 26% to 20% and 16% at GHSV of 2,000, 20,000 and 40,000, respectively. At GHSV of 2,000 and 20,000, the reaction appears to be in the kinetically controlled regime (below 540°C). At GHSV of 40,000, the reaction appears to be kinetically controlled up to 600°C. It was also determined that in the absence of copper, mixtures of GAC with SiO_2/Al_2O_3 or with the 50:50 mixtures of SiO_2/Al_2O_3 and ZSM-5 did not achieve conversion of NO to N_2 above

those found for GAC alone. These results also indicate that the stainless steel sheathed thermocouple imbedded in these mixtures does not exhibit catalytic activity.

3.5.2 Reduction of NO with Mixture of GAC and Cu-ZSM-5

The following section shows the results of NO reduction with GAC over Cu-ZSM-5.

3.5.2.1 Effect of Space Velocity. Figure 3.3 shows the effect of GHSV on the reduction of NO with 5 wt% GAC/Cu-ZSM-5 mixture in the presence of 10% oxygen as a function of temperature. The maximum NO conversions to N_2 of 57%, 37%, 15%, 10% and 8% are obtained at GHSV of 2,140, 20,000, 40,000, 50,000 and 80,000, respectively. The temperatures at which the maximum conversion is obtained increase with increasing space velocity. The maximum conversion values are plotted as a function of GHSV in Figure 3.4 for fresh catalyst. First, the curve decreases rapidly with increasing GHSV, and above GHSV of 50,000, it decreases much more slowly with conversion less than 10%. The reaction light off temperatures also increase with increasing GHSV.

In Figure 3.3, it can be seen that the NO conversion to N_2 does not achieve a plateau indicative of the mass transfer limited regime. After going through a maximum, the N_2 conversion decreases with increasing reaction temperature. The reason for this observation may be that the available GAC is consumed at the higher temperatures and there is then no source of reductant to react with NO.

3.5.2.2 Effect of Poisoning. In order to determine whether water decreases the activity of Cu-ZSM-5 for the carbon+NO reaction, two separate experiments were conducted, each using fresh samples of the same catalyst/GAC blend. In the first run, a physical mixture of 50 wt% GAC and 50 wt% Cu-ZSM-5 was contacted with a dry gas mixture of 590 ppm NO and 10% O_2 in He. In the second run, the helium flow was reduced to

accommodate the addition of 10% water while the NO and O_2 concentrations were maintained at the same concentration as in the first experiment. The amount of GAC mixed with Cu-ZSM-5 was increased to 50 wt% in this experiment in order to avoid the rapid carbon depletion due to oxidation found at elevated temperature in the experiments presented in Figure 3. Therefore, we used a greater quantity of GAC to provide a longer time period to obtain more accurate measurements. The curves obtained are shown in Figure 3.5.

Poor conversion rates to N_2 were obtained in both cases. Without water, the maximum conversion did not exceed 15% between 500°C and 600°C due to the high GHSV of 50,000. In the second run, maximum conversion of only 8% at 600 °C was achieved due to the water poisoning effect. Moreover, the light off temperature representing the onset of significant reaction increased by approximately 100°C. It should be noted that as a consequence of rapid carbon oxidation, the reaction temperature was appreciably higher than the inlet gas temperature measured by the furnace thermocouple. The thermocouple imbedded in the catalyst/GAC mixture showed a sharp increase in temperature, but the response time was inadequate to accurately measure the change in catalyst temperature.

3.5.3 Reduction of NO with Cu-GAC

The results of reduction of NO with Cu-GAC are summarized as follows:

3.5.3.1 Effect of Space Velocity. Yamashita et al. [16] established that metal-loaded carbon reduces NO in the presence of oxygen. The experimental results show that the C+NO reaction is catalyzed by Cu-GAC in the presence of 10% oxygen. Since the reaction of GAC with O_2 is fast, GAC is consumed rapidly at temperatures of 450°C and

above producing CO and CO_2. It is the NO+CO reaction that we believe is reducing NO. No C+NO reaction was observed in the absence of O_2.

Experiments at GHSVs of 2,140, 20,000 and 40,000 were conducted with 20% Cu-GAC in the presence of 10% of oxygen. The results are shown in Figure 3.6. In all cases above 350°C conversion to N_2 is high. At the higher space velocities, the conversion to N_2 increases sharply above 250°C in the pore diffusion regime. For the reaction at GHSV of 2,140, NO conversion to N_2 exceeding 90% is obtained at temperatures over 400°C. Conversion of NO to N_2 over Cu-GAC is much higher than that obtained over Cu-ZSM-5.

In Figure 6, at 450 to 600°C NO conversion to N_2 decreases by only 4% to 91% when GHSV is increased by an order of magnitude from 2,140 to 20,000. However, at 40,000 GHSV, conversion decreases to 80% for the same temperature range as above.

Figure 3.7 displays NO conversion to N_2 at GHSV of 50,000 and 80,000 when Cu content was decreased to 1 wt% of the Cu-GAC mixture. The maximum conversion to N_2 is obtained in the temperature range of 450 to 600°C. In this range, the conversion rate is essentially independent of temperature (mass transfer limited regime). At GHSVs of 50,000 and 80,000 the maximum conversions to N_2 are slightly above 60% and 50%, respectively. A comparison of the curves in Figure 3.6 and 3.7 shows that over the entire temperature range investigated, higher space velocities result in lower conversion.

3.5.5.2 Effect of Copper Concentration. In order to measure catalytic activity for the reduction of NO with Cu-GAC at GHSV of 50,000 in the presence of 10% oxygen, three concentrations of Cu were studied. Figure 3.8 shows that the light off temperature for the reduction of NO is 250°C for all three Cu concentrations with no significant difference in

the maximum conversion obtained over the temperature range studied. The conversion to N_2 increases rapidly between 250°C to 300°C and more slowly between 350°C and 600°C. The maximum conversion in the mass transfer limited region above 400°C is essentially the same for all three Cu loadings.

3.5.3.3 Effect of Poisoning. The effect of poisons was evaluated for the reaction of NO with Cu-GAC at 50,000 GHSV in the presence of 10% O_2 at a copper concentration on GAC of 1%. The three runs were carried out with exactly the same gas concentrations except that in the second run 10% He was replaced with water vapor, and in the third run 20 ppm SO_2 were added to the mixture containing 10% water. Care was exercised to avoid water condensation by keeping the temperature above the dew point. A fresh catalyst sample from the same batch was used in each run. Figure 3.9 shows the resulting conversion of NO to N_2 for the three runs.

Comparing the three curves, it can be seen that water and SO_2 both inhibit the reduction of NO with Cu-GAC. There is a large light off temperature increase indicating a large rate of reaction decrease when SO_2 is present. The shape of the three curves is very similar, suggesting that poisoning does not change the NO reduction mechanism, but the rate of reaction decreases. The reduction in conversion due to poisoning is consistent with a deterioration of catalytic activity due to a loss in active sites.

3.5.4 Reduction of NO_2 with GAC over Cu-ZSM-5 and Cu-GAC

Since a small fraction of NO_x in diesel exhaust gas is NO_2, researchers compared the GAC reduction of NO_2 to N_2 with that of NO reduction to N_2 over the two Cu containing catalysts. Experiments were conducted with 1% Cu-GAC and GAC admixed with Cu-ZSM-5 in the presence of 10% oxygen at GHSV of 50,000. Figure 3.10 shows that in

both cases the curves for NO_2 and NO conversion to N_2 are quite similar. The mass transfer limited regions start at very similar temperatures for each catalyst. The reaction mechanism for Cu-GAC+NO_2+O_2 is discussed as a part of reaction mechanism below.

Comparing the reduction of NO or NO_2 with Cu-GAC to the reduction of NO or NO_2 with GAC over Cu-ZSM-5, Figure 3.10 shows only slight differences in the maximum conversions and the light off temperatures. Light off temperatures for Cu-ZSM-5 for both NO and NO_2 are greater than that for Cu-GAC. It is possible to infer, as Suzuki et al. [1], that the slightly lower conversions of NO_2 to N_2 are a consequence of NO_2 being reduced to NO prior to the reduction to N_2.

3.5.5 Reduction of NO with CO

Figure 3.11 shows the effect of GHSV on the reduction of NO with CO in the presence of 10% oxygen as a function of temperature. Maximum NO conversions to N_2 of 61%, 35%, 18% and 9% are obtained at GHSV of 2,000, 20,000, 40,000 and 50,000, respectively. These values are very similar to those obtained in the reduction of NO with 5 wt% GAC/Cu-ZSM-5 mixture (Figure 3.3). Similarly, these curves exhibit a maximum at around 400°. However, at temperatures above 500°C, this reaction exhibits higher conversion to N_2 at higher GHSV. A possible explanation for higher conversions of NO at temperatures above 500°C is that CO is oxidized more slowly by O_2 at higher GHSV. Thus, more CO is available for reduction of NO, increasing the rate of reaction and thus the conversion.

Three runs were conducted to react NO with CO over Cu-ZSM-5 in the presence of O_2 at GHSV of 50,000 in order to test catalyst activity under dry and wet conditions. In the first run under dry conditions, 430 ppm NO, 430 ppm CO, and 10% O_2 and balance

He were mixed and fed to the reactor. In the second run, 10% of the balance He was replaced with water. The third run was conducted at the conditions of the first run using the same catalyst.

Results on the reduction of NO with CO over Cu-ZSM-5 were in excellent agreement with D'Itri et al. [24]. In the first run, the maximum conversion rate to N_2 did not exceed 10% at 400-450°C. In the second and third runs, no appreciable conversion was measured.

3.5.6 Isothermal Reduction of NO

It is difficult to carry out experiments under isothermal conditions because the Cu catalyzed reaction between carbon and O_2 is highly exothermic. However, we did conduct a series of experiments designed to approach isothermal conditions by diluting the catalyst consisting of 20% Cu on GAC with α-Al_2O_3 as a heat sink. The catalyst volume in the bed was maintained constant at 1.5 cm^3 by varying the volume fraction of the 20% Cu-GAC in the binary solid mixture from 100% down to 16.7%. The experimental conditions and results are summarized in Table 3. The same experimental protocol as described above was used in these experiments. Table 3 shows that the peak bed temperatures decreased from 763 to 627 °C as Cu-GAC decreased from 100 to 5 wt% of the bed. The conversion of NO to N_2 at these peak temperatures also decreased from 60.5% to 23.2%, while the peak CO concentration decreased from 11,200 to 211 ppm. NO_2 emerged only after CO disappeared from the outlet gas stream. It appears that the GAC was completely depleted at this point. Even though the amount of Cu-GAC was decreased to 5 wt%, the bed temperature still increased to 626°C. When the proportion of Cu-GAC in the bed was further decreased, the effluent gas contained concentrations of

N_2 and CO that approached the detection limits of the analytical instruments, creating relatively large measurement errors.

This set of experiments shows that the conversions of NO to N_2 reported in this paper strongly depend on the peak temperature obtained in the catalyst bed which can be well above the values of the inlet gas temperature used as the abscissas of Figures 2 to 11. Thus, at the same GHSV, higher conversions are obtained at higher peak temperatures. One must interpret the results presented in the paper in view of this consideration and the experimental protocol previously described. However, these experiments also show that the amount of CO produced is related to the amount of NO converted to N_2 lending further support to the hypothesis that CO is a key intermediate for the NO reduction to N_2.

3.5.7 Reaction Mechanism

Yamashita et al. [16] indicate that the Cu catalyzes the $C+O_2$ reaction and increases production of CO. In agreement with their work, we found the $C+O_2$ reaction produces a considerable amount of CO. To investigate the role of CO as a stable intermediate for the $GAC+NO+O_2$ reaction in the presence of copper containing catalysts, comparison of CO concentration formed in the reduction of NO was made according to similar C/Cu ratios of the reducing materials. As an example of the results in Figure 3.12, much higher CO concentrations were obtained using 1% Cu-GAC at GHSV of 50,000 compared to 50% GAC/Cu-ZSM-5. The highest CO concentration of approximately 1040 ppm for Cu-GAC was measured at 600°C in contrast to 77 ppm for Cu-ZSM-5. CO starts to form at low temperatures (>250°C) and more CO forms when the copper is impregnated directly on the carbon. This phenomenon indicates that the proximity of the catalyst to the

reducing material is very important. We believe that the initial reaction in both Cu-GAC+NO+O_2 and GAC+NO+O_2 over Cu-ZSM-5 is GAC+O_2 producing CO, which then reduces NO to N_2.

When NO is absent from the system, a higher concentration of CO is observed, as shown in Figure 3.12. In the presence of NO, CO is consumed by NO forming N_2 and CO_2. Comparing Figure 3.7 and Figure 3.12, it is evident that the higher the quantity of CO formed in the absence of NO, the higher the conversion to N_2 when NO is present. In the absence of the catalyst, very little NO is reduced in the temperature range investigated (Figure 3.2). The concentration of CO formed is comparable to the NO concentration. Thus, NO does not consume CO significantly. Researchers have also found that NO conversion to N_2 increases with the CO/NO ratio [25].

Suzuki et al. [8] found that the reactivity of NO_2 with carbon is high and the main product is not N_2 but NO. Consequently, NO to NO_2 oxidation is not beneficial for the NO removal reaction in the presence of O_2. On the other hand, they found much evidence to support the hypothesis that O_2 enhances the C+NO reaction through formation of surface oxygen complexes.

Summarizing the experimental observations above, the differences in the mechanism of the GAC+NO+O_2 reaction depends on whether or not a catalyst is present. Furthermore, the proximity of the catalyst to the reductant is very important. In the absence of the catalyst, NO conversion to N_2 appears to depend on the concentration of CO formed. Since the rate of the C+O_2 reaction depends on temperature and space velocity, appreciable conversion is only obtained at high temperature and low space velocity. When the catalyst is located on the carbon (Cu-GAC), it promotes substantial

formation of CO even at low temperatures and high space velocity. However, the conversion to N_2 is still determined by the CO concentration. Thus, the reaction mechanism depends on the $C+O_2$ reaction to CO regardless of the catalyst.

When the catalyst is located on a physically distinct carrier (Cu-ZSM-5), the location of the catalyst can be relatively far from the carbon sites. Therefore, CO formation is particularly sensitive to space velocity; the lower the space velocity, the higher the rate of CO formation. Thus, the residence time of the gases is important. At high GHSVs the low residence time of the gases does not favor CO formation. In this situation, N_2 formation is limited by the low concentration of CO. In addition, poor conversion to N_2 is obtained at high temperatures (Figure 3.3) due to the higher rate of $CO+O_2$ competing with the CO+NO reaction. At higher GHSV, we also obtained higher conversion. A possible explanation is that, due to the lower GAC consumption rate at higher GHSV, there is more GAC available to produce CO for reducing NO. Thus, the rate of reaction and conversion to N_2 is increased. A similar observation was reported by Ranier et al. [26]. They showed that the relative catalytic kinetics of $CO + O_2$ is slower than the competing CO + NO reaction over PdO/Al_2O_3.

The overall apparent mechanism in the presence of a catalyst can be summarized as follows:

$$2C + O_2 \rightarrow 2CO \quad (1)$$

$$CO \rightarrow CO\text{-}s \quad (2)$$

$$NO \rightarrow NO\text{-}s \quad (3)$$

$$CO\text{-}s + NO\text{-}s \rightarrow CO_2\text{-}s + N\text{-}s \quad (4)$$

$$CO_2\text{-}s \rightarrow CO_2 \quad (5)$$

$$2N\text{-}s \rightarrow N_2\text{-}s \quad (6)$$

$$N_2\text{-}s \rightarrow N_2 \quad (7)$$

$$NO\text{-}s \rightarrow NO \quad (8)$$

$$CO\text{-}s \rightarrow CO \quad (9)$$

$$CO\text{-}s + O\text{-}s \rightarrow CO_2\text{-}s \quad (10)$$

$$CO_2\text{-}s \rightarrow CO_2 \quad (11)$$

$$N\text{-}s + NO\text{-}s \rightarrow N_2O\text{-}s \quad (12)$$

$$N_2O\text{-}s \rightarrow N_2O \quad (13)$$

$$N\text{-}s + CO\text{-}s \rightarrow CNO\text{-}s \quad (14)$$

$$CNO\text{-}s + O\text{-}s \rightarrow NO\text{-}s + CO\text{-}s \quad (15)$$

$$H_2O \rightarrow H_2O\text{-}s \text{ (reversible)} \quad (16)$$

$$SO_2 \rightarrow SO_2\text{-}s \text{ (irreversible)} \quad (17)$$

Where, -s refers to an adsorbed component on the catalyst.

In the above mechanism, CO can be formed by direct oxidation of the carbon [step (1)]. NO and CO, once formed, stay on the solid surface and are adsorbed on the catalyst sites [steps (2) and (3)]. Finally, CO reacts with NO to form N_2 and CO_2 in steps (4) through (7). Steps (8) through (17) show possible side reactions. Principally, NO and CO can leave the solid material and go into the gas phase [steps (8) and (9)]. When CO reacts with oxygen, CO_2 forms [steps (10) and (11)]. Steps (12) through (15) show other reactions that could take place. Steps (16) and (17) indicate catalyst poisoning by water and sulfur dioxide, which reduces the availability of adsorption sites.

NO conversion to N_2 was plotted as a function of space velocity for GAC over Cu-ZSM-5, and CO over Cu-ZSM-5 at 400°C as shown in Figure 3.13. The values of NO conversion to N_2 were taken at 400°C because the maximum conversions were obtained at this temperature using either GAC or CO as a reducing agent. At GHSVs higher than 40,000, the maximum conversions occur at different temperatures for GAC and CO. Therefore, no data was plotted at GHSVs of 50,000 and 80,000. The line shown was obtained by a least-squares regression of both sets of data. That line fits the results of both experiments, supporting the hypothesis that CO is an intermediate in the catalytic reaction of GAC+NO+O_2. Nevertheless, the role of CO in this reaction is not yet proven and should be addressed in future work.

CHAPTER 4

FTIR STUDY OF THE LEAN NO REDUCTION WITH CATALYZED CARBONACEOUS MATERIALS

4.1 Introduction

Control of engine exhaust emissions currently involves engine operation within a small window close to stoichiometry where so called three-way catalysts can simultaneously convert NO, CO and unburned hydrocarbons to N_2, CO_2 and H_2O [27, 28]. Although this system is efficient in terms of emissions control, the restriction of operating close to stoichiometry imposes a penalty in terms of high fuel consumption. Engines may be operated efficiently at much higher (ca. 20:1) air/fuel ratios leading to improved fuel consumption. However, in the presence of excess oxidant and diesel engine practice of operating under lean conditions, the current three way catalysts are ineffective for NO_x reduction. For these lean burn conditions, many alternative types of catalysts have been considered, including copper-based materials [29-31] with Cu-ZSM-5 being the most widely studied [32-36]. These alternatives offer limited efficiency in terms of NO_x conversion and in particular offer poor stability, high light off temperatures and high sensitivity to SO_2. A recently proposed alternative [37-39] is to store the NO_x on the catalyst's surface during lean burn operation and then using engine management control, offer brief, regular intermissions in which the engine runs under stoichiometric conditions. This results in the release of the NO_x that can be reduced efficiently under these conditions by the standard three-way catalyst components.

Currently, little is known about the mechanistic details of the sequence of reactions and studies resulting in greater knowledge of the details may allow some of the

key problems associated with the system to be addressed. Infrared spectroscopy has already been applied to studies of catalyst surface conditions [31-36] and this approach is currently being extended to the area of NO_x storage and reduction (NSR) catalysts.

The use of carbons and activated carbons as reducing agents for NO removal from exhaust gases has been proposed in the literature because they are relatively inexpensive, as well as being highly feasible for applications in vehicles and other small sources [40 – 46]. The reaction of NO with carbon has not been as extensively studied as some of the other oxidant gas-carbon reactions. However, because of its impact as an atmospheric pollutant, the potential for the removal of NO by activated carbons has recently been receiving increased attention.

The objective of this study is to enhance our understanding of the interaction of soot and NO. This interaction is highly promoted by the catalytic oxidation of soot, and results in most of the NO being converted to N_2. The experiments we conducted reveal that soot oxidation/NO reduction involves a stable intermediate rather than the soot itself. This intermediate, possibly CO, is produced by the oxidation of soot, and can then participate in the reduction of NO to N_2 on the catalyst.

4.2 Experimental

The experimental set-up has been described in some detail previously [47]. Briefly, all experiments were carried out at a gaseous hourly space velocity of 50,000. The catalyst is placed on a coarse fritted quartz disk in the middle zone of the furnace. The temperature profile is flat with a variability of less than ±1°C at 500°C. The reactant gases enter the reactor from the top and are discharged from the bottom (downflow). The flow rate of

each gas is measured by calibrated rotameters. The catalyst temperature is continuously monitored by a calibrated 0.16 cm Chromel-Alumel (K-type) thermocouple. The catalyst or catalyst physically mixed with α-Al_2O_3 is taken from a dessicator, weighed, and placed on the fritted disk inside the reactor. Each experiment is started by loading a weighed fresh sample that was prepared by mixing Cu-GAC and α-Al_2O_3 in the desired proportions. The fresh sample inside the reactor and the FTIR gas cell are purged with helium for 2 hours to drive out any residual air and moisture. The oven temperature is then raised to 490°C, The temperature inside the catalyst bed will rise to 502°C and reach steady state in 10 min.. When the bed temperature is steady, the FTIR series of online measurements are initiated. For the first 5-10 min., only He flows through the system, then approximately 500 ppm of NO is introduced into the gas steam. After 10-15 min. of NO flow, 10% O_2 is introduced into the system. The rapid oxidation of GAC results in a temperature increase on the order of 700°C when only Cu-GAC is present. After the GAC is consumed, the temperature reverts back to the inlet gas temperature in about 5 min.. Thus, the total time of the temperature excursion is 9-10 min., consisting of 4-5 min. during which GAC is oxidized, followed by a 5 min. cooling down period to the pre-set inlet gas temperature. In these experiments, the temperature was recorded to correspond to each FTIR reading, then was plotted as a function of time. In order to obtain a relatively stable bed temperature, the α-Al_2O_3 was used as a heat sink by mixing with the Cu-GAC in different ratios in order to reduce the bed temperature increase during the rapid oxidation of GAC. The wt.% of Cu-GAC and the peak temperature corresponding to the Cu-GAC/α-Al_2O_3 mixing ratios are shown in Table 4.1. The results

experiments are presented as plots of gas content change in the effluent stream and the temperature change in the catalyst bed as a function of time.

4.2.1 Analytical

A Nicolet 520 FTIR equipped with a 2 m gas cell was used to monitor the following gas content changes as a function of time in the gas stream: NO, NO_2, N_2O CO, CO_2. The instrument was calibrated with certified gaseous mixtures in which helium was the balance gas. At least three different concentration mixtures in the range of interest and the origin were used to obtain the overall calibration. The FTIR is used in a scanning mode of 10 scans per sample. The inlet and effluent streams from the catalytic reactor are analyzed with this instrument. The reduction of NO to N_2 can be obtained by difference of NO_x between the inlet gas and effluent gas. In addition, an HP5890 GC equipped with TCD detector was used to analyze the effluent stream of the FTIR for N_2 to verify the FTIR results. The GC uses a 0.32 cm diameter by 9.14 m long stainless steel column packed with 100/120 mesh HayeSep DB to separate N_2 from the background. The results of the two instruments were consistent with each other within the experimental error range.

4.2.2 Catalyst

The GAC used was obtained from J.T. Baker Chemical Co., Philipsburg, NJ, who prepared it from charcoal. The surface area of this material, as received, is 428.8 ± 1.9 m^2/g. The α-Al_2O_3 used as heat sink was obtained from Exxon-Mobil Oil Co..

Cu-GAC is prepared by the impregnation method. The impregnation method (incipient wetness) consists of completely incorporating a solution of cupric nitrate,

which is made by dissolving the salt in deionized water to the desired concentration to obtain the desired metal weight percentage, 20% in our case. After drying at 150°C in He, the support material is soaked overnight with the exact water pore volume of cupric nitrate solution to obtain the desired level. The resulting slurry is dried at 100°C for 4 hours, followed by calcination in flowing helium at 550°C to convert the salt to the metal oxide. Calcination of the GAC supported catalyst is performed in the fixed bed quartz reactor with flowing helium.

4.3 Results and Discussion

4.3.1 NO Reduction with Plain GAC without Oxygen Present

An isothermal reaction was carried out at 502°C, GHSV =50,000; 1.5 ml (0.4836g) GAC was put in the reactor. Helium was flowed through the reactor for 2 hours to drive out residual air and moisture. Then the bed temperature was increased to 502°C, reaching steady state in 10 min.. While the bed temperature remained in steady state, the FTIR online measurement was initiated. The result is shown in Figure 4.1. After 10 min. of continued He flow, the 480 ppm NO was introduced into the system. During the 45 min. online measurement, the NO concentration in the effluent gas remained constant, the same as the inlet NO concentration. No NO_2 and N_2O or CO and CO_2 were produced; the bed temperature also remained constant. This experiment shows that without the catalyst component and O_2 present, NO can not directly react with GAC to produce N_2. At the experimental temperature used, no significant level of NO was absorbed by GAC.

4.3.2 NO Reduction with Cu-GAC with 10% O_2 Present

Figures 4.2 and 4.3 show the FTIR results of NO reduction with 20% Cu-GAC at two pre-set bed temperatures 400°C and 500°C with 10% O_2 present, GHSV of 50,000. The same experimental protocol applied as previously described. After the temperature reached steady state, helium flowed through the system. At 1000 s, when 530 ppm NO was introduced into the system, the bed temperature increased about 30°C then fell back to the pre-set temperature. At the same time, a small amount of CO_2 was detected in the effluent gas stream, which also then fall back to zero. Even though 530 ppm NO was detected in the inlet gas stream, only around 350 ppm NO was present in the effluent gas before O_2 was introduced into the system. Since the previous experiment shows that the amount of physical absorption of gas on GAC at these temperatures is very small or none, we assume that the difference of NO between inlet and effluent gas is due to the chemical absorption of NO on Cu sites. At 1800 s, 10% O_2 was introduced into the system. Due to rapid Cu-GAC oxidation, the bed temperature rapidly increased to a peak temperature and the NO concentration also dropped rapidly. CO_2 was produced immediately after O_2 was introduced into the system, and reached its peak concentration of 10.5% after 50 s of peak temperature. At the same time, NO concentration also dropped to its lowest point of 41.5 ppm. CO reaches peak concentration 23 s later. The differences between the two experiments are, in the case of the 400°C pre-set temperature, bed peak temperature is 670°C and CO maximum concentration is 32265.3 ppm; in the 500°C preset temperature situation, the bed peak temperature and CO maximum concentration are 770°C, 32280.1 ppm, respectively. Due to GAC depletion, the bed temperature falls back to the pre-set temperature in about 500 s, and the NO concentration recovered above 400 ppm. The

time from CO emerging to disappearing is about 300 s. During the same period, NO also experienced a rapid concentration change. CO_2 has a second peak due to CO oxidation, and is completely depleted after 540 s from the time that O_2 is introduced indicating total depletion of GAC. NO_2 could be detected only after most of GAC was depleted. The total concentration of NO and NO_2 in the effluent gas is 520 ppm, almost equal to the inlet NO concentration of 530 ppm. No significant level of N_2O was detected during the experiment.

Two experiments show that NO reduction happens in the same period as GAC rapid oxidation. When copper is present on the GAC, GAC oxidation is significantly improved, as is the NO reduction. At maximum, 94.2% of NO is converted to N_2, but very little NO is converted to N_2 when no catalyst is present under similar conditions [1]. CO emerged right after the NO concentration began to decrease when O_2 is introduced into the system, and reached peak concentration at the same time as NO reached its lowest concentration. When CO disappeared, the NO concentration also reached the end of rapid climb, and recovered in a much slower pattern in the following period. The CO and NO concentration rapid change have almost the same initial time and duration, indicating that CO plays an important role in NO reduction. Because we know from Figure 1 that NO cannot directly react with GAC, and that CO results from GAC oxidation, therefore, one could draw the conclusion that with the catalyst component present, GAC rapid oxidation provides the species that is needed to reduce the NO to N_2. In our case, CO may be one of these species.

It is difficult to carry out experiments under isothermal conditions because the Cu catalyzed reaction between carbon and O_2 is highly exothermic. However, we did

conduct a series of experiments designed to approach isothermal conditions by diluting the catalyst consisting of 20% Cu on GAC with α-Al_2O_3 as a heat sink. The catalyst mixture volume in the bed was maintained constant at 1.5 cm^3 by varying the volume fraction of the 20% Cu-GAC in the binary solid mixture from 100% to 16.7%. The same experimental protocol as described before was used in these experiments, bed temperature was preset at 500°C. Figure 4.4 shows the FTIR results for NO reduction over a mixture of 0.5 ml 20% Cu-GAC and 1 ml α-Al_2O_3. When 500 ppm NO was introduced into the system, only 350 ppm NO was detected in the effluent gas, some NO was believed to be absorbed in the Cu site of Cu-GAC for the same reason discussed above. As O_2 was introduced at 1250 s, the bed temperature immediately increased to 680°C, 90°C lower than the peak temperature when 100% 20% - Cu-GAC was used. The NO concentration decreased while no NO_2 and N_2O were produced but CO was produced. After 23 s past the peak temperature, the NO reached its lowest concentration, 200 ppm, and CO reached its peak concentration, 6790.8 ppm, in the effluent gas. Another 23 s later, CO_2 achieved its peak concentration of 5%. The NO concentration recovered and the CO concentration decreased as Cu-GAC was depleting. The initial time and duration of the NO concentration change is almost the same as the CO concentration change, and NO_2 emerged only after most of the CO disappeared, and leveled off when all of the Cu-GAC is depleted as indicated by the CO_2 level changing to 0. The NO also leveled off at the same time as the NO_2, the level-off concentrations are 380 ppm and 120 ppm, respectively. The total level-off NO, NO_2 concentration in effluent gas is equal to the NO concentration in the inlet gas, the N is well balanced. Figure 4.5 and Figure 4.6 show the FTIR results when the 20% Cu-GAC/α-Al_2O_3 volume

ratio changes from 1:4 to 1:5. The general change is the same as that for the volume ratio 1:2 discussed above, only that the bed peak temperature, Peak CO, CO_2 concentrations and peak NO conversion to N_2 are different due to a different Cu-GAC fraction. The corresponding experimental conditions and results are summarized in Table 4.1.

Table 4.1. shows that the peak bed temperatures decreased from 763 to 627°C as Cu-GAC decreased from 100 to 5 wt. % of the bed. The conversion of NO to N_2 at these peak temperatures also decreased from 60.5 to 23.2%, while the CO concentration at peak temperature decreased from 11,200 to 211 ppm. Maximum conversion of NO to N_2 decreased from 94.2 to 38.5%, while the maximum CO concentration decreased from 32280.1 to 2077.3 ppm. NO_2 emerged only after CO disappeared from the effluent gas stream. It appears that the GAC was completely depleted at this point. This indicates that when reductant (CO) produced from GAC oxidation is present in the system, NO is not subject to be oxidized to NO_2 even though there is excess O_2 available. Even though the amount of Cu-GAC was decreased to 5wt.%, the bed temperature still increased to 626°C. When the proportion of Cu-GAC in the bed was further decreased, the effluent gas contained concentrations of N_2 and CO that approached the detection limits of the analytical instruments, creating relatively large measurement errors.

This set of experiments shows that the conversions of NO to N_2 reported in this paper strongly depend on the peak temperature obtained in the catalyst bed, which can be well above the pre-set bed temperature. This bed temperature results from Cu-GAC rapid oxidation, and is determined by the amount of Cu-GAC available. The more Cu-GAC present in the system, the higher the bed temperature that can be achieved, and the more CO that is produced. The copper catalyzes the $C + O_2$ reaction and increases production

of CO [22]. The plain GAC + O_2 reaction produces less CO, and results in much lower NO reduction to N_2 [1]. We found in our experiments that the C + O_2 reaction produces a considerable amount of CO. We also found that NO is not oxidized to NO_2 when CO is present in the system, which indicates NO reduction is much faster than NO oxidation under the experimental conditions presented in this paper. It also indicates that abundant reductant species (intermediates) are present on the surface of catalyst because one should interpret that the CO detected is only the fraction that is being released into the gas phase and will be oxidized to CO_2 immediately with the excess O_2 that is present. CO concentration in the gas phase should be related to the total amount of CO produced by the C + O_2 reaction. However, these experiments show that the amount of CO produced is related to the amount of NO converted to N_2 lending further support to the hypothesis that CO is a key intermediate for the NO reduction to N_2.

CHAPTER 5

PREPARATION AND CHARACTERIZATION OF HIGHLY DISPERSED PALLADIUM CATALYSTS

5.1 Introduction

The most common commercial procedure for dispersing the catalytic species within the carrier is by impregnating with an aqueous solution containing a salt (precursor) of the catalytic element or elements [48-52]. Most preparations simply involve soaking the carrier in the solution and allowing capillary and electrostatic forces to distribute the salt over the internal surface of the porous network. The salt generating the cations or anions containing the catalytic element is chosen to be compatible with the surface charge of the carrier to obtain efficient adsorption or, in some cases, ion exchange. For example, $Pt(NH3)_2^{+1}$ salts can ion exchange with H^+ present on the hydroxy containing surface of Al_2O_3. Anions such as $PtCl_4^{-2}$ will be electrostatically attracted to the H^+ sites. The isoelectric point of the carrier (the charge assumed by the carrier surface), which is dependent on pH, is useful in making decisions regarding salts and pH conditions for the preparation.

Among three preparation methods (capillary impregnation, electrostatic adsorption, and ion exchange), the capillary impregnation or incipient wetness approach is the most commonly used, simplest, and easiest to control. Most laboratories and manufacturers are capable of implementing it. In this method, the maximum water uptake by the carrier is referred to as the water pore volume. This is determined by slowly adding water to a carrier until it is saturated, as evidenced by the beading of the excess H_2O [53]. The precursor salt is then dissolved in an amount of water equal to the water

pore volume. Once dried, the carrier pore structure is certain to contain the precise amount of catalytic species.

Catalytic performance of catalysts is strongly influenced by the preparation variables. The dispersion and distribution, and accordingly the chemical states of surface species depend on various preparation parameters, such as metal content, pH, calcination temperature, carrier properties, but to different extents [54 – 65]. A systematic study of catalyst preparation requires a number of tedious activities to find effective preparation variables. We believed that a group study would benefit from better understanding of how those variables affect catalyst properties and lead to establishing better preparation procedures.

5.2 Experimental

5.2.1 Catalyst Preparation

The γ-Al_2O_3 used in the present study was supplied by Mobil Corporation. It has 120 m^2/g surface area, and is 20 micron in size. All γ-Al_2O_3 samples were aged at 600°C for 6 hr before impregnation. Palladium nitrate and ammonia used in this study were of analytical grade.

5.2.1.1 Cat-A Series. This catalyst series consists of 4 catalysts with 1%, 2%, 3%, 4% palladium loaded on aged γ-Al_2O_3 mentioned before. Palladium nitrate corresponding to different metal loadings was dissolved in distilled water with a volume corresponding to 1g γ-Al_2O_3/water pore volume. Weighed 1g γ-Al_2O_3 was then dropped into this solution followed by soaking and drying over night in a sealed container. All palladium will be adsorbed on the γ-Al_2O_3 surface by then. The sample was further dried at 100°C for 3 h

in a quartz reactor with helium flow though the reactor. Finally, the sample was calcined in a 3-zone furnace. The temperature was raised stepwise to 250°C, 350°C, 450°C for 1 h at each temperature and finally kept at 450°C for 4 h. The helium flowed though the reactor during the whole calcination process.

5.2.1.2 Cat-B Series. This catalyst series consists of 3 catalysts with 3% palladium, and 3 catalysts with 4% palladium loaded on aged γ-Al_2O_3 and calcined at 200°C, 350°C, 480°C, respectively. Palladium nitrate corresponding to 3% or 4% palladium loading was dissolved in distilled water at a volume corresponding to 1g γ-Al_2O_3/water pore volume. Weighed 1g γ-Al_2O_3 was then dropped into this solution followed by soaking and drying over night in a sealed container, all palladium will be adsorbed on the γ-Al_2O_3 surface by then. The sample was further dried at 100°C for 3 h at a vertical quartz reactor with helium downflow through the reactor. Finally, the sample was calcined in a 3-zone furnace. The 3 samples of each Pd loading were calcined at 200°C, 350°C and 480°C for 4 h, respectively. The helium flowed through the reactor during the whole calcination process.

5.2.1.3 Cat-C Series. This catalyst series consists of 5 catalysts with 3% palladium loaded on aged γ-Al_2O_3 but impregnated at different pH conditions. Palladium nitrate corresponding to 3% palladium loading was dissolved in distilled water with a volume corresponding to 1g γ-Al_2O_3/water pore volume, the solution has pH = 1. Weighed 1g γ-Al_2O_3 was then dropped into this solution and the resulting slurry pH increased to 3. Then 7.2N NH_4OH solution was used to adjust the slurry pH to 5, 6, 8 or 10, respectively, immediately after completion of the alumina addition. This was followed by soaking and drying over night in a sealed container. All of the palladium will be adsorbed on the γ-

Al_2O_3 surface by then. The sample was further dried at 100°C for 3 h in a vertical quartz reactor with helium downflow through the reactor. Finally, the sample was calcined in a 3-zone furnace. The three samples were calcined at 350°C for 4 h, respectively. The helium flowed through the reactor during the whole calcination process.

5.2.2 Characterization

This section describes the experiments for catalyst characterization.

5.2.2.1 Pulse Chemsorption. The dispersion of palladium on γ-Al_2O_3 for all of the catalyst preparation was measured by using the pulse chemsorption method in an Altmira instrument. Weighed powder catalyst samples (0.1 ~0.15 g) were first reduced at 350°C for 3h with 30ml/min ultra high purity 5% H_2 in Argon, followed by flushing for 2h at the same temperature with 30ml/min ultra high purity Argon. Then pulse chemsorption was carried out with 30ml/min ultra high purity 5% H_2 in Argon at 80°C, with 30ml/min ultra high purity Argon as carrier gas. The number of active catalyst sites was calculated using the method provided in the Altmira instrument manual.

5.2.2.2 X-ray Diffraction (XRD). Powder diffraction patterns of the samples were measured on a Philips X'pert PW3040-MPD XRD.

5.3 Results and Discussion

5.3.1 Effect of Palladium Loading on the Dispersion of Palladium on Al_2O_3

Cat-A series catalysts consist of 4 catalysts with 1%, 2%, 3% or 4% Pd impregnated, respectively. The palladium dispersion and metal crystalline size were measured by the pulse chemsorption method in the Altmira instrument. The dynamic pulse flow technique [66-69] for adsorption measurement and the modified stoichiometry proposed by O'Rear

et al. [70] were used for the computation of the accessible metal fraction. Although the stoichiometric determinations need accurate measurements in static volumetric units, a rapid pulse technique can be safely used for obtaining reliable analysis of metal dispersion.

Figure 5.1 is one of the chemsorption experimental results, and Figure 5.2 is the calculated result for Pd dispersion on Al_2O_3 of the 4 catalysts. Figure 5.2 shows that Pd dispersion decreases as the metal loading increases from 1% to 4%, and Pd crystalline size grows as the metal loading increases, as shown in Figure 5.3. The calculated results of number of moles of active sites per gram of sample are shown in Figure 5.4. The active sites increase as the metal loading increases, reaching maximum value at 3% Pd loading. Further increase of Pd loading to 4% results in active sites decreasing. The active species in catalysts are suggested to be the monolayer-dispersed oxides on the supports [71].

It was first suggested by Russell and Stokes [72] that a maximum activity of catalyst occurred when the Al_2O_3 surface was covered completely by monolayer active species. It seems that until the Pd loading reaches 3%, the dispersion of Pd on this Al_2O_3 is monolayer. This is indicated by the fact that the Pd dispersion eventually stays constant in this metal concentration range and the number of active sites increases due to the metal concentration increasing. When the Pd loading reaches 3%, the metal reaches its dispersion capacity on the Al_2O_3, as indicated by the observation that the dispersion and the number of active sites are decreased as the Pd loading increases from 3% to 4%. One extra catalyst preparation, 8% Pd supported on Al_2O_3 has been made for this set of catalysts, the chemsorption results show that the dispersion of this catalyst decreases to

6.3% from around 20% of 1-3% Pd loading. The active sites for this catalyst decrease to 4.735 E-5 moles/g, which is lower than the 3% and the 4% Pd loading catalysts.

It has been discovered that many salts and oxides can disperse spontaneously onto the surface of supports to form a monolayer or sub-monolayer [73]. This is quite a widespread phenomenon. For a salt or oxide dispersed on a support, there is a monolayer dispersion capacity. When its loading exceeds the capacity, the surplus salt or oxide will remain as crystalline phase in the system together with its monolayer phase. In our case, 3% Pd loading seems to be the monolayer dispersion capacity. When the Pd loading exceeds 3%, the Pd crystalline phase will form on the surface of the Al_2O_3, and its size will grow as the loading increases, the XRD experimental results shown in Figure 5.5, exhibit consistent behavior. Further increases in the Pd loading will not compensate for the dispersion decreases resulting from crystalline growth. Rather, the active sites on the catalysts will decrease.

5.3.2 Effect of Calcination Temperature on the Palladium Dispersion on Al_2O_3

In this group of experiments, 6 samples consisting of three 3% Pd/Al_2O_3 and three 4% Pd/Al_2O_3, were calcined at three different temperatures, 200°C, 350°C, and 480°C. Figure 5.6 shows that Pd dispersion decreases from 31% to 12.6% for 3% Pd/Al_2O_3, 25% to 7.9% for 4% Pd/Al_2O_3 as the calcination temperature increased. Pd crystallite size grew 3.3 times for 4% Pd/Al_2O_3 and 2.5 times for 3% Pd/Al_2O_3, and the calculated active sites also decreased by the same magnitude when the calcination temperature increased from 200°C to 480°C, as shown in Figures 5.7 and 5.8. These observations indicate that the catalysts were going through the sintering process, induced by thermal effects. Because the Al_2O_3 carriers used, are aged at 600°C for 6 h before preparation of the

catalysts, it is most likely that the initially well dispersed Pd was sintering while the calcination temperature increased. The XRD pattern in Figure 5.9 also shows the growth in crystal structures. It is common for a highly dispersed catalytic species to undergo growth to better-defined crystals. With the temperature increasing, the active species on the surface tend to migrate together. As this process proceeds, the crystals grow larger. The surface to volume ratio decreases, leaving fewer catalytic atoms or molecules on the surface of the crystal available to the reactant. In other words, many active sites are buried within the crystal.

Two models have been proposed for the mechanism of the sintering process. The first mechanism was developed by Ruckenstein and Pulvermacher [74-78], who propose a migration of metallic particles. The crystallites move on the surface of the carrier until they meet a second particle, leading to a fusion of both particles into a bigger crystallite. But this mechanism cannot explain the redispersion effect observed with some metals.

The second model published by Wanke and Flynn [79-82] is based on the migration of molecular species. Atomic and molecular species can be formed from the smallest crystallite. They are then able to diffuse on the surface of the support until they are trapped by bigger crystallites. Thus the bigger crystallites will grow at the expense of the smaller particles.

For big crystallites, the rate of the loss of metal atoms to form molecular species will be lower than the rate of species binding, the reverse being true for small crystallites. When the rate is the same, the sintering process is completed. Therefore, in the case of the Wanke and Flynn mechanism, the sintering process will result in an equilibrium of the movement of molecular species with a net transfer (although not complete) of species

from small particle to large particle. In this case we can expect a bimodal size distribution after sintering, the small particles becoming smaller and the big particles becoming bigger. For the mechanism of Ruckenstein, the small particles will segregate leading to the formation of bigger crystallites with monomodal size distribution. In his case, the smallest crystallites will form only at the beginning of the process before moving on the carrier surface. Thus, the distribution will contain a large size range including the rest of the smallest crystallites. From published studies, the sintering process should correspond mainly to the mechanism of Wanke and Flynn.

5.3.3 Effect of pH on the Palladium Dispersion on Al_2O_3

Figure 5.10 shows the effect of pH on palladium dispersion and active sites. In acidic condition (pH < 7), the dispersion of palladium gently increases as pH increases. As pH exceeds 7, the resulting impregnation slurry is under basic conditions, and further increases of pH results in a tremendous increase in the palladium dispersion. The dispersion reaches a maximum of 48% when the slurry pH reaches 10 to 11, which indicates that excess NH_4OH is present. This dispersion is much higher than Engelhard 4%Pd/Basios, and a little lower than 1.5% Pt/Al_2O_3 catalysts, which have 42.6%, 51% dispersion respectively. The active sites on the surface show a similar change due to the pH increasing, also shown in Figure 5.10. Figure 5.11 shows a corresponding palladium crystallite size decrease with pH increasing from 3 to 10.

Initially, well dispersed Pd can migrate and agglomerate to form bigger crystallites during washing, drying, and high temperature calcination. It is often desirable to fix the catalytic species so those subsequent processing steps will not cause significant movement or agglomeration of well-dispersed catalytic species. When the pH of the

impregnation slurry was adjusted, the catalytic species were actually precipitated to the surface inside the pores of the carrier. When pH is less than 7, there is not enough OH^- to precipitate all the catalytic species. Most of those species still have good mobility and therefore the dispersion only increases slightly as the pH increases. When there is excess OH^- present, indicated by pH value 10-11, the Pd will be precipitated quickly on the surface inside the pores of Al_2O_3 as soon as the OH^- reaches the surface the Pd "sits on". The faster the pH was adjusted, the faster the Pd was precipitated, and the smaller the size of the crystal formed. This will disable most catalytic species mobility, resulting in a high Pd dispersion. In other words, lower pH leads to more aggregation of Pd and a more prominent steric hindering effect than does higher pH. XRD pattern changes shown in Figure 5.12 also support this conclusion.

One may realize that precipitation of catalytic species is done by presoaking carriers with NH_4OH in industrial practice. By presoaking carriers with NH_4OH, the addition of an acidic Pd salt, such as $Pd(NO_3)_2$, will precipitate hydrated PdO on the surface of the pores within the carrier. But one should bear in mind that the pores within the carrier may fill with NH_4OH solution, the $Pd(OH)_2$ may form and be crystallized before it reach the surface of those pores, Thus those small crystallites may aggregate to bigger crystallites, blocking the entry of the pores. As mentioned before, the $Pd(NO_3)_2$ solution has pH value of 1, presoaked alumina with NH_4OH is not strong (basic) enough to precipitate all the Pd. In contrast, by impregnating Al_2O_3 with $Pd(NO_3)_2$ solution first, Pd will get a chance to become well distributed on the surface of the pores, the addition of NH_4OH will precipitate the Pd on the site where they were dispersed, and the resulting slurry pHs were adjusted to the value desired.

CHAPTER 6

THE LEAN CATALYTIC REDUCTION OF NITRIC OXIDE WITH CARBONACEOUS MATERIAL OVER PALLADIUM CATALYSTS

6.1 Introduction

In recent years, emissions regulations have challenged diesel engine designers to develop new technologies for controlling the emissions of nitrogen oxides (NO_x) and soot particulates from diesel engines. Emissions regulations are becoming more stringent.

On October 6, 2000, EPA published its final rule for the previously adopted diesel heavy-duty engine standards [83]. The standards (less than 2.5 g/bhp.h NOx plus nonmethane hydrocarbons and 0.1 g/bhp.h soot) are to be implemented in the 2004 model year. Emission standards for 2007 and later were adopted by EPA on December 21, 2000 [84]. These regulations call for 90% reduction in particulate matter (PM) and 90% reduction in NO_x for heavy-duty diesel engines compared to the 2004 standards. In addition, a 97% reduction in the allowable levels of sulfur in diesel fuel was adopted, corresponding to 15 ppm S, beginning June 15, 2006 [84]. Advances in engine technology have made it possible for the diesel engine to meet particulates emissions levels. However, the reduction of both NO_x and particulates emissions cannot be accomplished by engine modifications alone. Processes for diesel exhaust treatment will have to be developed. In doing so, catalytic NO_x reduction under lean conditions is a key requirement to meet the stringent EPA regulations. Catalytic reduction of NO_x with hydrocarbons in the presence of excess oxygen has been widely studied [85-88]. However, sufficient unburned hydrocarbons in the exhaust gas are not available for the selective catalytic reduction in the presence of excess oxygen (NO_x-HC-SCR) [89-90].

Since catalytic reduction of NO_x with hydrocarbons over Cu-ZSM-5 was reported by Iwamoto et al. [91], many studies have been conducted on catalytic NO_x reduction in diesel engines involving both catalyst development and system modifications. Many kinds of catalyst have been proposed for NO_x reduction [85-88, 92]; However, these catalysts have disadvantages, e.g., low durability under hydrothermal conditions, low SO_x resistance, or a narrow temperature window at which the high NO_x conversion is achieved.

This chapter presents experimental results of NO_x reduction with granular activated carbon (GAC) as a surrogate for diesel soot over palladium catalysts under lean conditions. The ultimate goal is to use these catalyst particles in a rotating fluidized bed reactor to capture soot and to promote the reduction of NO_x with that soot thereby effecting the simultaneous removal of NO_x and soot. It should be noted that the success of this procedure depends on the availability of sufficient soot or other reductants to stoichiometrically remove the NO_x present in modern diesel engines.

6.2 Experimental

6.2.1 Catalyst Preparation and Characterization

This Research studied two different sizes of catalyst particles. The first, provided by Engelhard Corporation, consisted of PdO supported on either CeO_2, Al_2O_3, or TiO_2, with a particle size of approximately 2 μm. The other, PdO supported on 80 μm γ-Al_2O_3 particles, was prepared in the NJIT catalyst laboratory. Preparation methods and characterization of catalyst used in this study are summarized in Table 6.1 and Table 6.2. The catalyst is prepared from palladium nitrate using the capillary impregnation method.

First, the γ-Al_2O_3 was aged at 500°C for 12 hours. The catalyst was then prepared by immersing alumina powder in the precursor nitrate solutions, followed by drying and calcination in air at 500°C for 4 hours.

6.2.2 Activity Test on a Laboratory Scale

Relative catalyst activity was measured for the reduction of NO with granular activated carbon (GAC) to produce N_2. These measurements were conducted in a downflow reactor system with synthetic exhaust gas. The synthetic exhaust gas for the NO reduction was composed of 590 ppm NO, 10% O_2, with He as the balance. The reactor bed was composed of physically mixed catalyst and GAC at a volume ratio of 1:1. Activity tests were carried out at a gaseous hourly space velocity (GHSV) of 50,000 and 80,000 over the temperature range of 200-600°C, with GC analyses for N_2 conducted each 50°C. Other components in the product mixture were monitored using a Nicolet FTIR.

Each experiment is started by loading a weighed fresh sample from the same batch that was prepared by mixing catalyst and GAC in the desired proportions. A fresh sample is used for each constant temperature experiment. The fresh catalyst/GAC mixture inside the reactor is purged with He for 30 min to drive out any residual air and surface moisture. The desired gaseous reactant mixture, without O_2, is then introduced and the desired steady state temperature is achieved after 5-10 min. Then the 10% oxygen component is introduced into the gas mixture. The minimum inlet gas temperature required to cause the rapid oxidation of GAC depends on the catalyst and GHSV. At GSHV of 50,000, this temperature is 450°C for 4% PdO/CeO_2, 500°C for 4% PdO/Al_2O_3, and 550°C for 4% PdO/TiO_2. The rapid oxidation of GAC results in a temperature increase of approximately 650-750°C. After the GAC is consumed, the temperature

reverts back to the inlet gas temperature in about 3 min. Thus, the total time of the temperature excursion is 9-10 min, consisting of 4-5 min during which the GAC is oxidized, followed by a 5 min cooling down period to the pre-set inlet gas temperature.

The concentration of N_2 was measured at the inlet as well as the outlet of the reactor by the TCD detector of an HP model 5890 dual detector GC using a 9.1 m HayeSep DB column. The CO and CO_2 concentrations were measured by the GC FID detector after passing the samples over a nickel methanation catalyst to convert them to methane after separation with a 1.8 m Porapak Q column. The results are presented as plots of conversion of NO to N_2 as a function of inlet gas temperature. As soon as the observed temperature passes through a maximum, the representative gas flows to the sampling loop through the column to the TCD. The effluent gas from the catalyst bed travels through the lower section of the reactor below the fritted disc (36.5 cm length, 2.5 cm diameter) and then through polypropylene tubing (4.5 m length, 3.2 mm diameter) to the sampling loop (2 cm^3). At a GHSV of 50,000, the time delay for injection into the GC is approximately 8.9 s in the sampling loop for a total of 10.7 s. The average N_2 conversion from the reduction of NO thus obtained is very reproducible.

GHSV is calculated by dividing the total gas flow rate (cm^3/h) at the temperature and pressure of the experiment by the total solid sample volume (cm^3). NO conversion to N_2 is calculated by $2[N_2]_{out}/[NO]_{in}$. The inlet and outlet streams were also monitored by FTIR at low temperatures in order to obtain nitrogen balances. The inlet concentration of nitrogen from NO was balanced with nitrogen present as NO, NO_2 and N_2O by FTIR and N_2 by GC. The concentration of N_2O was less than 10 ppm and 20 ppm under conditions of rapid GAC oxidation.

6.2.3 Short-Term Catalyst Poisoning Test with a Simulated Exhaust Gas at Laboratory Scale

Short-term catalyst poisoning tests were conducted by using PdO/Al_2O_3 catalyst to reduce NO in order to check the effect of water and sulfur on catalyst performance. The catalysts were exposed to a simulated exhaust gas consisting of 590 ppm NO, 10% O_2, 20 ppm SO_2, 10% water, with helium as balance at 550°C for up to 30 hours. The partial pressure of the water was determined from the fraction by percentage of water vapor needed in the reaction system, The water temperature corresponding to this partial pressure for a saturated water/gas system is then determined from a standard table (45°C for 10% water). The desired concentration of water vapor in the simulated exhaust gas is then obtained by bubbling the feed through water maintained at this temperature. The catalysts were examined by the same procedure used in the activity tests described above.

6.2.4 Isothermal Reaction

Isothermal reactions were conducted with the PdO/Al_2O_3 catalyst at GHSV of 50,000. A Nicolet 520 FTIR equipped with a 2 m gas cell was used to measure the concentration of the following gases as functions of time: NO, NO_2, N_2O, CO, CO_2. The instrument was calibrated with certified gaseous mixtures in which He was the balance gas. At least three different mixtures in the range of interest were used to obtain the overall calibration. The FTIR was used in a scanning mode of 10 scans per sample. Both inlet and effluent streams from the catalytic reactor were analyzed. The reduction of NO to N_2 can be obtained from the difference in NO_x concentrations in the inlet gas and the effluent gas. In addition, the GC instrument previously described was used to analyze the stream

leaving the FTIR for N_2 to verify the FTIR results. The results of the two instruments were consistent with each other to within acceptable experimental error.

Each experiment is started by loading a weighed sample that was prepared by mixing the catalyst and GAC in the desired proportions. The fresh catalyst/GAC mixture inside the reactor and the FTIR cell are purged with He for 2 hrs to drive out any residual air and moisture. Once the FTIR spectrum exhibits a good baseline, the oven temperature is raised to 490°C. The temperature inside the catalyst bed increases to 520°C, reaching steady state in approximately 10 min. The FTIR series online measurements are then initiated. After He flows through the system for 10 minutes, 500 ppm NO is introduced into the gas stream. After He and NO flow for 15 minutes, 10% O_2 is introduced into the system. The rapid oxidation of GAC results in a temperature increase on the order of 700°C when catalyst/GAC volume ratio is 1:1. After the GAC is consumed, the temperature reverts to the inlet gas temperature in about 3.5 minutes. Thus, the total time of the temperature excursion is 5-6 minutes, consisting of 1.5-2 minutes during which GAC is oxidized, followed by a 3-4 minutes cooling down period. In this experiment, the temperatures corresponding to each FTIR reading were recorded.

In order to obtain relatively stable bed temperatures, the experiments were carried out with catalyst/GAC volume ratios varying from 1:1 to 5:1. The mass of catalyst and GAC volume ratios, and peak temperature for each experiment are given in Table 6.4. The results of the experiments are presented as plots of concentrations in the effluent stream and the temperature in the catalyst bed as functions of time.

6.2.5 NO_x Reduction Test with an Actual Engine Bench

Figures 6.1 and 6.2 show schematic diagrams of the catalytic reaction system and the rotating fluidized bed reactor (RFBR) for the NO_x reduction experiments in an actual engine bench, respectively. The specifications of the diesel engine and operational conditions of the engine are given in Table 6.5.

The exhaust gas from the diesel engine (1981 Volkswagen Rabbit) is fed to the RFBR through calibrated orifice meters. A variable-speed motor provides rotating speeds between 0 to 5000 rpm. The perforated cylinder distributor, described in Chapter 2, was used in all experiments. The soot particle size and particle number distributions in the inlet and outlet of the RFBR were measured with an API Aerosizer system (Amherst Process Instruments, Inc.).

The inlet and outlet concentration of NO, NO_2, N_2O, CO, CO_2, and organic compounds were analyzed online with the FTIR gas analyzer (Nicolet, MAGNA-IR 560 E.S.P.). Dry air was used to remove moisture from the FTIR before each experiment. Three experiments were carried out with the filter granules (bed particles) consisting of 500 g, 60-80 μm Al_2O_3 (low fines), CuO/Al_2O_3, and PdO/Al_2O_3 catalyst for blank, control, and catalytic reduction, respectively. The RFBR was set to rotate at 1200-rpm before the engine was started in order to prevent the exhaust flow from blowing out the filter granules. During the experiments, the engine was operated at 1450 – 1700 rpm, 48 – 51 ft-lb. Load. The inlet and outlet gas could attain temperatures of 635°C and 350°C, respectively. The rotating speed of the RFBR was then adjusted to 900 – 1200 rpm to keep the bed in the fluidized region. When the gas temperature reached steady state (inlet 550 to 625°C, outlet approximately 350°C), the FTIR gas analysis cycle was initiated.

Each cycle consisted of 25 minutes during which the inlet gas was analyzed and 35-40 minutes during which the outlet gas was analyzed. Two cycles of gas analysis and particle measurements were carried out for each experiment. The results were consistent within experimental error.

6.3 Results and Discussion

6.3.1 Laboratory Screening Tests of Catalysts for NO Reduction

The catalytic activities of various palladium-based catalysts were measured at inlet gas temperatures from 200 to 600°C. The results, shown in Figure 6.3 indicate that all catalysts have high activity. However, the $PdO/\gamma\text{-}Al_2O_3$ showed the highest activity among the tested catalysts. The activity of this catalyst is excellent. It has a light-off temperature of 450°C. Over 80% maximum conversion of NO to N_2 is obtained once the inlet gas temperature exceeds 500 °C.

The PdO/CeO_2 catalyst has a slightly lower light-off temperature of 400°C, giving over 70% maximum conversion of NO to N_2, which is obtained when the inlet gas temperature is exceeds 450°C. Among three catalysts, PdO/TiO_2 has the highest light-off temperature of 500°C, with maximum conversion attained only after the temperature exceeds 550°C.

From the BET surface areas shown in Table 6.1, the PdO/Al_2O_3 catalyst has the highest surface area of 132.6 ± 2.1 m^2/g. Its highest area may contribute to its highest activity. The surface area of PdO/TiO_2, which has lower activity, is 42.6 m^2/g. The performance of PdO/CeO_2 catalyst is of interest. It has a specific surface area similar to PdO/Al_2O_3, but its maximum conversion is similar to PdO/TiO_2. However, PdO/CeO_2

has a much lower light-off temperature than PdO/TiO_2, and is also lower than that of PdO/Al_2O_3. This finding may be a consequence of the fact that CeO_2 is one of the oxygen storage components in 3-way automotive oxidation catalyst [93].

In order to confirm whether CeO_2 has activity in NO reduction, the NO reduction was measured at inlet gas temperatures from 200 to 600°C by using only CeO_2 as a catalyst, as shown in Figure 6.4. The activity of CeO_2 as a NO_x reduction catalyst is very low; the maximum conversion reached only 15%. This is almost the same conversion as that obtained with GAC in the absence of a catalyst [94]. However, the change in conversion to N_2 as a function of the temperature curve exhibits behavior similar to that of the PdO/CeO_2 catalyst, albeit at much lower conversion. Both curves have the same light-off temperature and temperature at which maximum conversion is reached. Therefore, even though CeO_2 does not have activity for NO reduction to N_2, it does promote a reduction in the reaction temperature. This phenomenon is very important in helping elucidate the catalytic mechanism of the reaction. Since CeO_2 is an oxidation catalyst, it can promote the oxidation of GAC, and thus bring NO reduction temperature down. Therefore, it appears that NO reduction with GAC begins with GAC oxidation to produce intermediate(s) needed for the NO reduction to N_2 on the surface of the catalyst.

The three catalysts exhibited low activity before reaching light-off temperature with the conversion rate increasing only slightly with increasing temperature. It appears that the reaction rate is governed by a catalytic kinetics reaction in this region. After the light-off temperature is achieved, the conversion rate changes rapidly from less than 10% to 70-90%. As the temperature is increased further, conversion levels off, indicating that the reaction becomes mass transfer controlled [95].

The conversion of NO to N_2 was also studied by varying the amount of O_2 fed into the reaction system. These results are presented in Figure 6.5. The NO reduction to N_2 is enhanced significantly with increasing concentration of oxygen up to approximately 5% and then with further oxygen increase it remains constant. It appears that increasing oxygen concentration promotes the heterogeneous and catalytic oxidation of GAC until the surface saturates, after which further increase in oxygen concentration produces no beneficial effects. This experimental observation is also consistent with the assumption that GAC oxidation produces the intermediates needed to reduce NO to N_2. Therefore, any process that affects GAC oxidation would affect NO reduction in this reaction system.

A new palladium catalyst was prepared, supported on 80 μm particles of γ-Al_2O_3.The BET surface area of this catalyst is higher than that of the Engelhard catalysts (see Table 6.1). The activity test of this catalyst is shown in Figure 6.6. As can be observed, both the Engelhard PdO/γ-Al_2O_3 catalyst and the PdO/γ-Al_2O_3 catalyst prepared in our lab behave similarly when treated at the standard conditions mentioned above. Apparently, the γ-Al_2O_3 surface area contribution to the reaction rate was not of primary importance.

6.3.2 Effect of Space Velocity

The catalytic activities of the palladium catalysts were also measured at two different space velocities (50,000 and 80,000 GHSV) in the inlet gas temperature range of 200 to 600°C. All three palladium catalysts showed good performance at both space velocities. However, PdO/Al_2O_3 still showed the highest activity among the tested catalysts.

The test results for PdO/CeO_2 are shown in Figure 6.7. The two curves show the expected behavior, i.e., higher GHSV reduces activity. The catalysts have the same light-off temperature at both space velocities. In the case of GHSV 50,000, the reaction reached a maximum conversion of 80% at a temperature of 450°C and remained constant to 600°C. When GHSV was increased to 80,000, conversion reached only 65% at the temperature of 450°C, approximately 10% less than that at the GHSV of 50,000. However, with increasing temperature, the conversion of NO to N_2 at GHSV of 80,000 increased slowly, eventually reaching the same maximum conversion as the GHSV of 50,000 catalyst sample at the temperature 600°C.

The effect of space velocity on PdO/Al_2O_3 was also studied; the results are shown in Figure 6.8. The light-off temperature does not change as GHSV changes from 50,000 to 80,000. In this case, also, conversion to N_2 decreases at GHSV 80,000 compared to GHSV 50,000. A final conversion of 90% is achieved at 600°C for both space velocities. Tests with PdO/TiO_2 gave similar results for GHSV as a function of temperature. Conversion decreased with the increasing space velocity, but reached the same conversion at 600°C. The results are shown in Figure 6.9.

6.3.3 Effect of SO_2 and H_2O on the Activities of Palladium Catalysts

The palladium catalysts were also examined with a simulated gas mixture that contained 20 ppm SO_2, 10% H_2O vapor, 590 ppm NO and 10% O_2 with the balance being helium. The same experiments were carried out with all three catalysts after exposure to SO_2 and H_2O for 15 hours. The BET surface area was also measured after the experiment. The tested activities and BET surface area are shown in Figure 6.10-12 and Table 6. 3.

The experimental results show that this exposure to SO_2 and H_2O has the following effects on palladium catalysts: (1) The shape of the conversion (activity) curve after exposure does not change appreciably from that of the fresh catalyst, but it is shifted by approximately + 50°C (i.e., to achieve the same conversion the temperature must be increased by that amount), (2) The NO conversion to N_2 is decreased on average 5 to 10%, (3) There is no change in the BET surface area of catalysts.

Since the PdO/Al_2O_3 catalyst has the highest activity, it was chosen to conduct a short-term poisoning experiment for about 30 hours. The results are plotted against time in Figure 6.13. Comparing the 15 hrs poisoning curve with the fresh catalyst curve, the shape of the curve again does not change, but the light-off temperature is shifted to the higher temperature 500°C, approximately 50°C higher than the fresh catalyst. In the mass transfer limited regime, the conversion rate levels out at 70%, beginning at a temperature of 550°C. This behavior is consistent with the catalyst losing active sites [95].

After 30 hours of poisoning by SO_2 and water, the shape of the curve changed further. Curve C in Figure 6.13 has a much smaller slope than those of curves A and B with the light-off temperature remaining at 500°C. After light-off, the slope remains smaller than those of curves A and B, indicating that the reaction rate is decreasing, passing from chemical kinetic control to pore diffusion control [95]. At a temperature of 600°C, the mass transfer limited region does not appear to have been reached.

6.3.4 Isothermal Reaction

Due to the highly exothermic reaction between GAC and O_2, it is extremely difficult to control the bed temperature. However, an experimental approach to maintaining a relatively constant bed temperature was carried out; namely, the GAC content in the

mixture of catalyst/GAC in the reaction bed was decreased. In the case of PdO/Al_2O_3 with volume ratio 1:1 of catalyst/GAC (Figure 6.14), a peak temperature of 770°C is achieved after 200 s of O_2 in the system with the O_2 introduced after approximately 1600s. A maximum of 79% NO is converted to N_2 after 25 s past the peak temperature. At approximately the same time CO (150 ppm) and CO_2 (7%) peaked. No significant NO_2 and N_2O were detected at this time. NO_2 appeared only after CO disappeared from the effluent gas stream (300 s after O_2 is added into the system). GAC is almost totally depleted at 400 s from the time O_2 was added. This disappearance is signaled by the CO_2 concentration approaching zero, at the same time that the total NO_x returned to the initial level.

Figure 6.15-16 shows the results when the catalyst/GAC volume ratio is changed to 5:1. The bed peak temperature changes from 770°C to a 540°C temperature plateau that remains 600s (300s after O_2 was added into the system). The conversion of NO to N_2 also reaches a maximum of 15% after 400 s from the time O_2 was added into system. Significant quantities of CO were not detected. CO_2 reached a maximum level of only 4000 ppm with a very slow depletion rate, indicating that GAC is depleted at a very slow rate. Figure 6.17 shows the results at the same catalyst/GAC ratio (5:1), but with the initial temperature increased to 610°C with all other conditions kept unchanged. They are similar to those of the catalyst/GAC volume ratio 1:1 experiment. Measurements showed that 75% of the NO is converted to N_2, the peak bed temperature is 730°C, peak CO_2 level decreased to 4% and no significant CO was detected due to the much smaller amount of GAC present. A run was made in which γ-Al_2O_3 was used instead of PdO/Al_2O_3 at an initial temperature of 608°C. Figure 6.18 shows that no NO conversion

to N_2 is detected, bed temperature remained constant, CO_2 only reached a 3000 ppm maximum level. Thus a very slow GAC depletion rate is indicated.

This set of experiments shows that the conversion of NO to N_2 is strongly dependent on the bed temperature. Higher GAC content or higher initial temperature result in faster GAC thermal reactions, which in turn raise the bed to a higher temperature. Consequently, higher conversion of NO to N_2 is obtained. Thus a high rate of NO conversion is obtained from a high rate of GAC thermal reaction. From a kinetic viewpoint, one would expect the rate of NO conversion to increase when the available reductant content increases. The results of these experiments support the conclusion that the rate of NO reduction in the case of the NO + GAC reaction depends on the amount of reductant, and on the bed temperature. Since solid GAC can not reach the PdO/Al_2O_3 catalyst pore structure, the active reductant must be one of the intermediates of the GAC + O_2 reaction which is capable of migrating between the catalyst and GAC boundary. Clearly, CO_2, the final product of this reaction, cannot be the reductant.

6.3.5 NO_x Reduction Test Using the Exhaust from Diesel Engine

The γ-Al_2O_3, CuO/Al_2O_3, and PdO/Al_2O_3 catalysts were examined with actual diesel engine exhaust gas by using a rotating fluidized bed reactor (RFBR). An RFBR provides good contact between filter granule (catalyst particles) and soot particles, therefore providing good mass transfer [96]. The tests were carried out with the focus on NO_x reduction, soot elimination, and the reaction profile.

Table 6.6 shows the FTIR results of three engine bench experiments. With plain γ-Al_2O_3 as filter granules the average concentration of NO, NO_2, N_2O, CO, and CO_2 in the inlet and outlet exhaust gases were the same (120 ppm, 19 ppm, 2 ppm, 220 ppm, 5%,

respectively, in the first test cycle; 150 ppm, 20 ppm, 2 ppm, 300 ppm, 6% in the second test cycle). No NO_x reduction activity was observed in this experiment. When CuO/Al_2O_3 particles were used as filter granules, the average inlet concentrations of NO, NO_2, N_2O, CO, and CO_2 were 150 ppm, 19 ppm, 2 ppm, 280 ppm, 5.5%, respectively, in the first test cycle; 160 ppm, 19 ppm, 2 ppm, 300 ppm, 5.5% in the second test cycle. The average outlet concentrations of NO, NO_2, N_2O, CO, and CO_2 were 136 ppm, 19 ppm, 2 ppm, 225 ppm, 4.9%, respectively, in the first test cycle; 145 ppm, 19 ppm, 2 ppm, 225 ppm, 5% in the second test cycle. Only approximately 10% NO and 19-25% CO were removed from the exhaust in the above two testing cycles. With PdO/Al_2O_3 as filter granules, The average concentrations of NO, NO_2, N_2O, CO, and CO_2 in the inlet were 120 ppm, 19 ppm, 2 ppm, 320 ppm, 4.2%, respectively, for the first test cycle; 140 ppm, 19 ppm, 2 ppm, 250 ppm, 4.5% for the second test cycle. The average outlet concentrations were 90 ppm, 19 ppm, 2 ppm, 50 ppm, 4.2%, respectively, for the first test cycle; 112 ppm, 19 ppm, 2 ppm, 35 ppm, 4.3% for the second test cycle. NO reduction of 20-25% and 90% CO oxidation were achieved using this catalyst.

The API aerosizer measurements reveal an interesting result, shown in table 6.7. For each experiment, the test results from the two cycles were highly reproducible. In each experiment, the preponderance of particles in the inlet gas are in the 0.1 - 1 μm size range. In the outlet gas, besides particles in the 0.1 – 1 μm range, a small fraction of 1 – 10 μm particles is present [97]. Comparison of the inlet and outlet particle size distributions shows that the number of particles in the 0.1 –1 μm range in the outlet is significantly less than that in inlet gas. The number of residual soot particles in this range is much smaller than the observed number when plain Al_2O_3 and CuO/Al_2O_3 were used

as filter granules. The greatest reduction of soot in the 0.1 – 1 μm range thus occurs with the use of the PdO/Al_2O_3 catalyst, with which over 20% NO_x reduction was observed. The larger particles (1-10 μm) observed in the outlet gas are most likely due to attrition of the filter granules. The resulting fines are blown out of the RFBR as discussed by Qian et, al. [98].

The bench experiments show that the RFBR exhibited high capability to capture soot particles. The highest filtration efficiency of RFBR achieved was over 95% in certain fluidized conditions [99]. With an active catalyst, the captured soot particles can act as a reducing agent, resulting in over 20% NO reduction in our experiment with PdO/Al_2O_3 present. In the same experiment 90% of the CO in the exhaust gas was oxidized to CO_2. Plain Al_2O_3 (no PdO) did not show any reaction activity, i.e., no NO, CO, or HC was removed from the exhaust gas, even though high filtration efficiency was observed. In the experiment using CuO/Al_2O_3 as filter granules, much lower reaction activity was observed (compared to PdO/Al_2O_3). Even though the NO reduction efficiency in this actual engine experiment is much lower than in the laboratory screening test with the same palladium catalyst, these experiments do demonstrate the validity of the RFBR concept for this application. Many factors affect the NO reduction in this particular bench experiment, such as heat loss, the control of the bed fluidization condition, and reactor design. With further research, better understanding of RFBR principles and optimization of RFBR design can be expected to result in improved NO reduction in future implementations.

6.3.6 Calculation of Activation Energy

In heterogeneous catalytic reactions, the overall reaction process can be separated into a sequence of individual steps that are shown below (Heck and Farrauto, 1995):

1. Mass transfer of the reactants from the bulk fluid to the external surface of the catalyst.
2. Diffusion of the reactant from the pore mouth through the catalyst pores to the immediate vicinity of the internal catalyst surface.
3. Adsorption of reactant onto the catalyst surface.
4. Reaction on the surface of catalyst.
5. Desorption of the products from the surface.
6. Diffusion of the products from the interior of the catalyst to the pore mouth at the external surface.
7. Mass transfer of the products from the external catalyst surface to the bulk fluid.

The overall reaction rate is determined by the slowest step in the mechanism. In the chemical kinetic region, where the diffusion steps 1, 2, 6, and 7 are fast compared to the reaction step, the reaction rate is proportional to exp (-Ea/RT), where Ea is the activation energy. Thus, the rate of conversion increases with temperature. In the pore diffusion region, steps 1, 3, 4, 5, and 7 are fast compared to diffusion steps 2 and 6. In this region, the rate of conversion also increases with temperature but is less sensitive to temperature than in the chemical kinetic control region. In the bulk mass transfer region, steps 2, 3, 4, 5, and 6 are faster than the mass transfer steps 1 and 7. The rate equation in the mass transfer control region is almost independent of temperature (Fogler, 1986). The corresponding activation energies are of the following orders: Chemical kinetics, Ea > 10 kcal/mole, Pore diffusion, Ea = 6-10 kcal/mole, Bulk mass transfer, Ea = 2-4 kcal/mole.

The ability of a catalyst to increase a reaction rate can be measured by obtaining the Arrhenuis parameters. The activation energy of the reaction is the key figure of merit for comparing reaction rates. The catalyzed reaction usually involves three rate processes: (1) adsorption, (2) the formation and breakup of an activated complex, and (3) desorption of products. Each of these has its own activation energy. The rate of reaction is also determined by the number of active sites and by the concentration on the catalyst surface of various adsorbed species. The calculation of the apparent activation energy of a reaction may provide insight into possible mechanisms and assist in identifying the rate-controlling step.

The formation rate of each product can be written by the conventional Arrhenius-type power-law expression as follows:

$$r = k\, C_C^{\,n1}\, C_{NO}^{\,n2}\, C_{O2}^{\,n3} \qquad (6.1)$$

Where the rate constant, k, in Arrhenius form is given by

$$k = A \exp(-Ea/RT) \qquad (6.2)$$

Or in logarithmic form

$$\ln r = - Ea / RT + \ln A + n_1 \ln Cc + n_2 \ln C_{NO} + n_3 \ln C_{O2} \qquad (6.3)$$

Where:

A is the pre-exponential factor, cm^3/g cat.-s,

Ea is the apparent activation energy, kcal/mol,

R is the gas constant, kcal/mol-K

Ci is the concentration, mol/cm^3

n_i is the reaction order of each species that participates in the rate limiting step

k is rate constant, mol/g cat.-s,

Although the reaction orders have not been reported, it is generally assumed that the reaction order in soot concentration should be zero in the temperature range of this study. The linear relation between ln r and T^{-1} suggests that Equation (6.3) can be simplified to Equation (6.4) and that $\ln A\sum C_i$ and Ea can be obtained from the intercept and the slope for each reactant.

$$\ln r = - Ea / RT + \ln(A\prod C_i^{ni}) \quad (i = C, NO, O_2) \tag{6.4}$$

Figure 6.19 shows a plot of conversion versus W/V (where W is the mass of catalyst and V is the gas flow rate) for the NOx reduction with GAC over PdO/Al_2O_3 catalyst in the temperature range of 350°C to 450°C (typical conversions were below 30% thus minimizing product reactant reactions). The flow rate was varied to give a suitable range of space times. By using linear regression, one can obtain values for the rate constant k. Ea and A are then obtained as the slope and intercept from a plot of the logarithm of the rate constants versus 1/T for the reaction (Figure 6.20).

$$\ln k_1/k_2 = - Ea/R\ (1/T_1 - 1/T_2) \tag{6.5}$$

Figure 6.19 shows that at the lower temperatures of 350°, 400°C and 450°C, it is reasonable to use linear regression to calculate rate constants at each temperature. But for 500°C, as mentioned above, the reaction occurs very rapidly with the carbon being consumed within a minute. Thus, the conversion considerably exceeds 30%. When W/V is less than 0.015 g-sec/cm^3, a relatively good linear regression was obtained with experimentally tested points. It was assumed that a conversion of 70% operates for the first point, representative of the kinetic regime, and in reasonable agreement with the points at lower temperatures. Eventually, the conversion of NO_x to N_2 levels off with

increasing W/V, indicating that the reaction has become mass transfer limited [2]. The Ea calculated from Equation (6.5) in the temperature range of 350° to 500°C is 24.1 kcal/mol (99.2 kJ/mol). This value suggests that in the temperature range of 350 to 500°C the reaction is kinetically controlled (Figure 6.20).

6.3.7 Reaction Mechanism

Suzuki et al. [8] found that the reactivity of NO_2 with carbon is high and the main product is not N_2 but NO. Consequently, NO to NO_2 oxidation is not beneficial for the NO removal reaction in the presence of O_2. On the other hand, they found much evidence to support the hypothesis that O_2 enhances the C + NO reaction through formation of surface oxygen complexes.

It is assumed that the adsorbed species on the catalyst surface are formed at the boundary or spill over from the remote sites to the boundary and that carbon in close vicinity takes part in the reaction. Gaseous oxygen is adsorbed dissociatively on the catalyst surface, resulting in adsorbed atomic oxygen that reacts rapidly with the reactive free carbon site to give an oxygen-containing active intermediate, C*[O]. Suzuki et al. [8] examined the carbon surface after the reaction with a gaseous mixture of NO and oxygen by X-ray photoelectron spectroscopy and confirmed the presence of the following nitrogen groups complexed with carbon: pyridinic, pyrrolic, -NO, $-NO_2$. The former two and latter two groups might correspond, respectively, to C*[N] and C*[N, O] intermediates involved in the reaction. The N_2O peak may suggest that the presence of [NO*] and C*[O] species adsorbed on the porous solid material, which then reacted according to following equation:

$$C^*[O] + 2[NO^*] \rightarrow N_2O + CO_2$$

It also implies that the formation of nitrogen and N_2O are competitive reactions with the common intermediate of NO_{ad}. The competing reactions are:

$C^*[O] + [NO^*] \rightarrow [N^*] + CO_2$

$[N^*] + [N^*] \rightarrow N_2$

$[N^*] + [NO^*] \rightarrow N_2O.$

They also reported that the coexistence of NO and oxygen can enhance the oxidation of soot with the intermediate C*[O]. This intermediate can react with either O_{ad} or NO_{ad} to produce CO_2 and nitrogen and plays an important role in the reduction.

Kagawa et al. [100] investigated the catalytic combustion of soot deposits from diesel-powered engines and proposed the following mechanism for soot-O_2 reaction to account for the observed half-order kinetics with respect to the oxygen partial pressure.

$O_2\ (g) \rightarrow 2O_{ad}$

$C_f + O_{ad} \rightarrow C^*[O]$

$C^*[O] + O_{ad} \rightarrow CO_2\ (g)\ (+ C_f)$

Detail regarding the nature of the C*[O] intermediate is unclear, but the presence of such an oxygen-containing reactive surface complex was confirmed on the char surface after reaction with gaseous oxygen.

The heterogeneous reactions of NO and N_2O at the char surface are generally recognized to be the most important reactions in reducing both NO and N_2O [101] (Pels. 1995). The products of NO-carbon reaction are generally found to be N_2, CO and CO_2. The overall reaction can be expressed as follows:

$C + 2NO \rightarrow CO_2 + N_2$ (1)

$C + NO \rightarrow CO + 1/2N_2$ (2)

$CO + NO \rightarrow CO_2 + \frac{1}{2} N_2$ (3)

Reaction (3) is a catalytic reaction, based upon the observation that NO reduction by carbon is enhanced in the presence of CO. The relative importance of the carbon consuming reactions (1) and (2), and the catalytic reaction (3) in the presence of CO was studied by Furusawa et al. (1985) [102] by measuring the material balance over the temperature range prevailing in a fluidized-bed combustor (FBC). Their results showed that, at low temperature (994 and 1078 K), the molar amount of CO_2 was less than that represented by the stoichiometry of reaction (3), indicating that the carbon consuming reactions become significant. The contribution of the carbon consuming reactions to the total reduction of NO is enhanced with increasing temperature and with a decrease in the ratio of CO/NO. The catalytic reduction of NO was found to be dominant even at higher temperatures, if the partial pressure of CO was sufficiently higher than that of NO. The above-discussed overall reactions can be considered to be phenomenological observations, showing the complexity of the reaction system.

The mechanisms of NO-carbon reactions are quite complex, involving several reaction steps and elementary processes. Several mechanisms have been proposed (Smith et al., 1959; Chan et al., 1983; De Soete, 1990) and modified (Suuberg et al., 1990; Teng et al., 1992; Yamashite et al., 1993) [103-108]. The complexity of the mechanism for NO-carbon reaction likely arises from the chemical and physical structure of carbon, and is due to the formation of the products. Formation of N_2 from the NO-carbon reaction requires the combination of dissociated N atoms on the carbon surface, while for the N_2O-carbon reaction, nitrogen atoms are already bonded (Smith et al., 1959) [103]. Carbon atoms in carbonaceous materials can be characterized as reactive and unreactive

sites, with the carbon-oxygen complexes on the surface being important intermediates in NO- and N_2O-carbon reactions. The consensus is that there exist two types of intermediate complexes; unstable and stable carbon-oxygen complexes, each leading to different product release and temperature dependencies. The properties of the surface complexes and their role in the reaction could be closely related to the properties of the active sites in the carbonaceous material. To understand the mechanism in terms of elementary processes and the product release, it is important to clarify the properties of active sites and surface complexes.

From the work of Smith et al. (1959) [103] till the present, two generally accepted conclusions about the mechanism of the NO-carbon reaction have been made based on experimental observations:

- The first step is chemisorption of NO on carbon surface, as was also observed in our experiments.
- Carbon-oxygen complexes are important intermediates in the reaction.

There are two issues of interest that would be helpful in clarifying aspects of the mechanism, namely, the behavior of NO adsorption on the carbon surface and the routes of N_2, CO and CO_2 formation.

At temperatures below 473 K to as low as 198 K, chemisorption of NO on carbon occurs along with the formation of carbon-oxygen complexes. N_2 is the only product in this temperature range:

$$2NO + 2C \rightarrow 2C(O) + N_2 \qquad (4)$$

It has been suggested that the oxygen atom of the NO molecule is held by the surface (Smith et al., (1959) [103], i.e., NO is adsorbed in O-down orientation. The oxygen

complexes were then postulated as the sites for physical adsorption. This leads to a mechanistic model including two reversible reactions:

$$NO + C^* + C(O) \leftrightarrow C(O...ON)C^* \quad (5)$$

$$NO + C^{**} + C(O) \leftrightarrow C(O...ON)C^{**} \quad (6)$$

where C* and C** are used to differentiate the different nature of the carbon sites. These subsequently form different types of C(O...ON)C, followed by two reactions that produce CO and CO_2 as observed experimentally at higher temperatures.

$$NO + C(O...ON)C^* \rightarrow CO_2 + N_2 + C(O) \quad (7)$$

$$NO + C(O...ON)C^{**} \rightarrow CO_2 + N_2 + CO \quad (8)$$

Some interesting points concerning this model were raised by Teng et al. (1992) [107] which are summarized here:

- N_2 is also a significant high temperature product (> 1000°K), implying the existence of long-lived N-containing complexes which are able to desorb as N_2 in the absence of NO. It was proposed, based on the work of Zarifyzanz et al. (1967) [109], that NO adsorption also occurs in an N-down orientation to form N-containing complexes C(N).
- Chu and Schimidt, (1993) [110] observed the formation of a high melting point $(CN)_x$ polymer during the graphite-NO reaction by transmission electron microscopy (TEM), atomic force microscopy (AFM), Auger electron spectroscopy (AES) and electron energy loss spectroscopy (EELS). Suzuki et al. (1994) also identified the surface nitrogen species by X-ray photoelectron spectroscopy (XPS). Both studies confirmed the existence of C(N) species, which are responsible for high temperature

N_2 evolution. Thus, reaction (4), if applied to the higher temperature regime, could be split into two steps:

$2C + NO \rightarrow C(O) + C(N)$ (4a)

$2C(N) \rightarrow N_2 + 2C$ (4b)

- Desorption of C(O) to form CO is an important step for all practical oxidizing carbon gasification processes, and must be present in the mechanistic model:

  $C(O) \rightarrow CO.$ (9)

- The route to CO_2 formation, instead of reactions (10) and (11), was proposed to follow:

  $C + C(O) + NO \rightarrow C(O_2) + C(N)$ (10)

  $C(O_2) \rightarrow CO_2.$ (11)

The significance of this reaction model is the introduction of the idea that there exist rapid turnover sites at which desorption of the surface species is fast. Thus these sites are "empty" under gasification condition. The gasification of carbon by NO involves two parallel processes: (1) somewhat slow desorption of relatively stable surface complexes; (2) processes involving NO attack on active unoccupied sites that result in essentially immediate desorption of gaseous products. These are represented stoichiometrically by the reactions:

$(1 + x)C_f + C(O) + NO \rightarrow CO_2 + C(N) + xC_f$ (12)

$(2 + y)C_f + NO \rightarrow CO + C(N) + yC_f$ (13)

At the present time, no conclusive NO-carbon reaction mechanisms can be found. However, from the reaction steps as discussed above, it is reasonable to summarize the reaction mechanism by the following reaction steps:

$NO + 2C \rightarrow C(O) + C(N)$ (4a)

$2C(N) \rightarrow 2C + N_2$ (4b)

$C(O) \rightarrow CO$ (9)

$C + NO + C(O) \rightarrow C(O_2) + C(N)$ (10)

$C(O_2) \rightarrow CO_2$ (11)

$CO + C(O) \rightarrow CO_2 + C$ (14)

It is obvious that the above reactions are not equally important in the overall reaction scheme and that their contributions to the final product releases depend on the reaction conditions, particularly on the reaction temperature. It is generally agreed that the first step is chemisorption of NO on the carbon surface with dissociation of the N-O bond to produce N- and O-carbon complexes. The formation of N_2 involves either the combination of dissociated N atoms on the surface of the N-N bond formed simultaneously with the dissociation of one or both N-O bonds (Suuberg et al., 1990) [106]. This was found throughout the reaction temperature range. The formation of CO and CO_2 is similar, to the carbon-O_2 reaction, both in terms of the characteristics of carbon-oxygen complexes and temperature dependence. The CO comes mainly from the desorption of the relatively stable carbon-oxygen surface complex and is dominant at high temperatures. CO_2 might be partially formed from unstable carbon-oxygen surface complexes and the interaction between the surface complexes and reactant species, as shown in reactions (10), (11) and (14).

It was found that reaction rate increases, by a factor of about 3 for char in the presence of 3% CO, compared to the case where CO is absent (Johnsson, 1990)[111]. The enhancement of NO reduction in the presence of CO, as suggested by Chan et al.

(1983) [104], may be due to either a direct reaction of CO catalyzed by the char surface as in reaction (3) or a reaction of CO with chemisorbed oxygen deposited by NO on the surface, creating a free active site for further reaction with NO as represented by reactions (14) and (4). As the temperature is increased, the rate of desorption of chemisorbed oxygen to form CO by reaction (9) increases. Thus the concentration of carbon-oxygen complexes decreases and the importance of reaction (14) diminishes. Therefore, the existence of two competing parallel reaction schemes may be represented by reactions (14) and (9). The results of Furusawa and coworkers (1985) [102] showed that the increased contribution of catalytic reaction with increasing CO concentration might be attributed to the rate of reaction (14).

It has been generally agreed that the presence of oxygen enhances the rate of NO chemisorption on carbon, and consequently the rate of the NO-carbon reaction (Chan et al., 1983[104]; Mochida et al., 1985, 1991 [112-113]; Yamashita et al., 1991, 1993[114, 108]; Suzuki et al., 1994[115]). Three possibilities have been proposed to explain the enhancement effect of O_2. Yamashita et al [108, 114] considered the enhancement by the oxidation of NO to NO_2, which easily reacts with carbon to form N_2 and NO. NO can be oxidized again to NO_2. Chu et al. (1993) [110] found that NO_2 produced from NO and O_2 reacts with carbon at a higher rate than O_2. This was further supported by Gray and Don (1990) [116] in their study of N_2O-carbon reaction kinetics. However, the NO oxidation to NO_2 is important only at low temperature (573-773 K) (Rodriguez-Mirasol et al., 1994a, b) [117]. At higher temperatures the enhancement of NO reduction over char in the presence of O_2 is most probably due to the high CO concentration formed during combustion, as discussed in the previous section. Chan et al. (1983) [104] suggested that

in the presence of diffusion limitation for the O_2-char reaction, oxygen will penetrate into the particles as CO. The product of the O_2 reaction therefore enhances the NO reduction. More specific study of the role of oxygen was performed by Yamashita et al. and Suzuki et al. (1994) [8]. They found that the reactivity of NO_2 was greater but that the main product was not N_2 but NO. The transformation of NO to NO_2 was not so beneficial for the NO removal reaction in the presence of O_2. They argued for the hypothesis that O_2 enhances the carbon-NO reaction through formation of a surface oxygen complex, that the presence of O_2 strongly enhances char oxidation and surface intermediates are continuously renewed. During the reaction, the char surface is largely covered with C(O) complexes, due to the reaction of O_2 with free carbon sites:

$$O_2 + 2C_f \rightarrow 2C(O) \qquad (15)$$

Such surface complexes can be divided into active and stable C(O) groups. The stable C(O) complex is unimportant in the reduction of NO, but the active C(O) complexes can easily react with NO, i.e., via reactions (10) and (11). These reactions also create free sites, where NO can be reduced according to reaction (4). Although the newly formed free sites would be attacked mainly by O_2, the probability of a reaction with NO is also increased.

All these possibilities can be supported by experimental observations. The predominant mechanism probably depends on reaction conditions, especially the O_2 concentration and the temperature. However, based on the extensive studies recently reported, it may be concluded that the function of O_2 in the NO-carbon reaction is to produce more reactive intermediates for NO reduction. The carbon-O_2 reaction forms many surface oxygen-containing complexes.

Summarizing the experimental observations, the differences in the mechanism of the GAC + NO + O_2 reaction depends on whether or not a catalyst is present. Furthermore, the initial temperature is very important. In the absence of the catalyst, no significant amount of NO is converted to N_2. When the palladium catalyst is present, it promotes substantial C + O_2 reaction when the initial temperature is above a required threshold, which depends on the GAC content. Therefore, the conversion to N_2 is determined by the content of GAC and the initial temperature. Thus, the reaction mechanism depends on the C + O_2 reaction to produce the reductant species.

The overall apparent mechanism in the presence of a palladium catalyst can be summarized as follows.

$NO \rightarrow NO\text{-}s$ (1)

$O_2 \rightarrow 2O\text{-}s$ (2)

$O\text{-}s + C \rightarrow (CO)$ (3)

$(CO) \rightarrow (CO)\text{-}s$ (4)

$(CO)\text{-}s + NO\text{-}s \rightarrow CO_2\text{-}s + N\text{-}s$ (5)

$2N\text{-}s \rightarrow N_2$ (6)

$CO_2\text{-}s \rightarrow CO_2$ (7)

$O\text{-}s + (CO) \rightarrow CO_2$ (8)

$N\text{-}s + NO\text{-}s \rightarrow N_2O\text{-}s$ (9)

$N_2O\text{-}s \rightarrow N_2O$ (10)

$O\text{-}s + NO\text{-}s \rightarrow NO_2\text{-}s$ (11)

$NO_2\text{-}s \rightarrow NO_2$ (12)

$NO + 2C \rightarrow (CO) + (CN)$ (13)

where -s refers to an adsorbed component on the catalyst and (CO) refers to carbon oxygen complexes.

In the above mechanism, O_2 will be adsorbed on the surface of the catalyst and dissociated (step (2)). Then active oxygen migrates to the carbon surface and reacts with carbon to form (CO) (step (3)). This reaction is much faster than O_2 directly reacting with carbon. Finally, (CO) migrates to the catalyst sites and reacts with NO that is adsorbed on catalyst sites to form N_2 and CO_2 (step (4) to (7)). Steps (8) to (12) show the other side reactions.

CHAPTER 7

CONCLUSIONS

The presence of copper promotes the reduction of NO with GAC in the presence of 10% O_2 whether the copper is ion exchanged onto a zeolite or deposited in elemental form on GAC. Cu reduces the oxidation temperature for GAC to react with O_2 to form CO.

The fraction of NO reduced to N_2 with GAC over Cu-ZSM-5 in the presence of 10% O_2 is relatively small. The conversion to N_2 decreases sharply with increasing space velocity. Conversions to N_2 at 400°C over Cu-ZSM-5 with GAC obtained at GHSVs in the range of 2,000 to 50,000 are very close to the conversions with CO as the reducing agent using the same catalyst at the same reaction conditions. This similarity suggests that CO is a stable intermediate in the reaction.

The conversion of NO to N_2 over Cu-GAC in the presence of 10% O_2 is much greater than that for GAC/Cu-ZSM-5. In the absence of NO, high concentrations of CO are produced by the Cu-catalyzed reaction of GAC+O_2 even at relatively low temperatures. For the same conditions, the quantity of CO produced with GAC/Cu-ZSM-5 is over 200 times smaller. Regardless of the catalyst, the conversion to N_2 decreases with increasing space velocity and the presence of H_2O and SO_2. The conversion of NO to N_2 over Cu-ZSM-5 over the temperature range 200-600°C increases to a maximum as the temperature is increased and then decreases to low levels as the temperature is increased further. The location and magnitude of this maximum is sensitive to space velocity. Increasing the temperature causes lower conversion as GHSV is increased. In contrast, conversion to N_2 over Cu-GAC continues to increase throughout this

temperature range. Moreover, higher conversions are obtained over Cu-GAC than over Cu-ZSM-5 with less sensitivity to GHSV, suggesting that this reaction is much faster.

NO_2 behaves similarly to NO in the reaction with either GAC over Cu-ZSM-5 or Cu-GAC. It appears that the reaction of NO_2 with GAC is to produce NO+CO and that CO is a key intermediate for the NO reduction to N_2.

An attempt was made to conduct isothermal experiments by adding an increasing amount of α-Al_2O_3 to the catalyst bed as a heat sink. We found that the maximum conversion of NO to N_2 based on our experimental protocol depends on the peak temperature developed in the bed. This bed temperature is decided by the amount of Cu-GAC available and the pre-set temperature. The more Cu-GAC present and the higher the bed temperature that can be developed, the more CO is produced, and the more NO is converted to N_2. The experimental evidence indicates that CO is a key intermediate for the NO reduction to N_2. Nevertheless, the results presented in this paper provide a clear and consistent picture of the effect of copper catalysis in promoting the GAC oxidation to CO, followed by CO reduction of NO to N_2.

The author concludes that Cu containing catalysts are efficient promoters of the NO_x + soot reaction under lean conditions at high space velocity. However, they can be easily poisoned by water and SO_2. Consequently, it appears necessary to find other catalysts that are more resistant than Cu-based catalysts to H_2O and SO_2 poisoning at diesel engine operating conditions.

In the preparation of palladium catalysts with γ-Al_2O_3 as the carrier, the Pd dispersion on the surface of the carrier decreases with increasing metal loading due to the monolayer dispersion capacity. A 3-4% Pd loading results in the optimum number of

active sites. Higher calcination temperatures result in lower Pd dispersion and larger Pd crystallite size due to the sintering process that results from thermal effects. Lower pH leads to more aggregation of Pd and a more prominent steric hindering effect than does higher pH. Therefore lower Pd dispersions were observed at lower pH.

By investigating the reduction of NO with GAC under lean conditions, it was shown that palladium catalysts have high activities for the reduction of NO to N_2 with solid carbonaceous material. Among the catalysts tested, PdO/Al_2O_3 exhibited the highest activity with a 90% maximum conversion when the mixture is preheated to 500°C. The PdO/CeO_2 catalyst has the lowest light-off temperature. This may be due to the CeO_2 oxidative activity, which can promote GAC oxidation. However CeO_2 does not have activity for reduction of NO to N_2. In our experiments, over 80% of the NO is reduced to N_2 over PdO/Al_2O_3 at GHSV of 50,000 and the catalyst showed a relatively low dependence on space velocity with 80% NO conversion maintained even at the high GSHV of 80,000. The palladium catalyst also showed a high resistance to SO_2 and water poisoning. For example, a 70-80% NO conversion was obtained at a temperature of 550°C after 15 hours of SO_2 and water application; 40% NO conversion was still maintained after 30 hours of SO_2 and water application.

An attempt was made to conduct isothermal experiments by adjusting the catalyst/GAC ratio in the catalyst bed. It was found that the maximum conversion of NO to N_2 based on the indicated experimental protocol depends on the peak temperature developed in the bed which is associated with GAC content and the preheat temperature. The results presented in this paper provide a clear and consistent picture that a palladium

catalyst promotes the GAC oxidation to a carbon-oxygen intermediate (CO), followed by this intermediate reducing NO to N_2 while the intermediate is oxidized to CO_2.

Bench experiments were carried out to test whether the RFBR concept is applicable to diesel engine exhaust control. Even though the RFBR design and experimental conditions such as catalyst employed, fluidization conditions, reaction temperature, and engine operation conditions are far from optimum, the experimental results show that RFBR did achieve a NO reduction of 20%, and a CO, HC, soot removing efficiency of over 90%. By optimizing the experimental conditions, one would expect a greater reduction in NO.

APPENDIX A

FIGURES OF EXPERIMENTAL RESULTS

This section includes all figures of experiment results for Chapter 2 to Chapter 6.

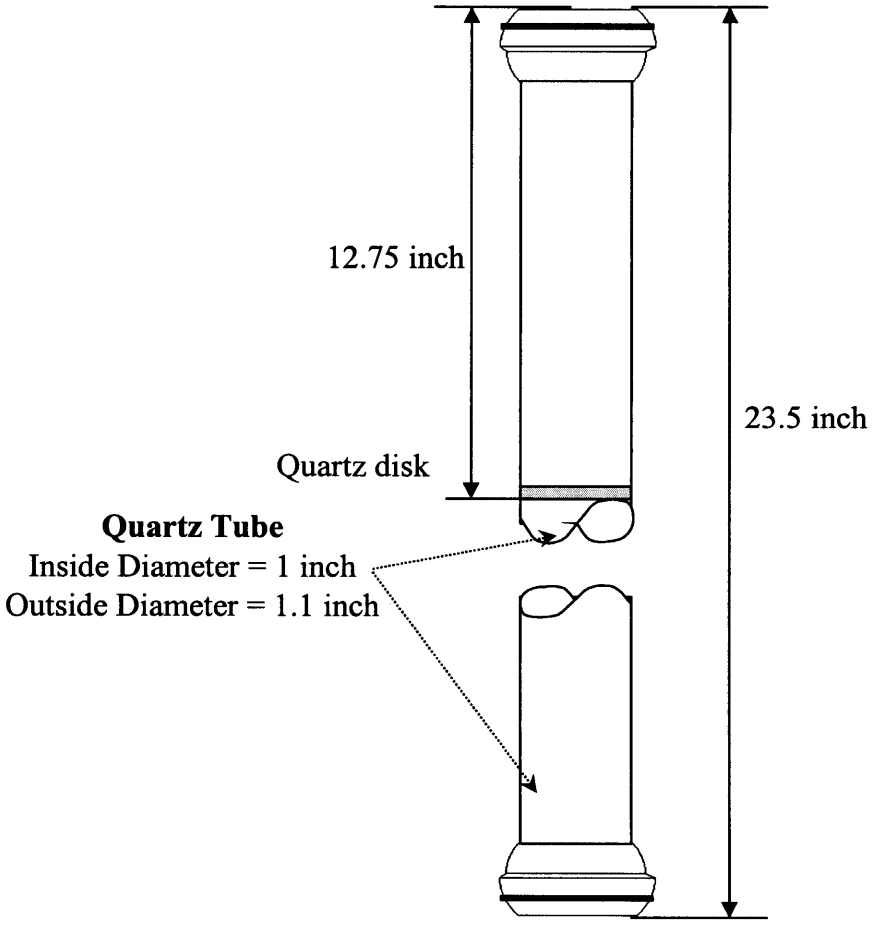

Figure 2.1a Packed bed reactor.

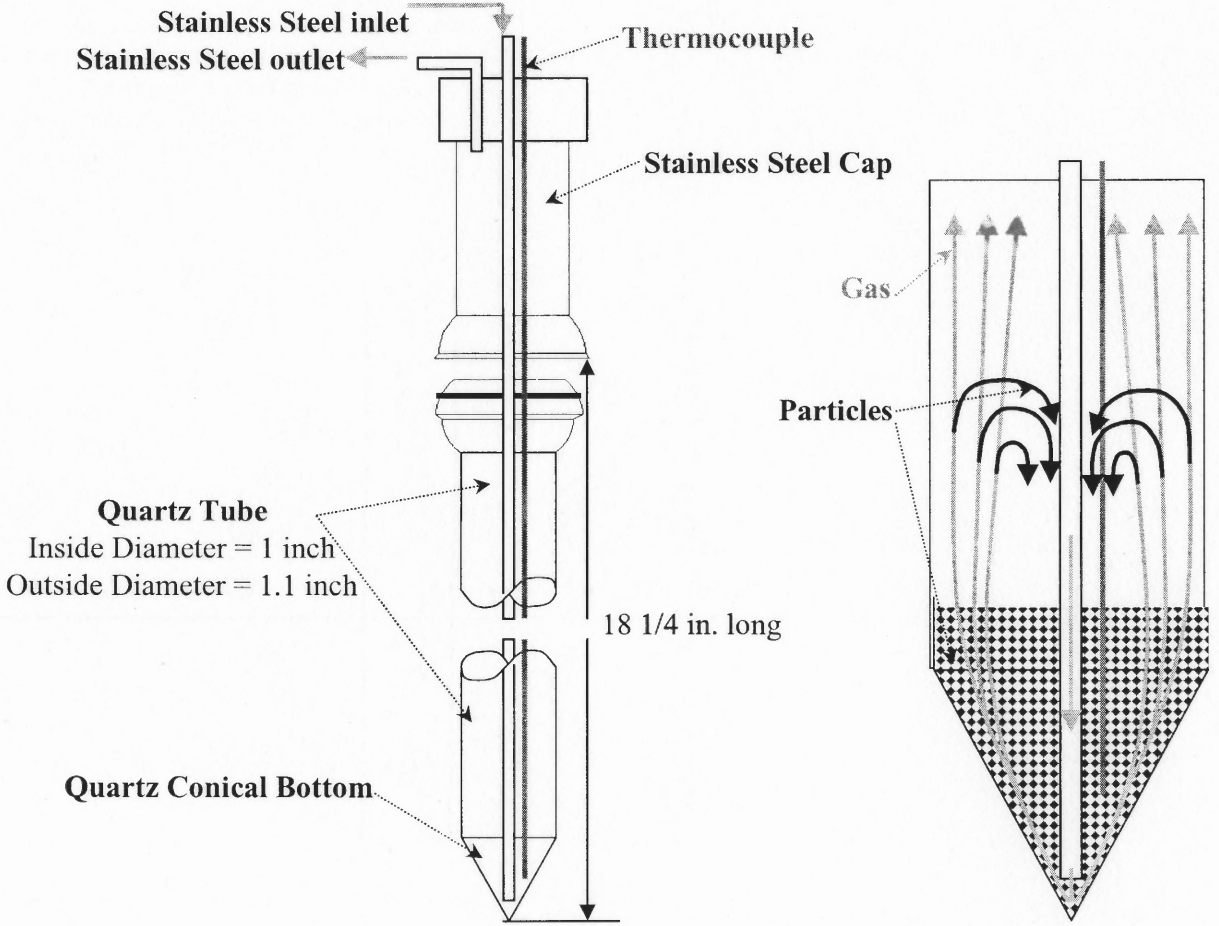

Figure 2.1b Fixed fluidized bed reactor (RFB).

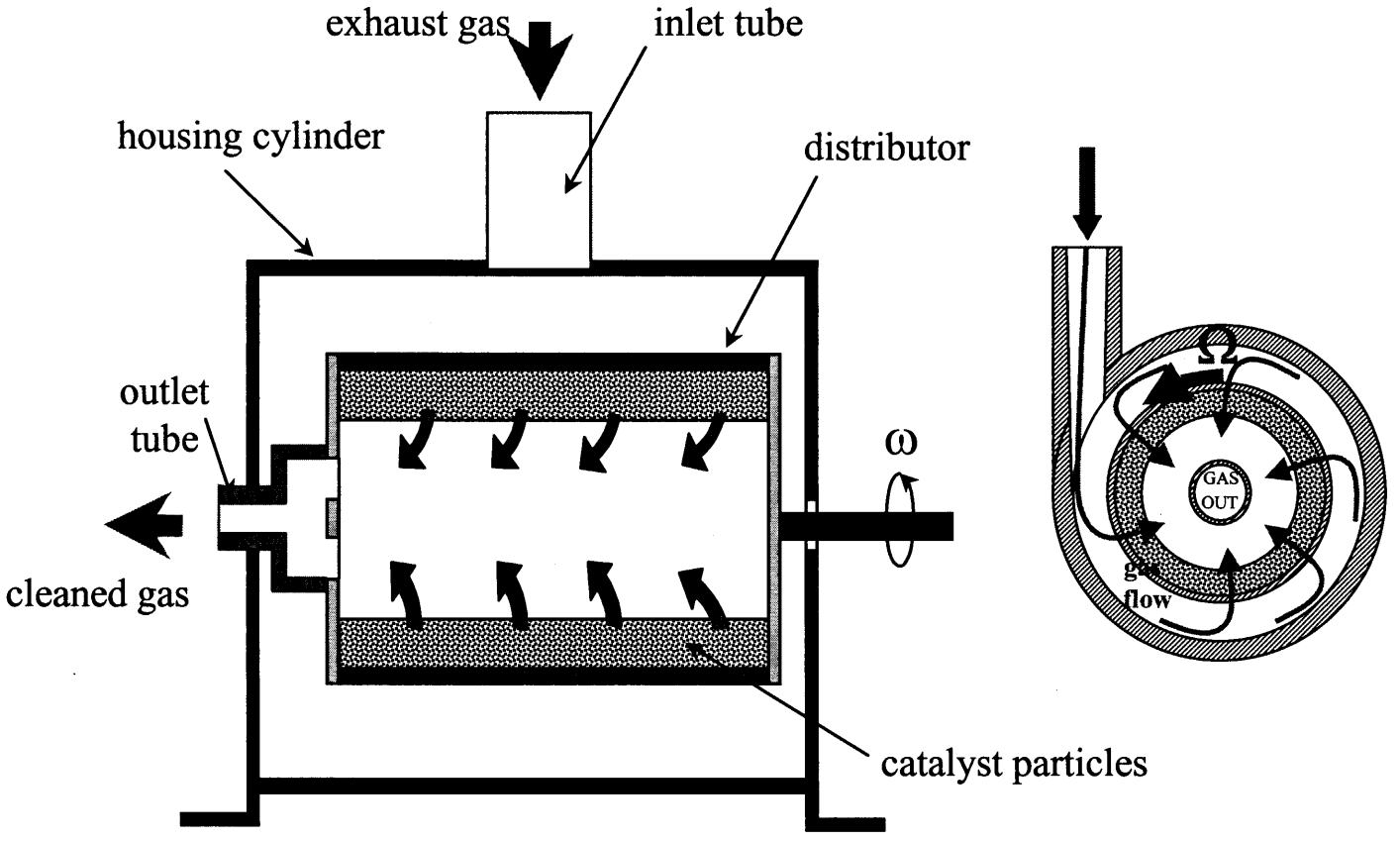

Figure 2.2 Rotating fluidized bed reactor.

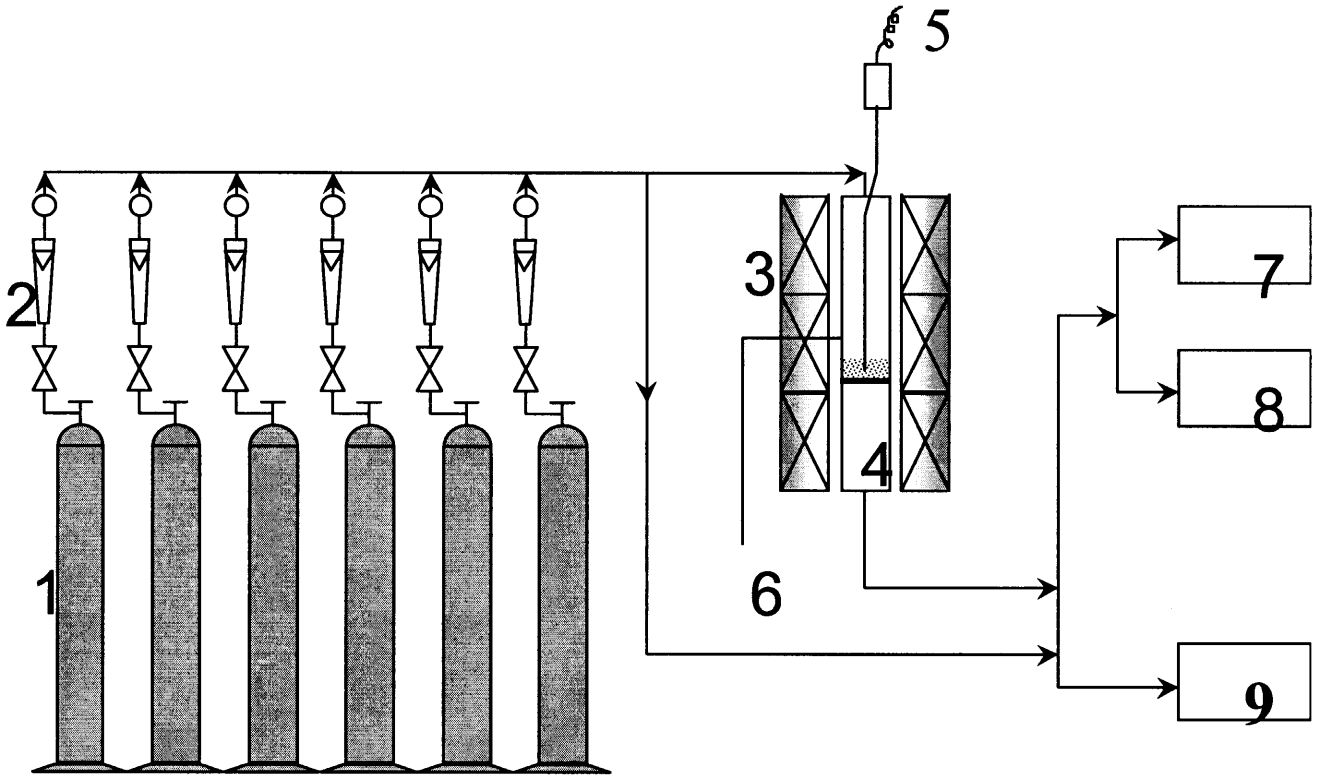

Figure 3.1 Schematic diagram of experimental apparatus

1. Cylinders (He, NO, NO_2, O_2, CO, SO_2), 2. Flowmeters, 3. 3-ZoneFurnace, 4. Quartz Reactor, 5. Thermocouple,

6. Temperature Controller, 7. HP5890 GC-FID, 8. HP5890 GC-TCD, 9. Nicolet G Series 520 FT-IR.

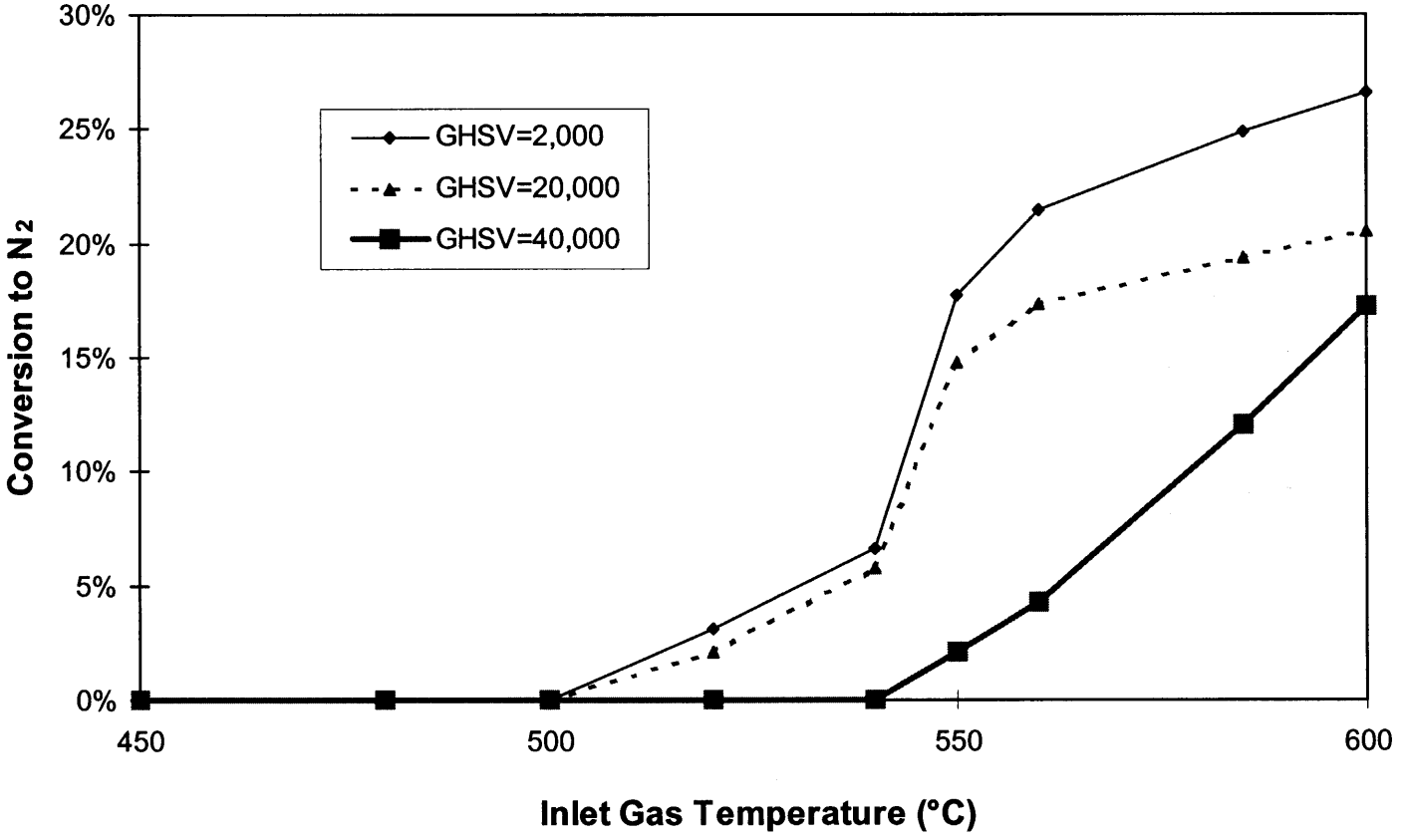

Figure 3.2 Effect of space velocity on reduction of NO with GAC, [NO] = 590 ppm, [O_2]=10%.

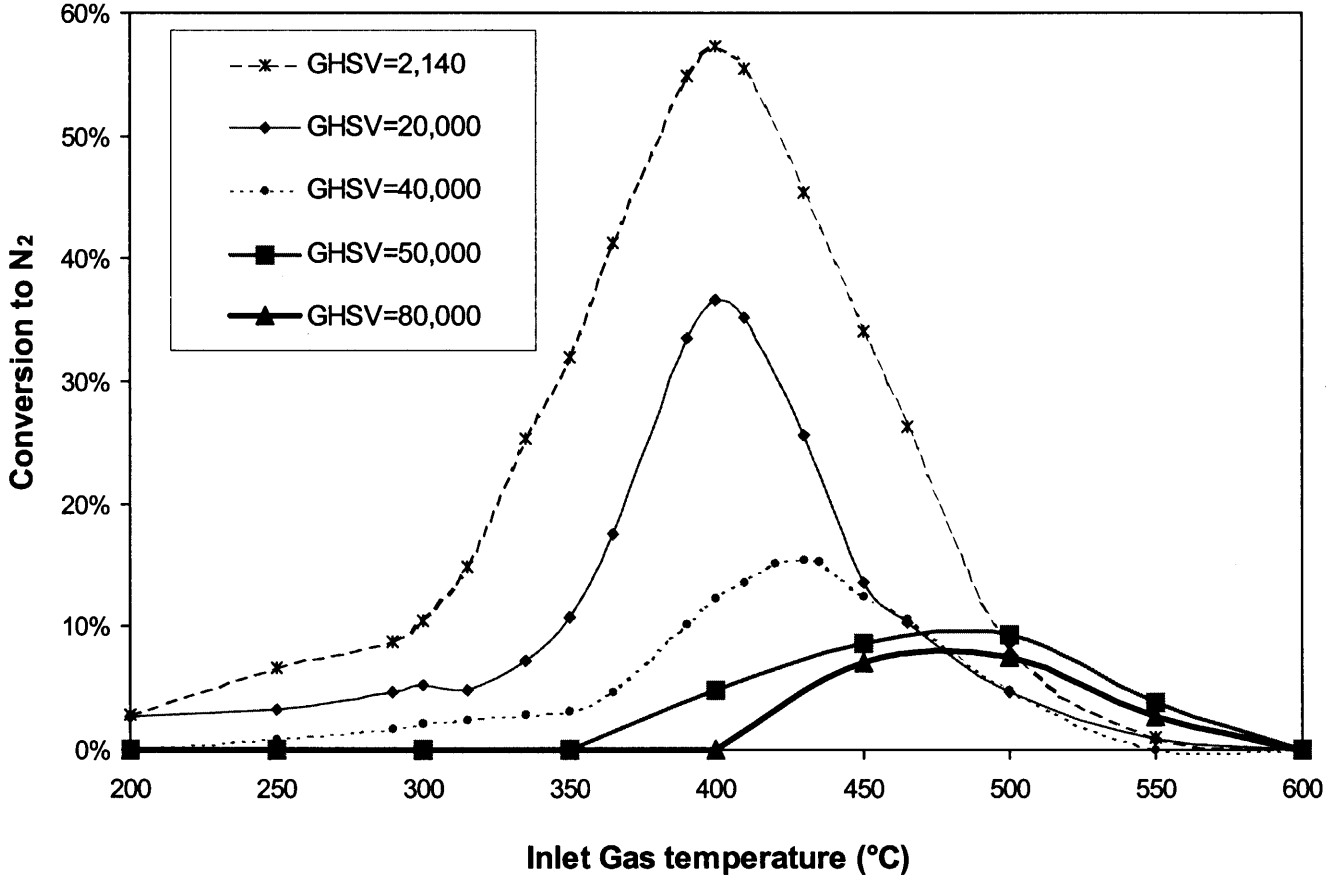

Figure 3.3 Effect of space velocity on reduction of NO with GAC over Cu-ZSM-5, [NO] = 590 ppm, [O_2] = 10%, [GAC] = 5%, [Cu-ZSM-5] = 95%.

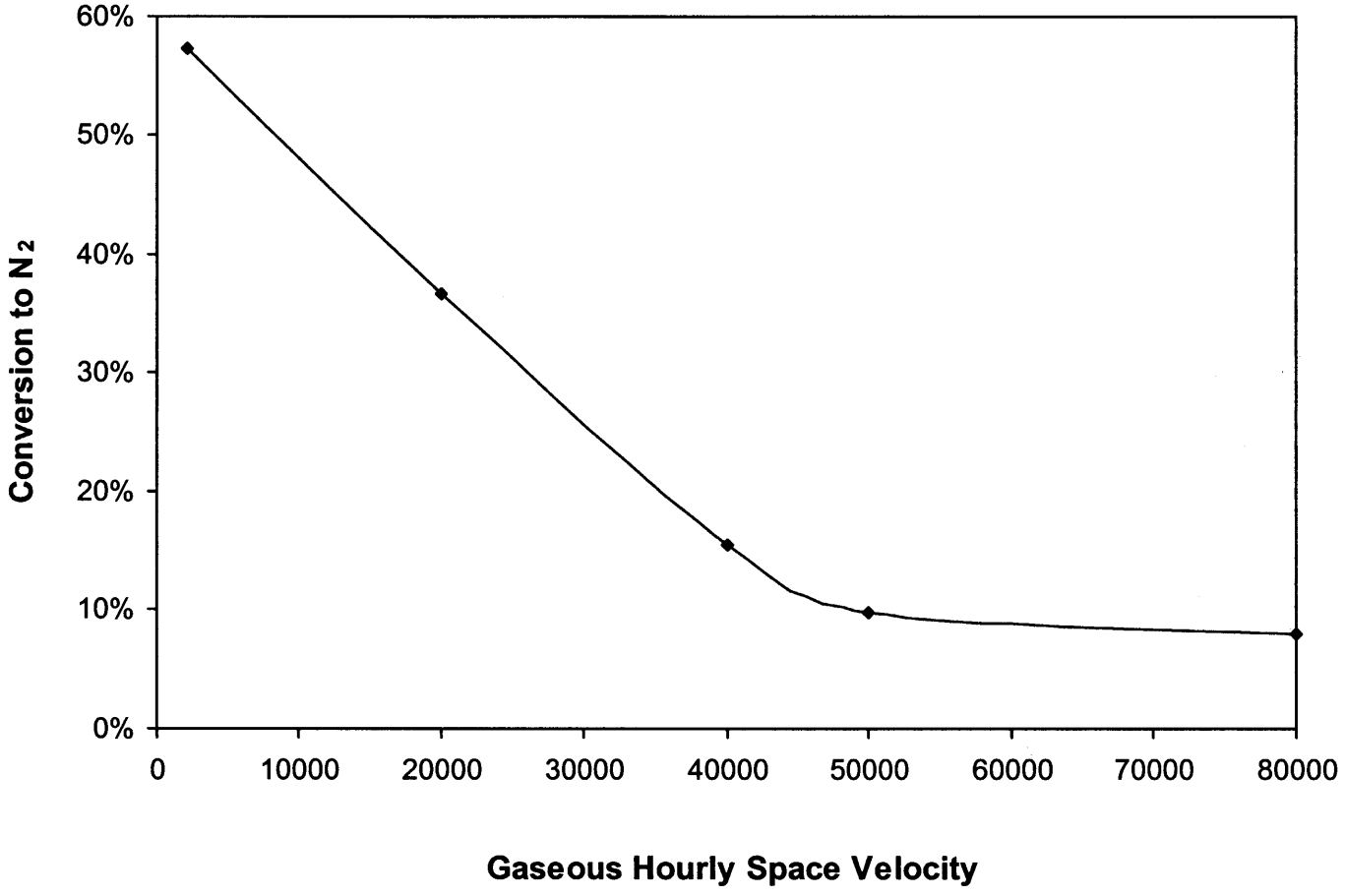

Figure 3.4 Effect of space velocity on the maximum conversion values of the reduction of NO with GAC over Cu-ZSM-5, [NO]=590 ppm, [O_2]=10%, [GAC]=5%, [Cu-ZSM-5]=95%.

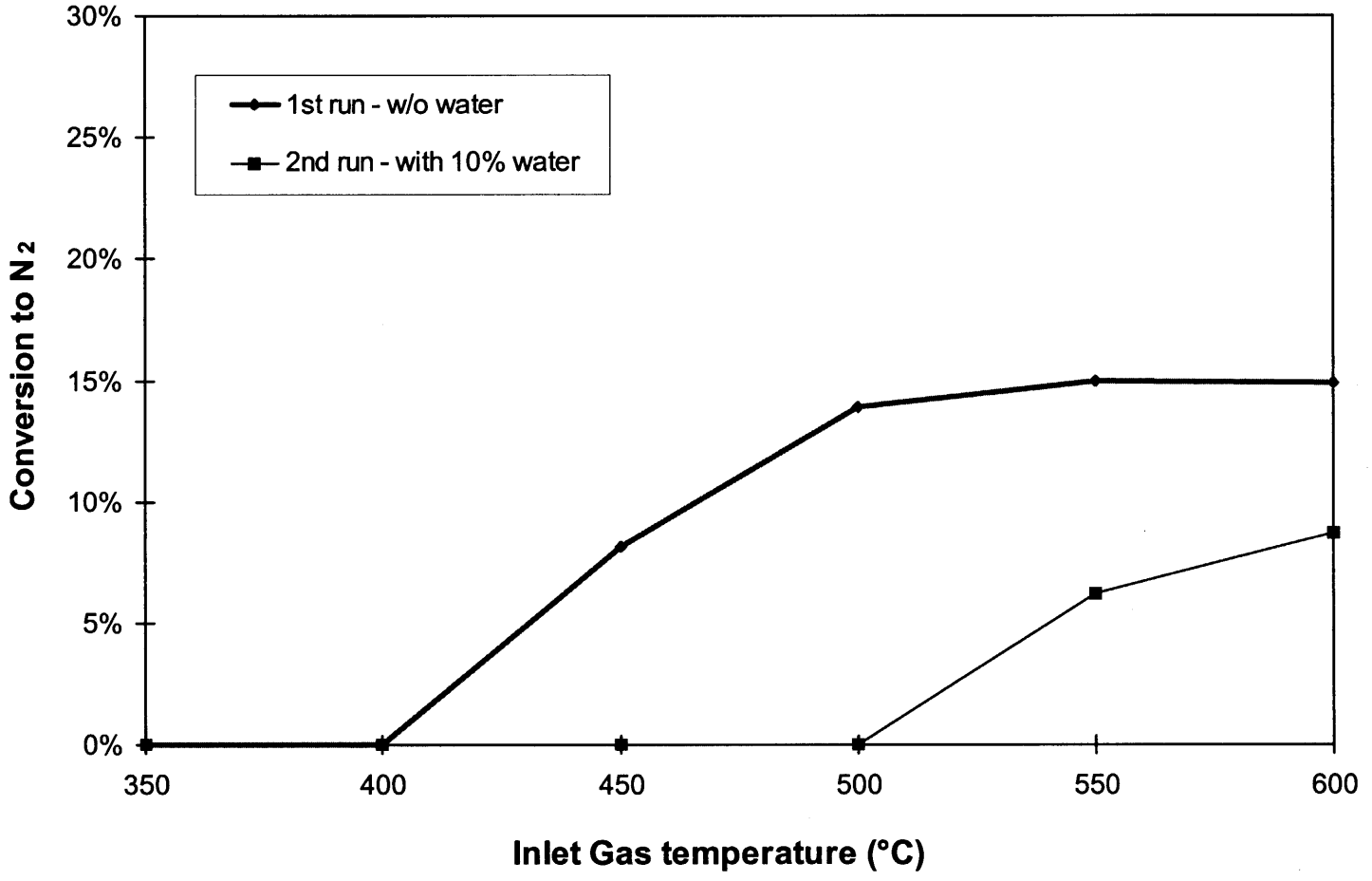

Figure 3.5 Effect of water poisoning on reduction of NO with GAC over Cu-ZSM5, GHSV=50,000, [NO]=590 ppm, $[O_2]$=10%, [GAC]=5%,[Cu-ZSM-5]=95%.

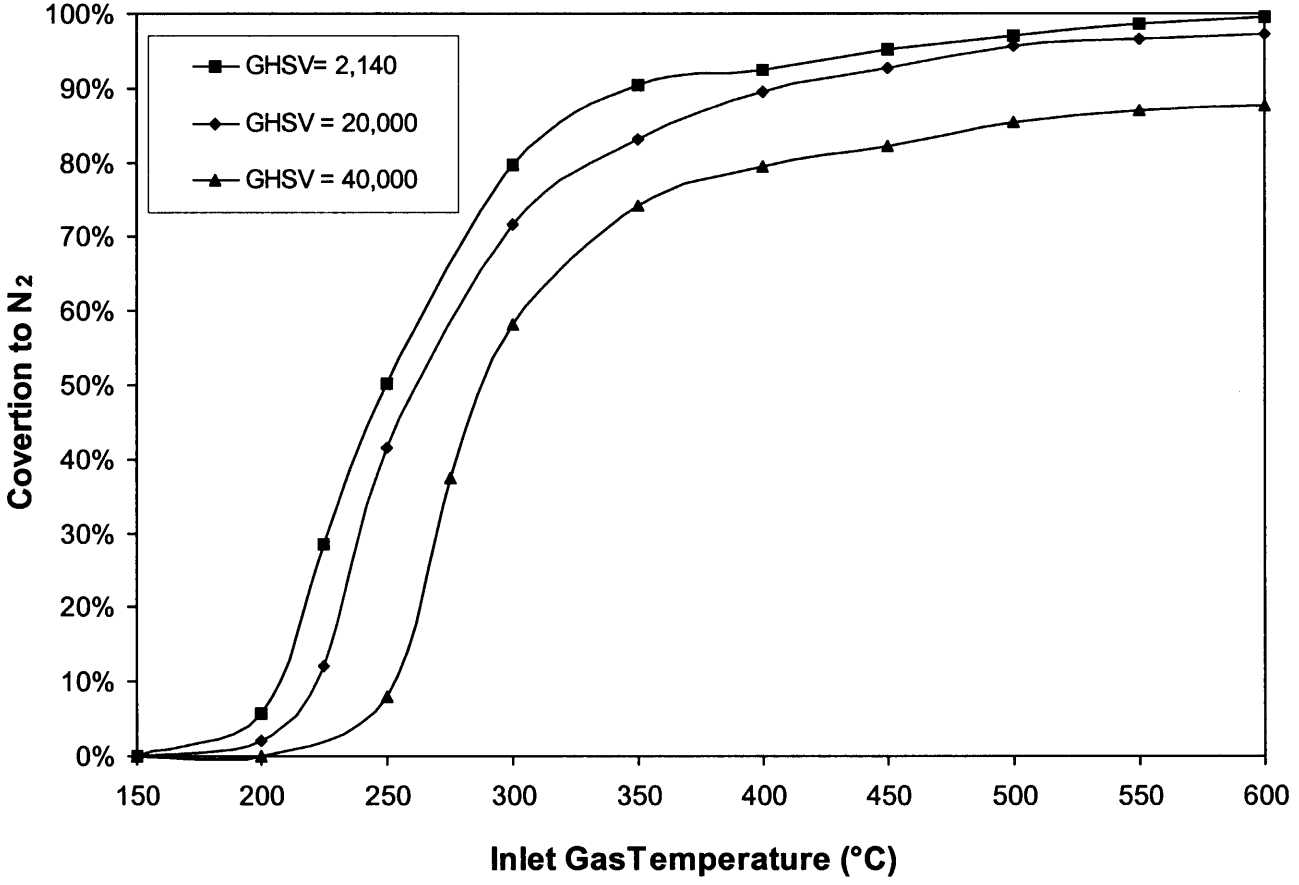

Figure 3.6 Effect of space velocity on the reduction of NO with Cu-GAC, [NO]=590 ppm, $[O_2]$=10%, [Cu]=20%.

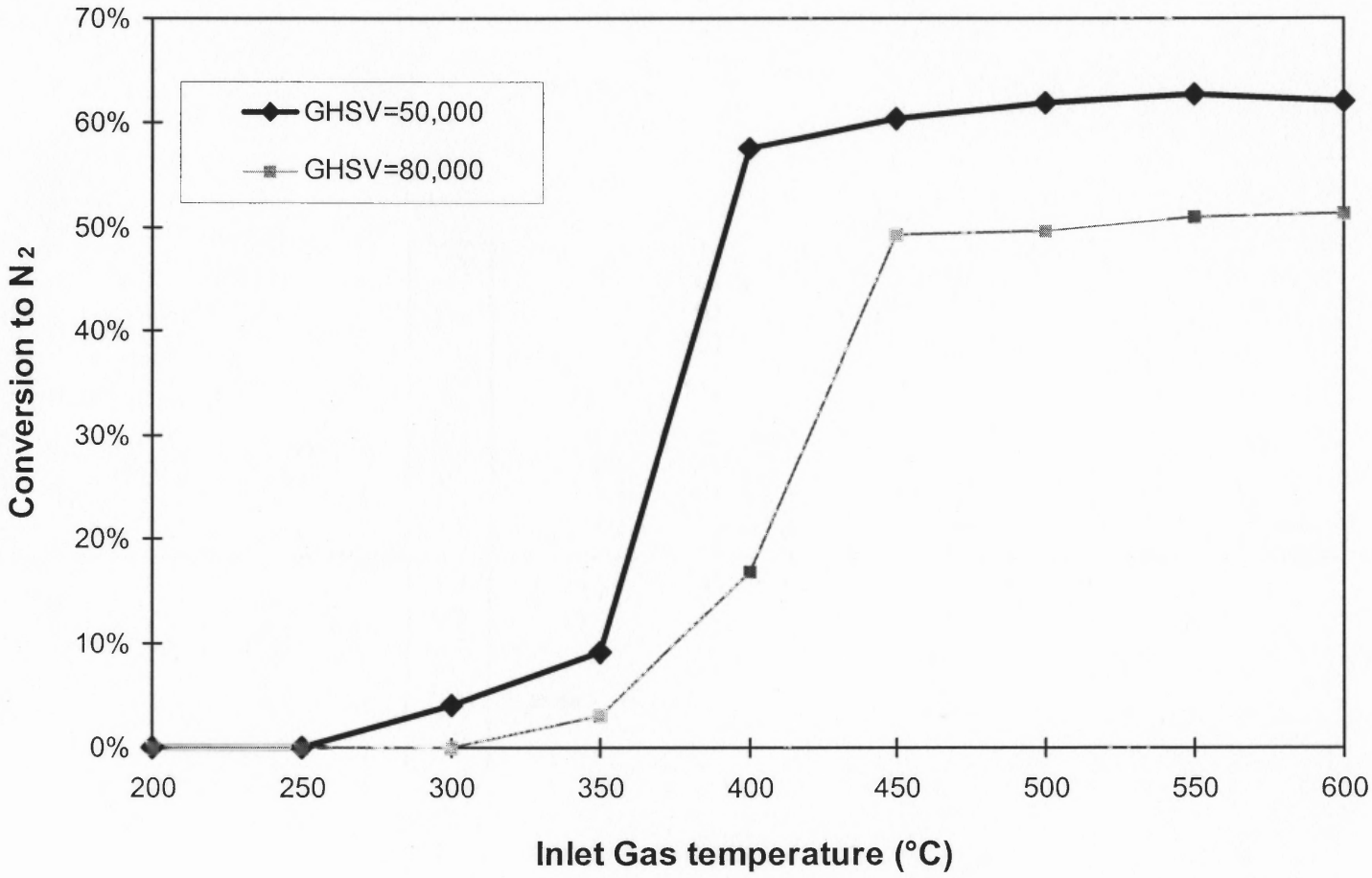

Figure 3.7 Effect of space velocity on reduction of NO with Cu-GAC,[NO]=590 ppm, [O_2]=10%, [Cu]=1%.

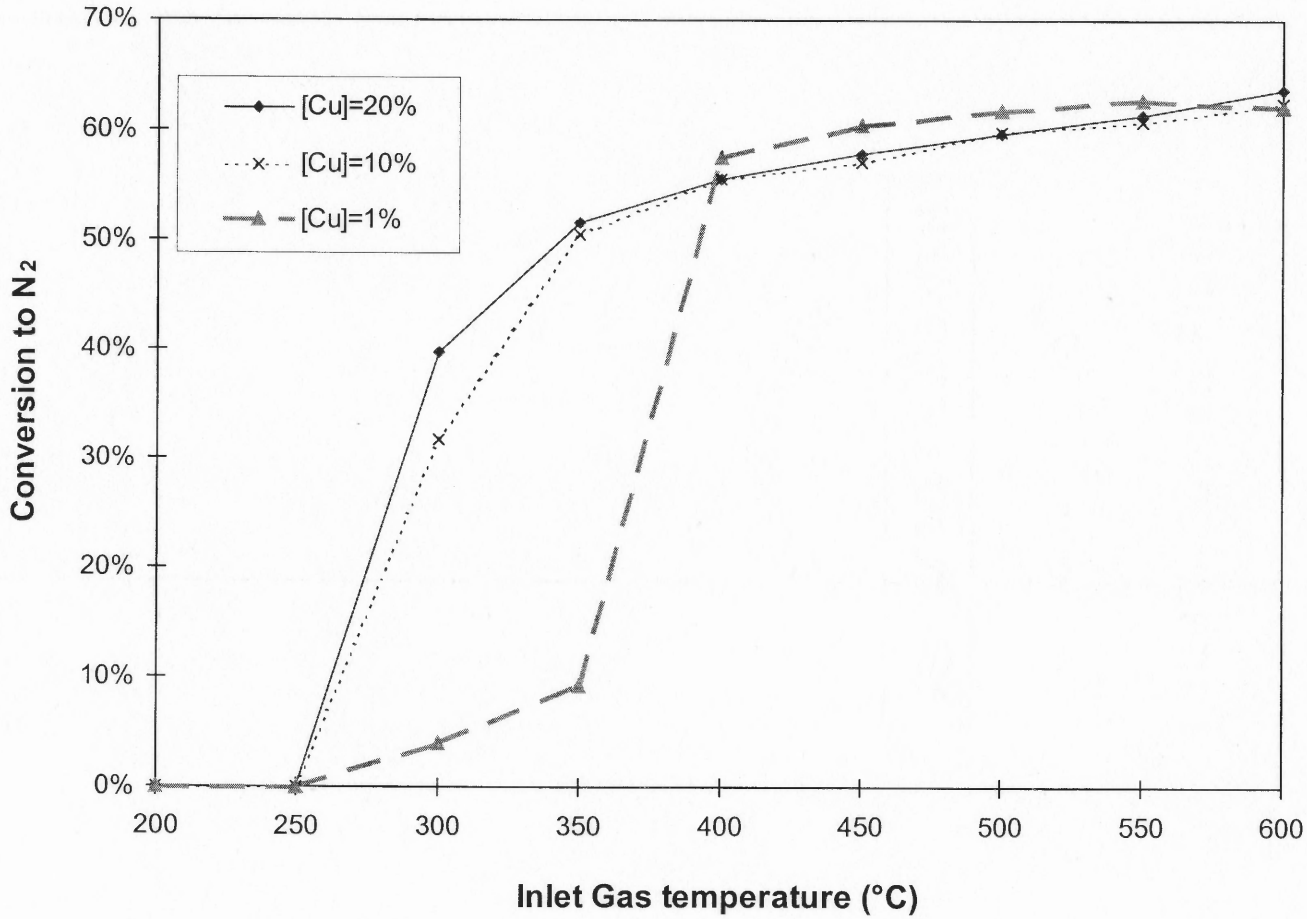

Figure 3.8 Effect of Cu concentration on the reduction of NO with Cu-GAC, GHSV=50,000, [NO]=590ppm, $[O_2]$=10%.

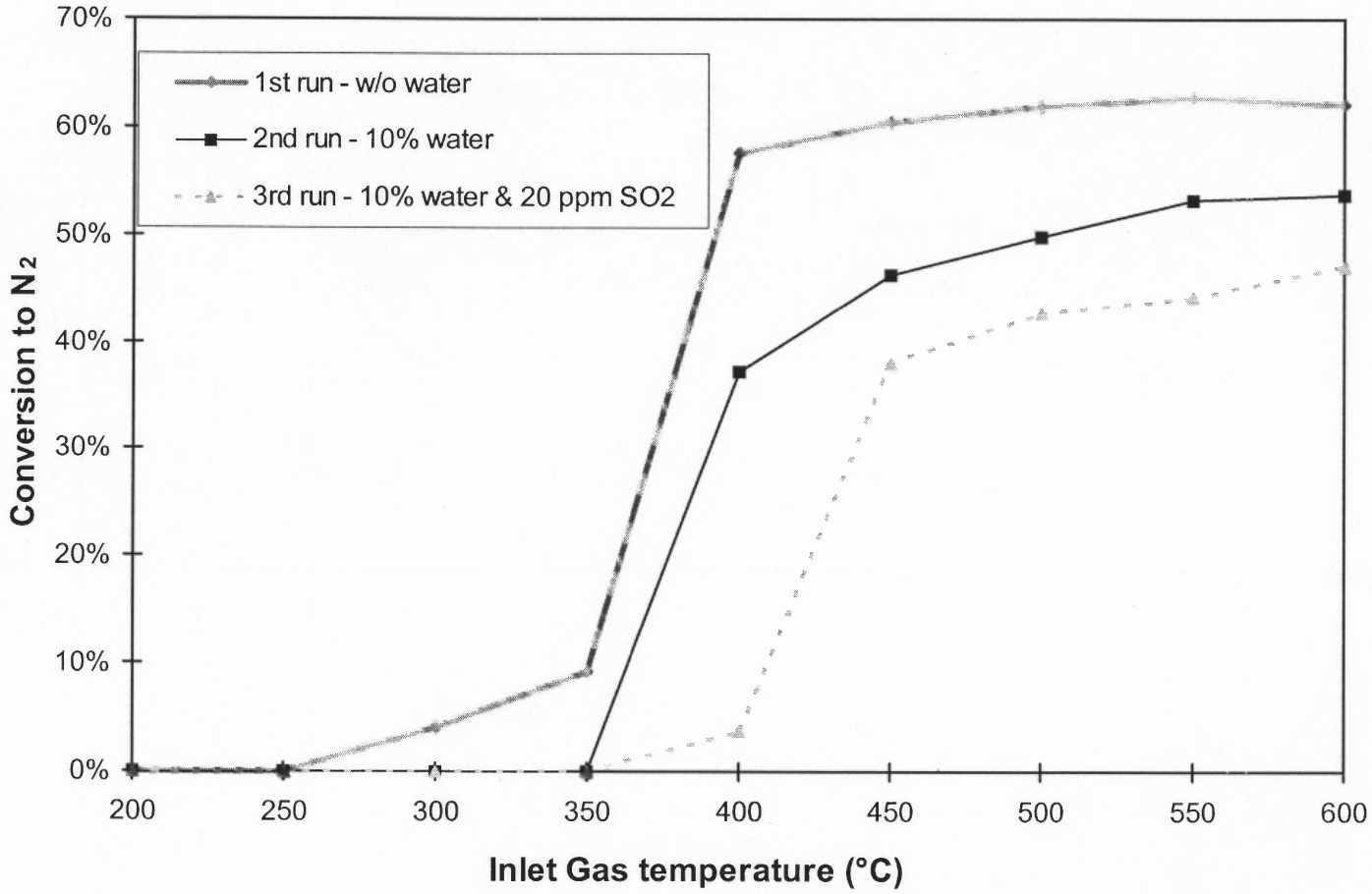

Figure 3.9 Effect of poisons on reduction of NO with Cu-GAC, GHSV=50,000,[NO]=590 ppm, $[O_2]$=10%, [Cu]=1%.

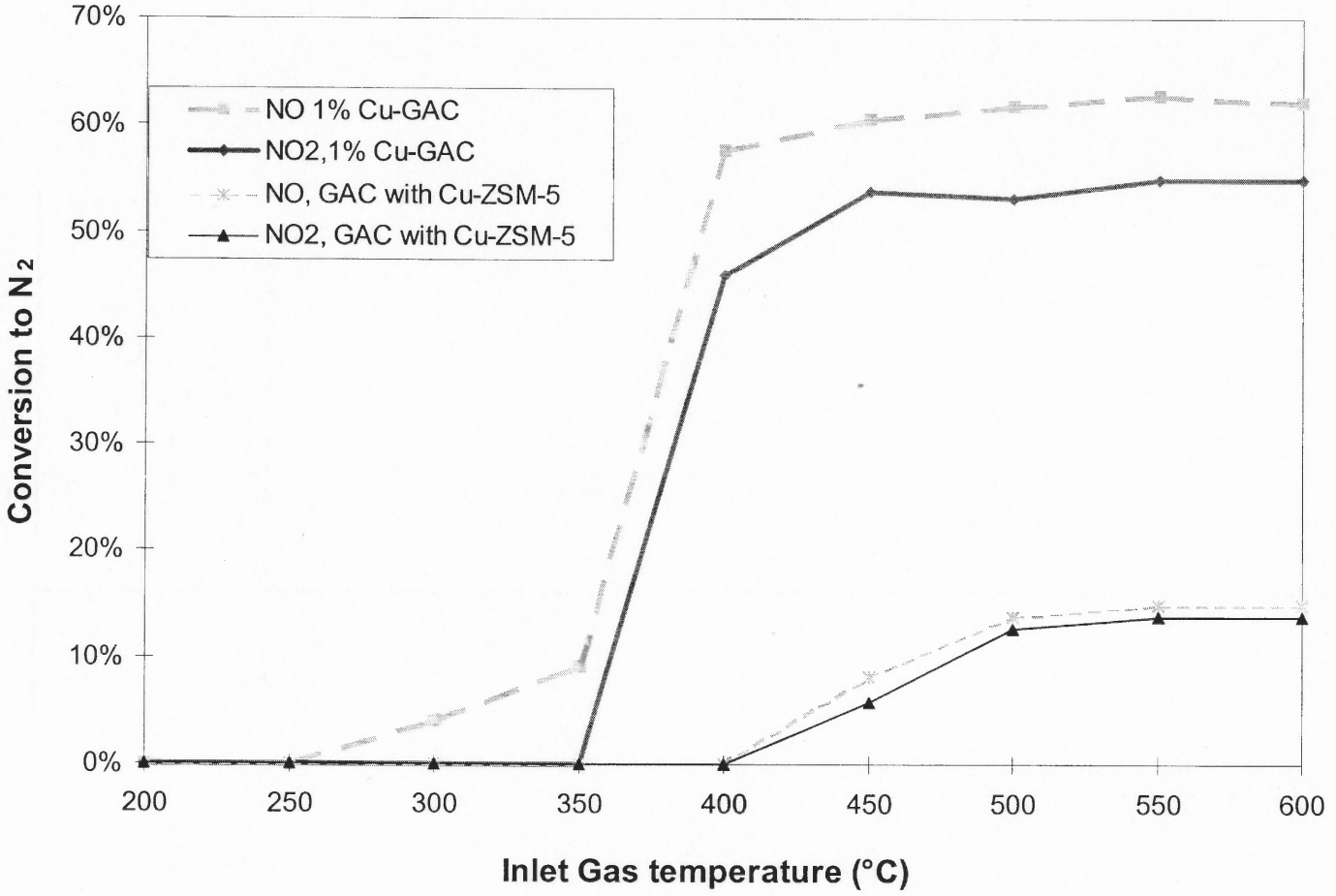

Figure 3.10 Reduction of NO and NO_2 with different reductants, GHSV=50,000, $[NO_2]$=590 ppm, $[O_2]$=10%.

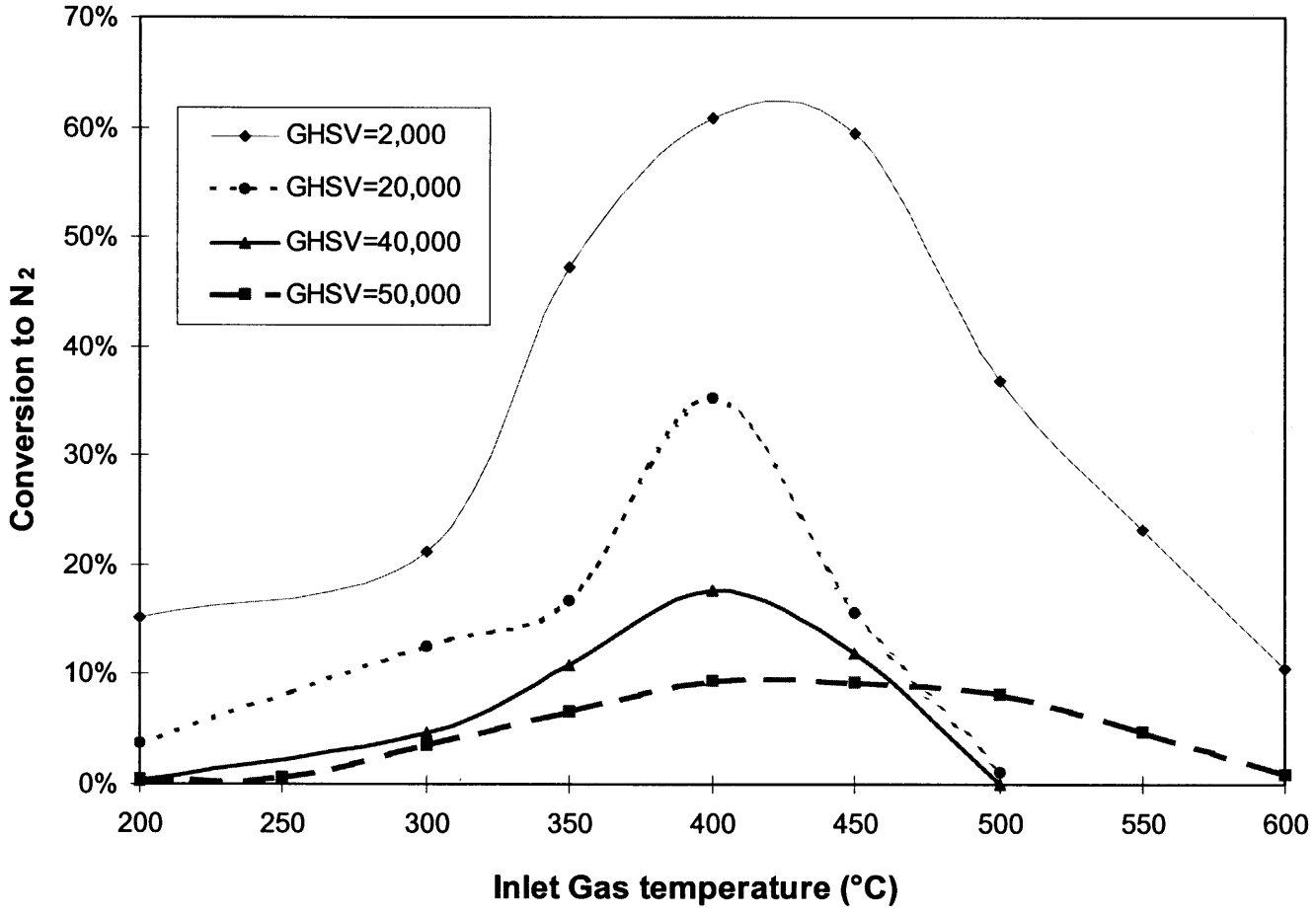

Figure 3.11 Effect of space velocity on reduction of NO with CO over Cu-ZSM-5, [NO]=[CO]=490 ppm, $[O_2]$=10%.

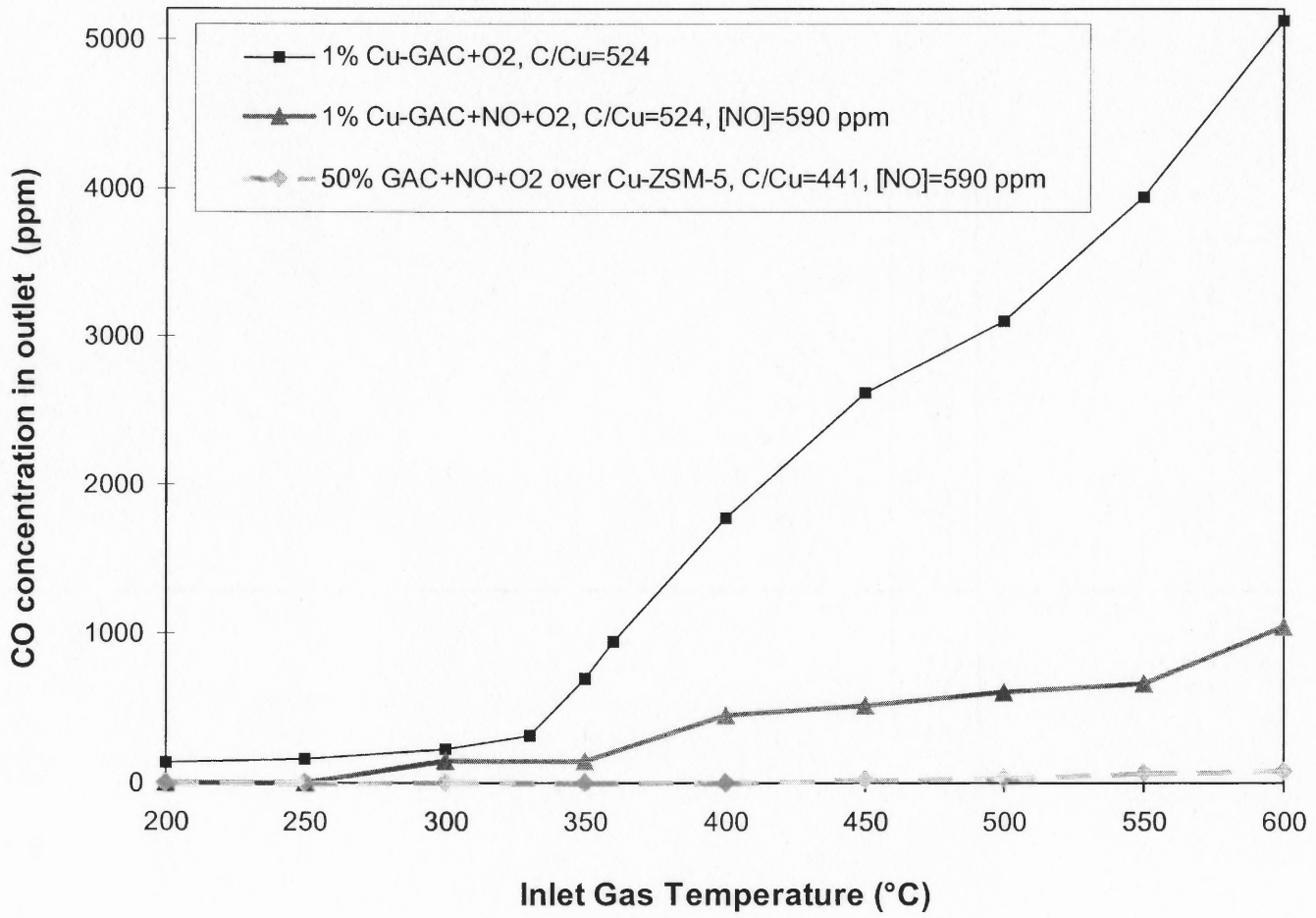

Figure 3.12 Oxidation of GAC promoted by Cu containing catalysts , GHSV=50,000, $[O_2]$=10%.

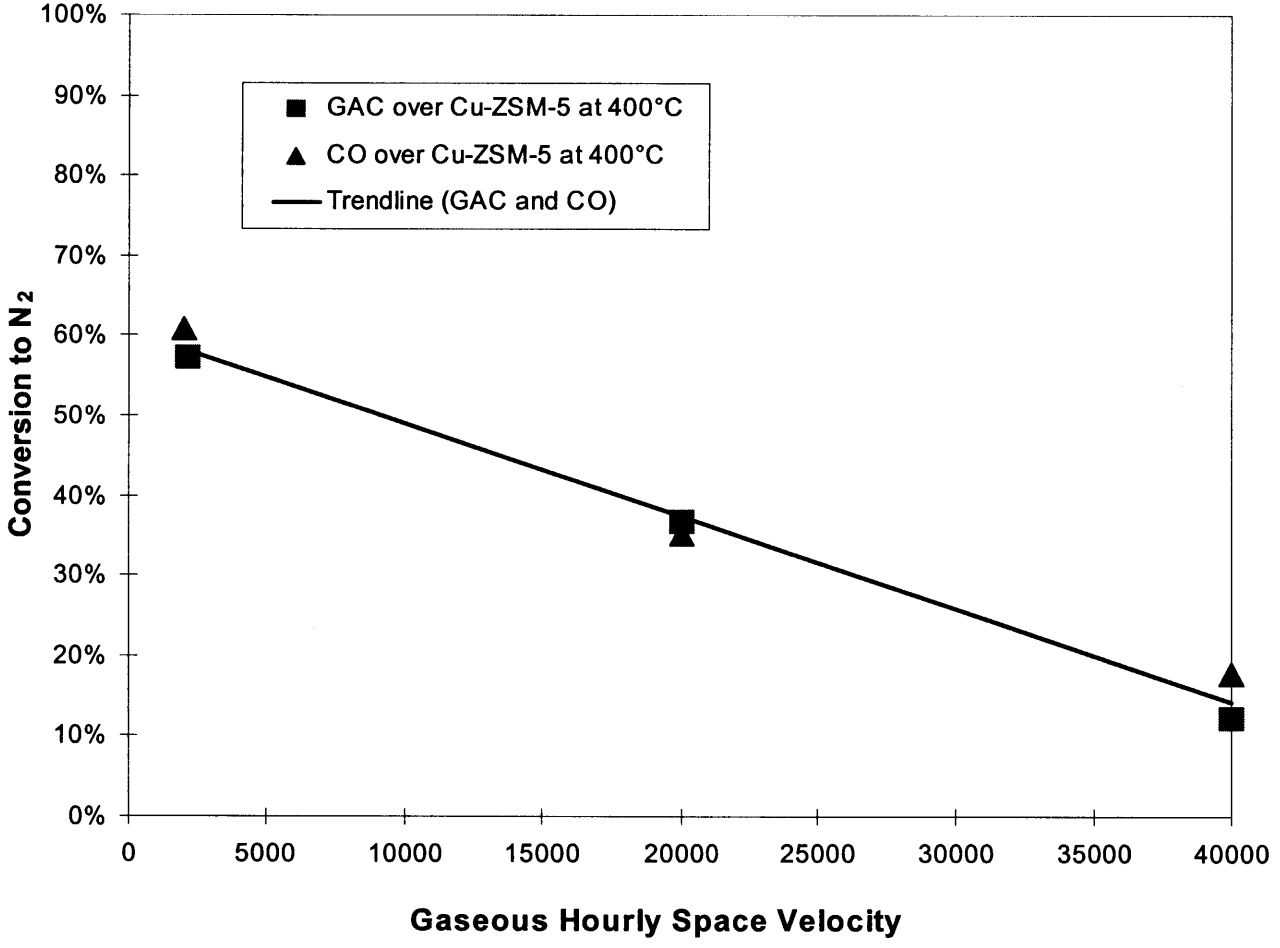

Figure 3.13 Comparison of CO and GAC as reductants over Cu-ZSM-5.

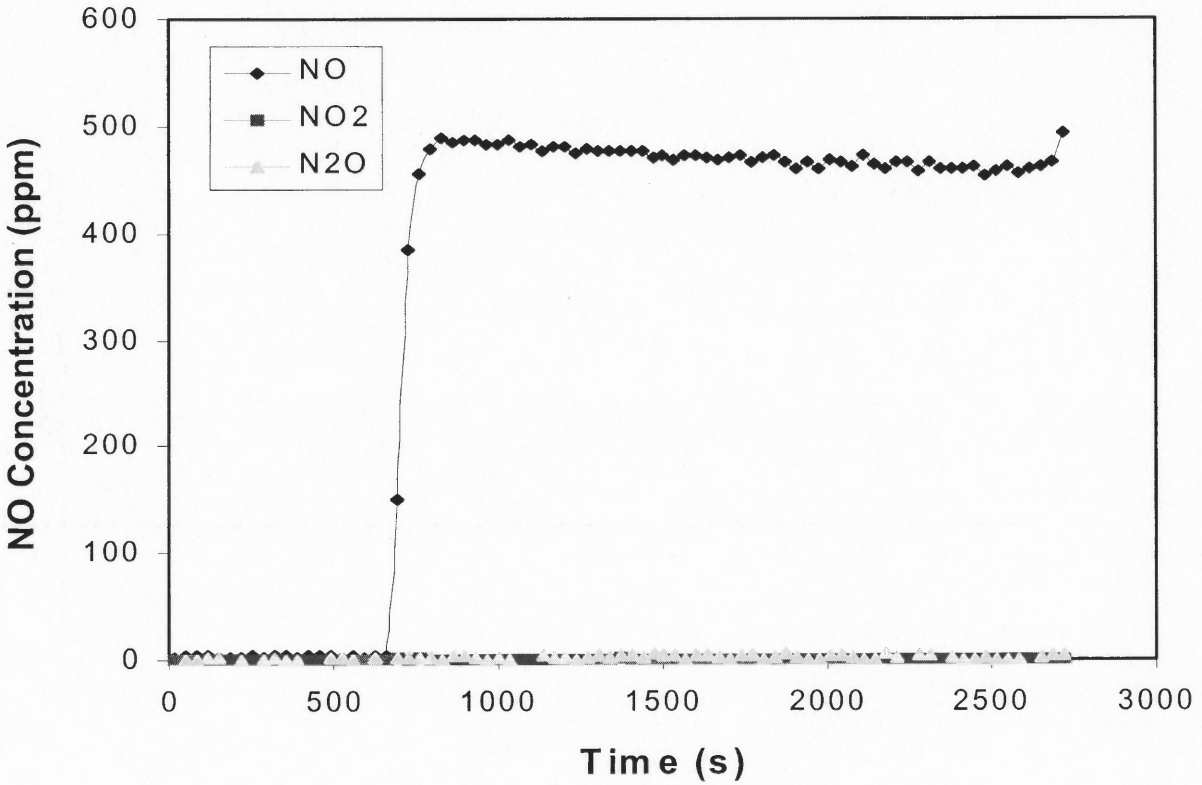

Figure 4.1 NO + GAC at T = 502°C, GHSV = 50,000, [NO] = 480 ppm.

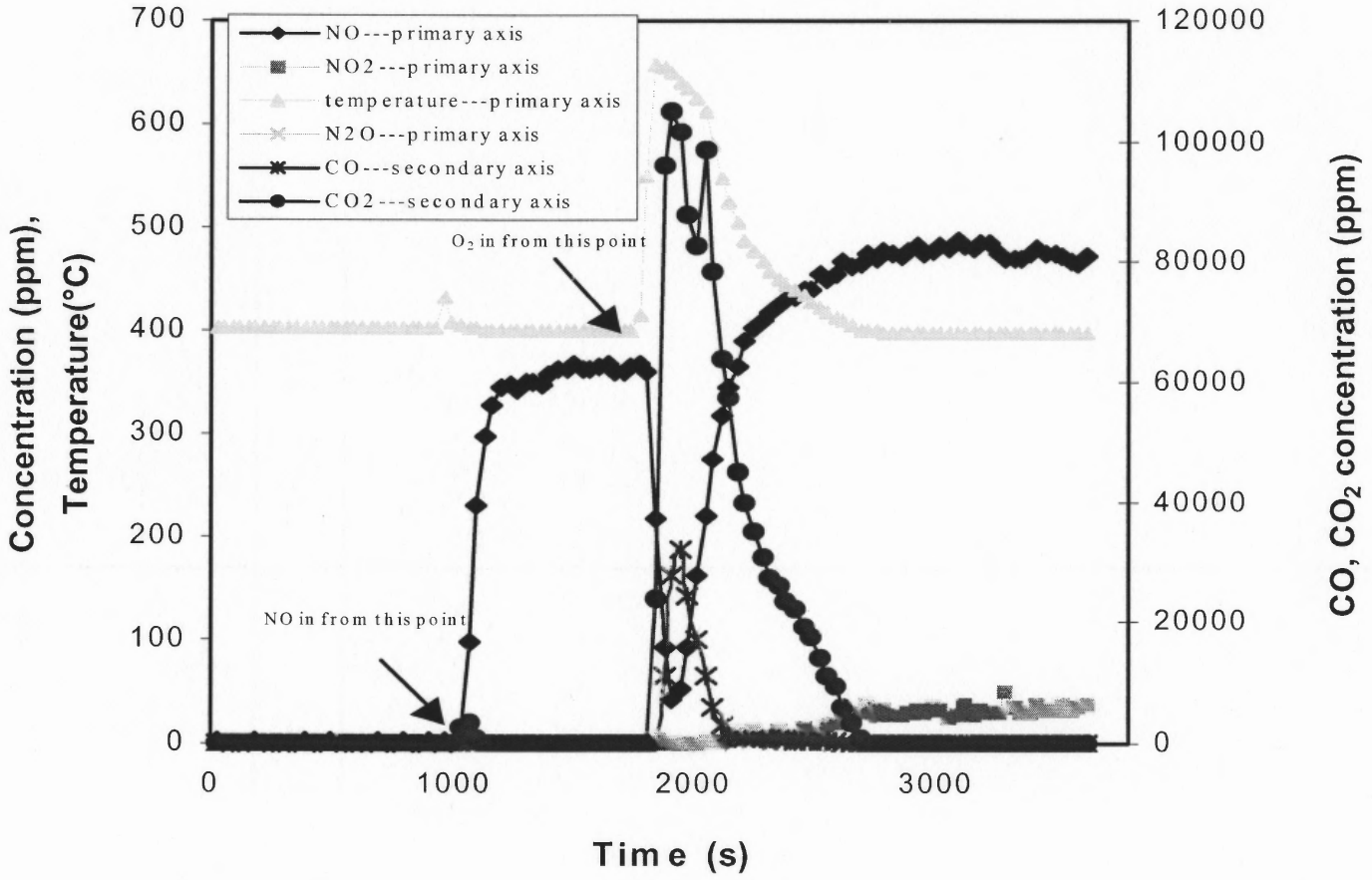

Figure 4.2 1.5ml (0.3895g) 20% Cu-GAC + NO + O_2, GSHV = 50,000, [NO] = 530 ppm, [O_2] =10%.

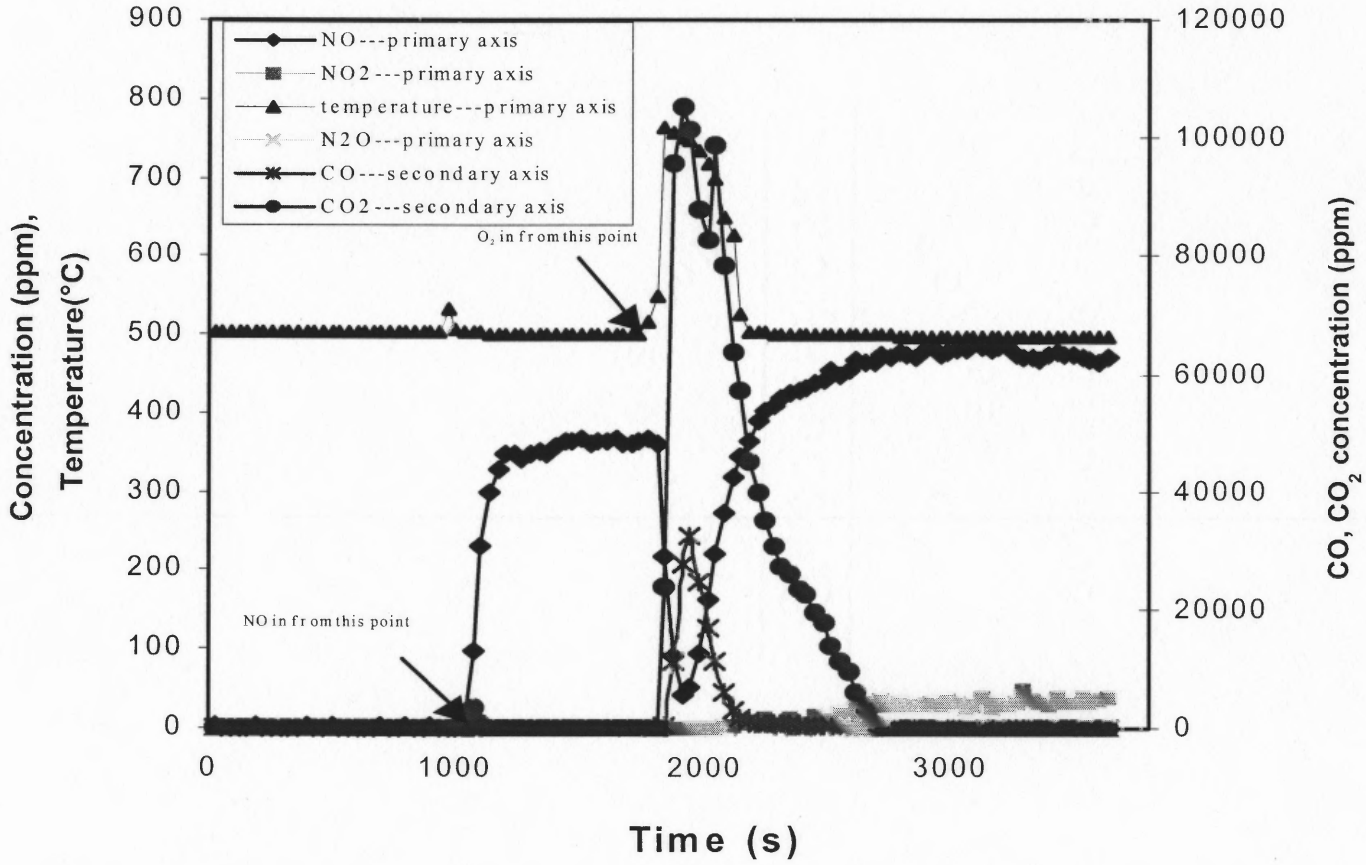

Figure 4.3 1.5ml (0.4016g) 20% Cu-GAC + NO + O_2, GSHV=50,000, [NO] = 530 ppm, [O_2] =10%.

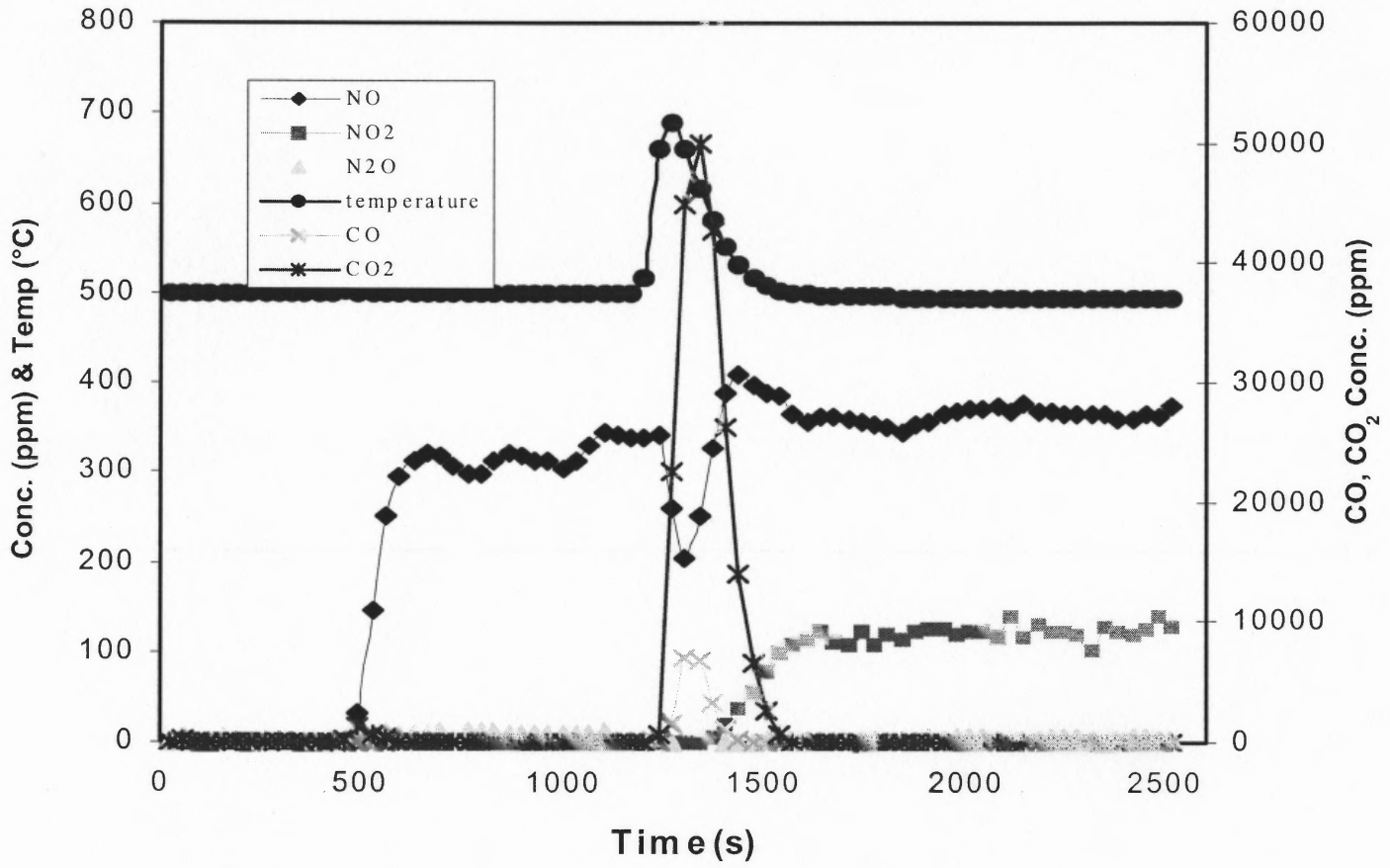

Figure 4.4 NO + O_2 over 0.5 ml (0.2146g)20% Cu-GAC + 1 ml (1.5321g) α-Al_2O_3,[NO] = 500 ppm, [O_2] =10%, GHSV = 50,000.

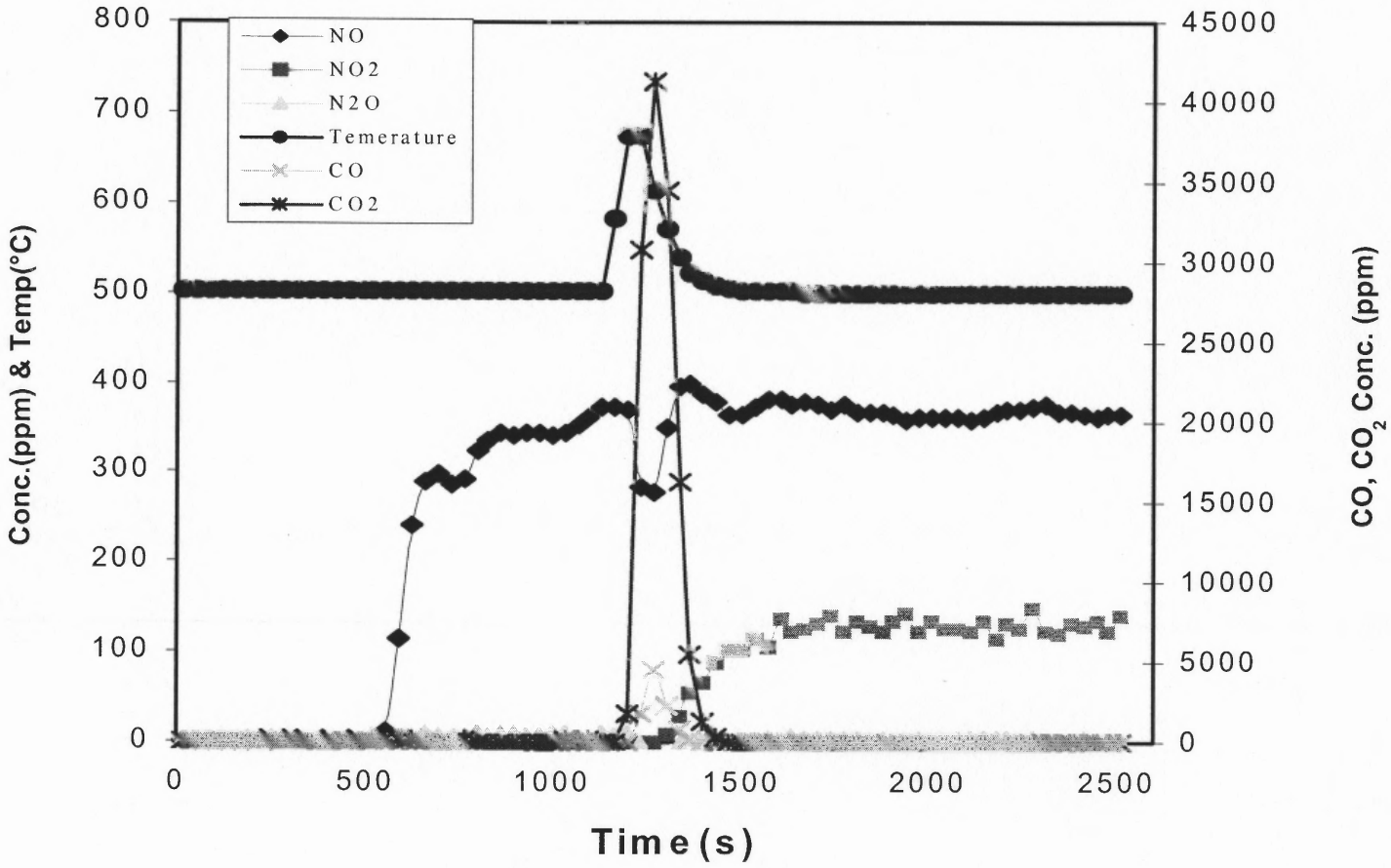

Figure 4.5 $NO+O_2$ over 0.3 ml (0.1325g) 20% Cu-GAC + 1.2 ml (1.8362g) α-Al_2O_3, GHSV = 50,000, [NO]= 510 ppm, $[O_2]$ =10%.

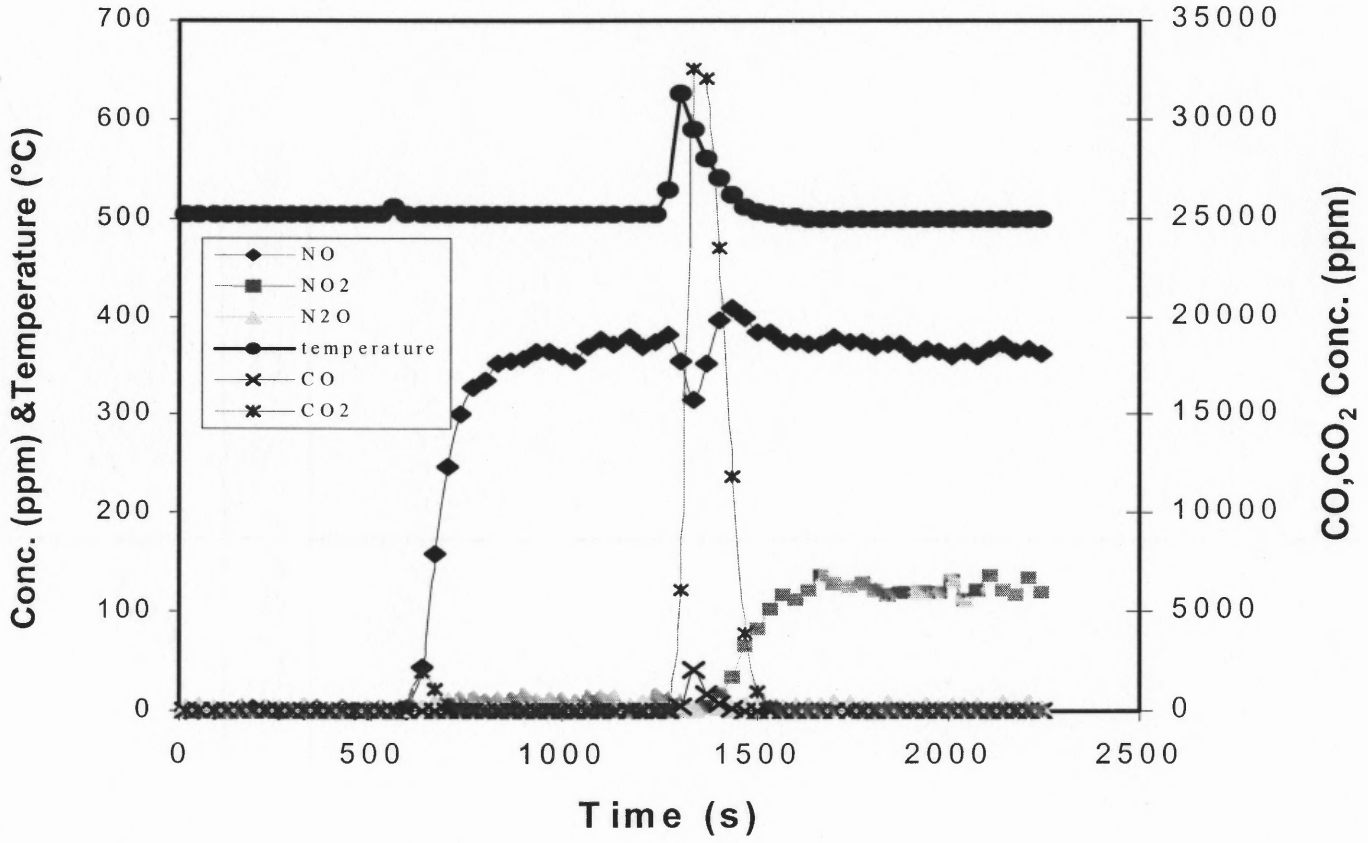

Figure 4.6 NO + O_2 over 0.25 ml (0.096g)20% Cu-GAC + 1.25 ml (1.9241g) α-Al_2O_3, [NO] = 520ppm, [O_2] = 10%, GHSV = 50,000.

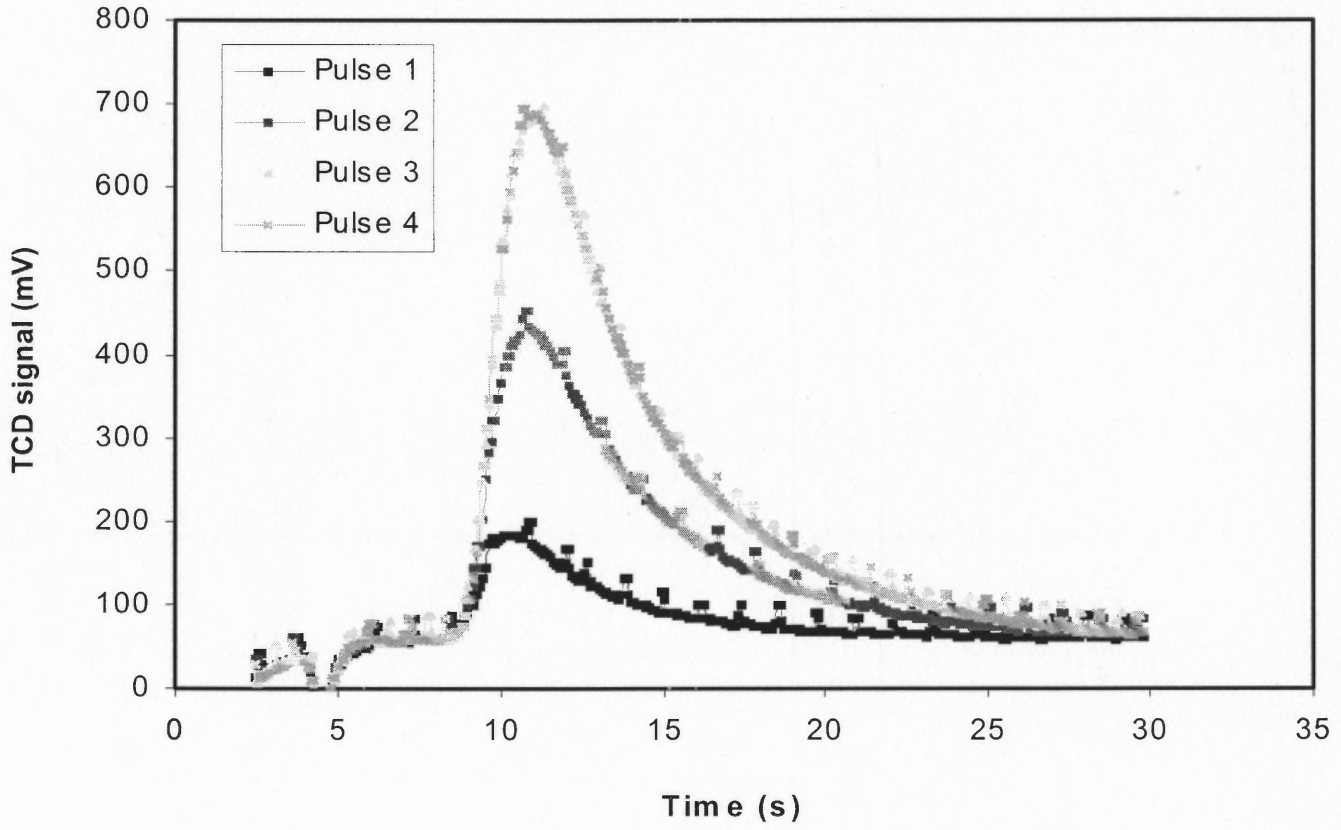

Figure 5.1 Ultra-High purity 5% H_2 Pulse chemisorption on 0.1392g 3% PdO/Al_2O_3 .

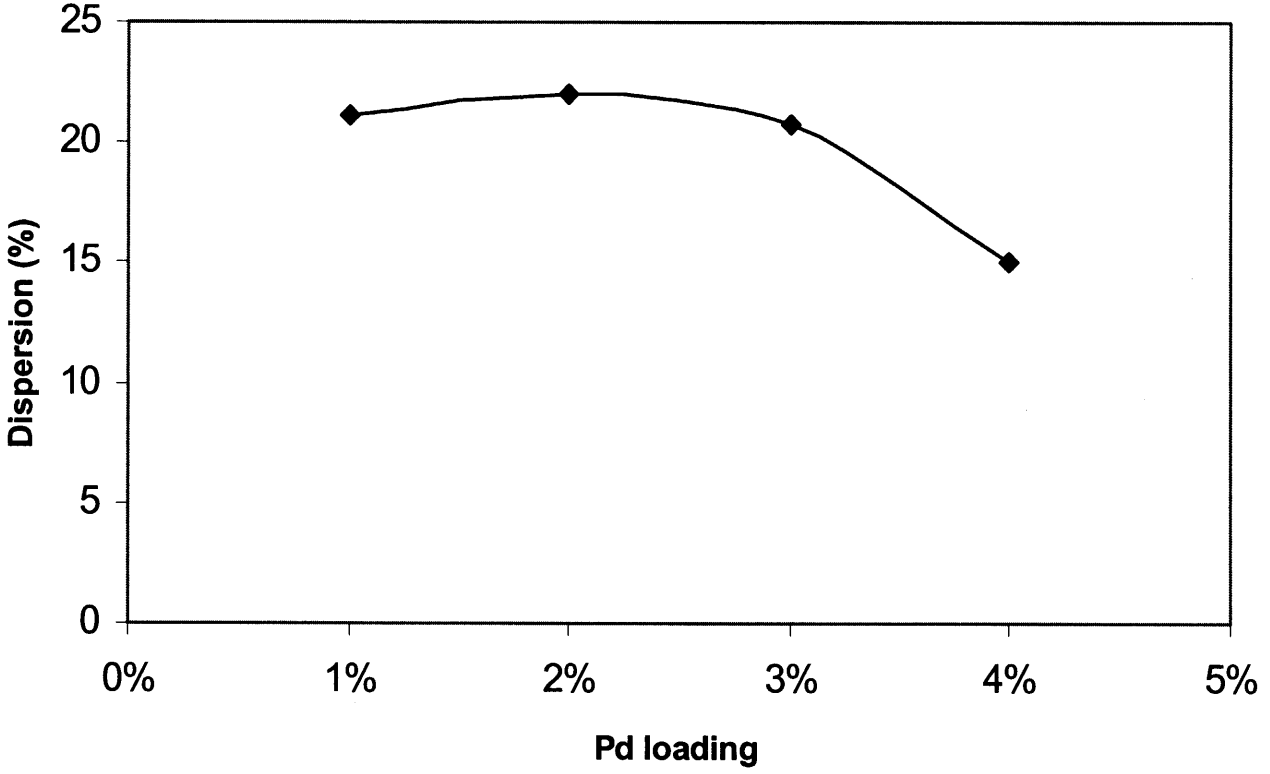

Figure 5.2 Effect of Pd loading on metal dispersion.

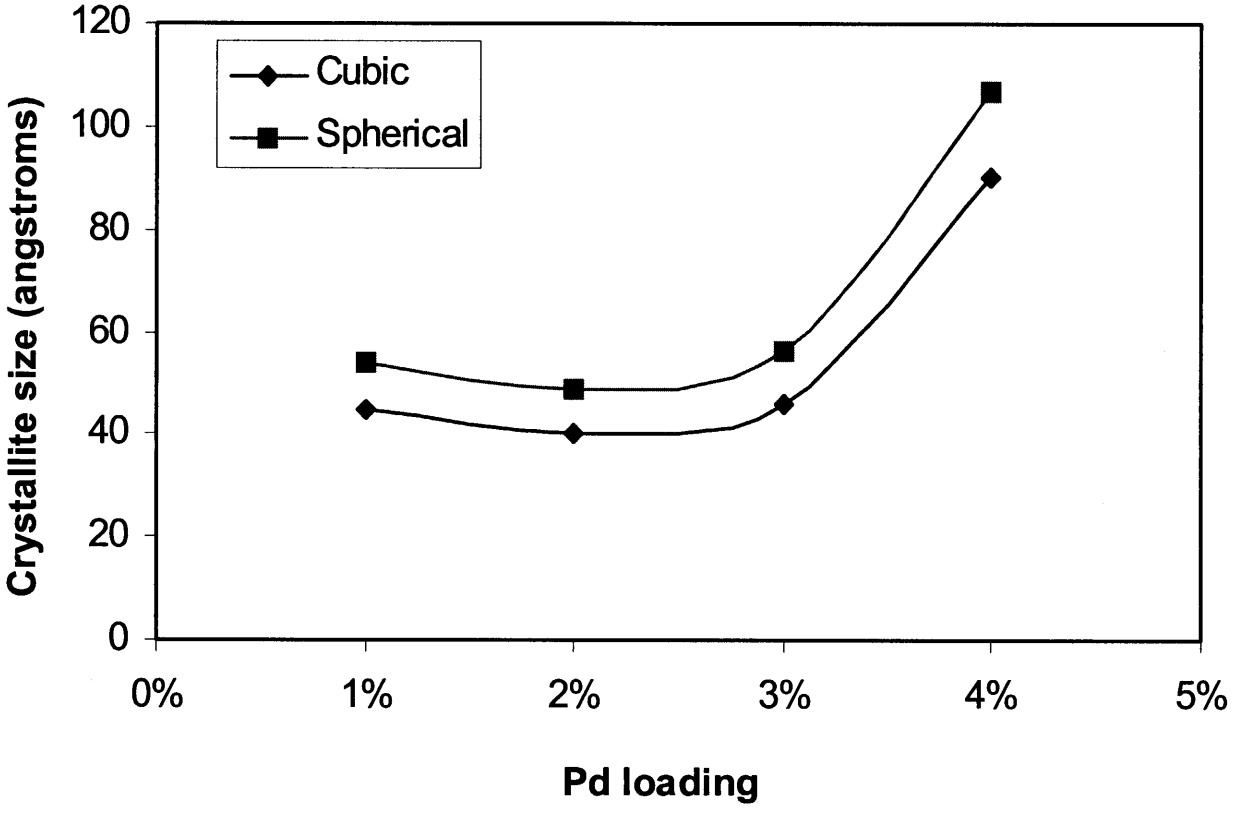

Figure 5.3 Effect of Pd loading on metal crystallite size.

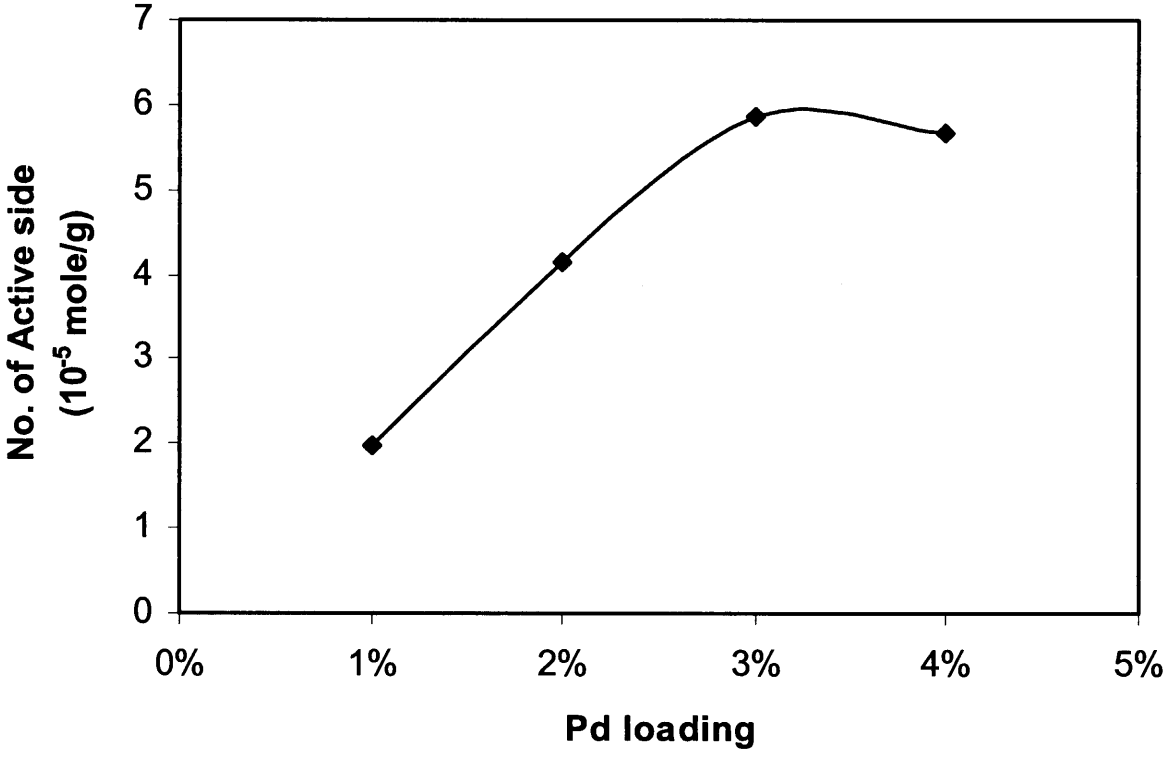

Figure 5.4 Effect of Pd loading on the moles of active site.

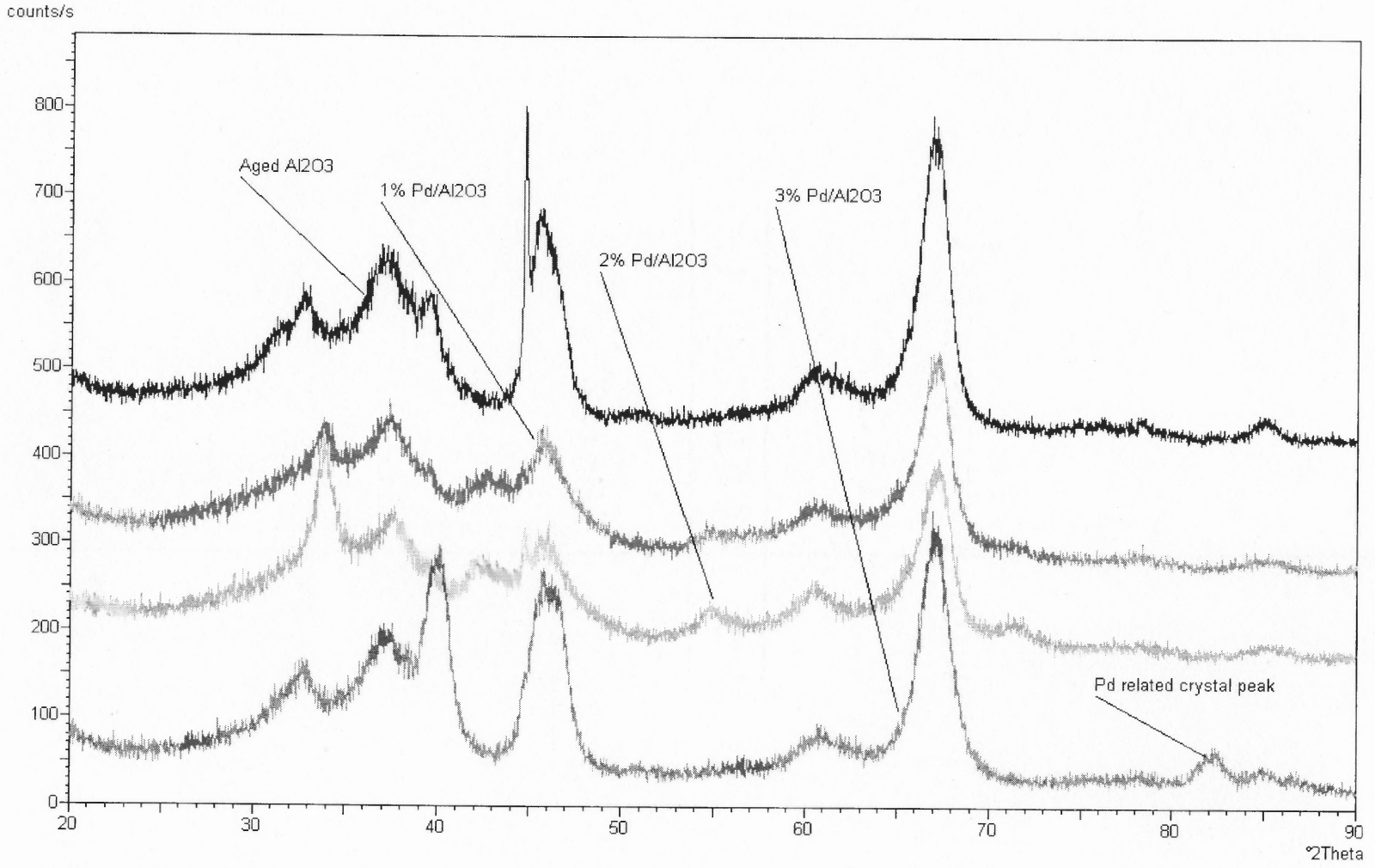

Figure 5.5 XRD pattern of 1-4% Pd on 150 m^2/g γ-Al_2O_3.

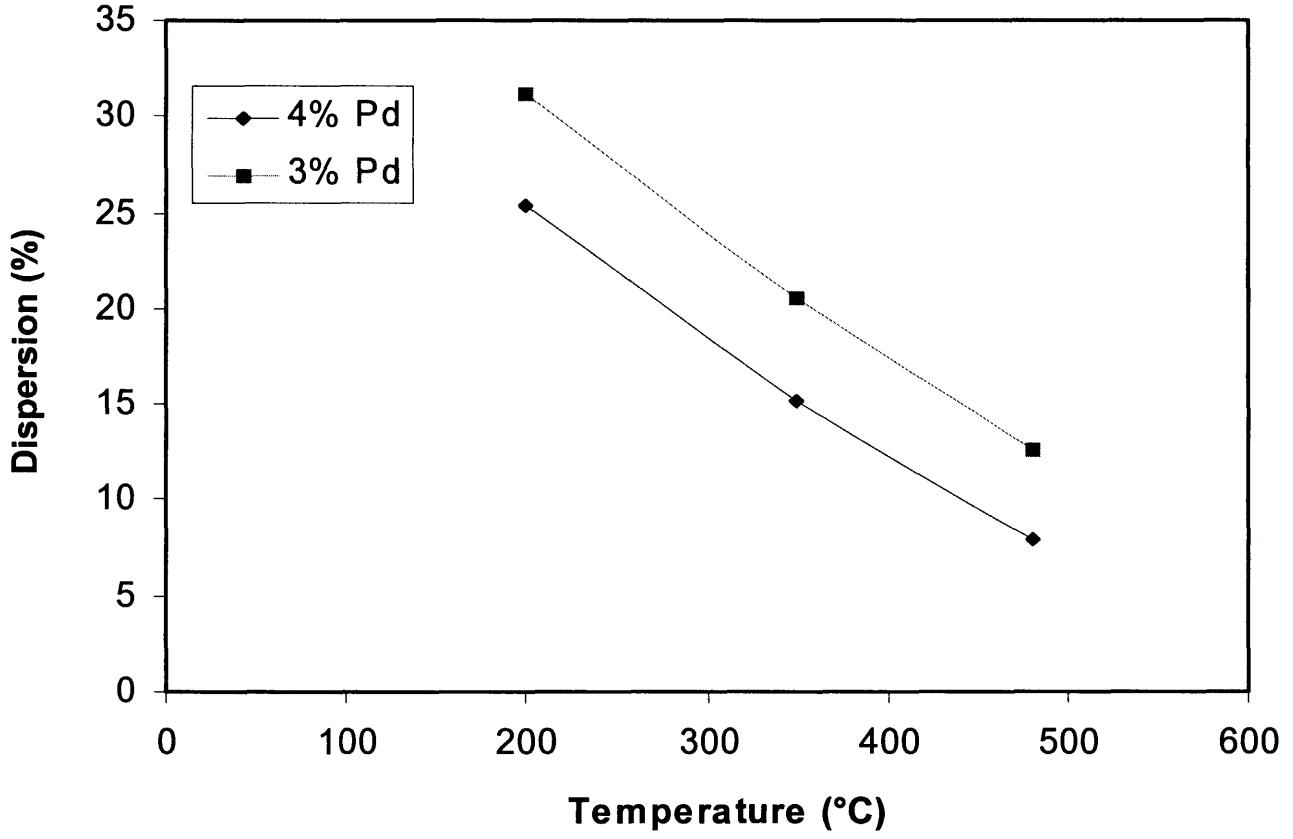

Figure 5.6 Effect of calcination temperature on Pd dispersion.

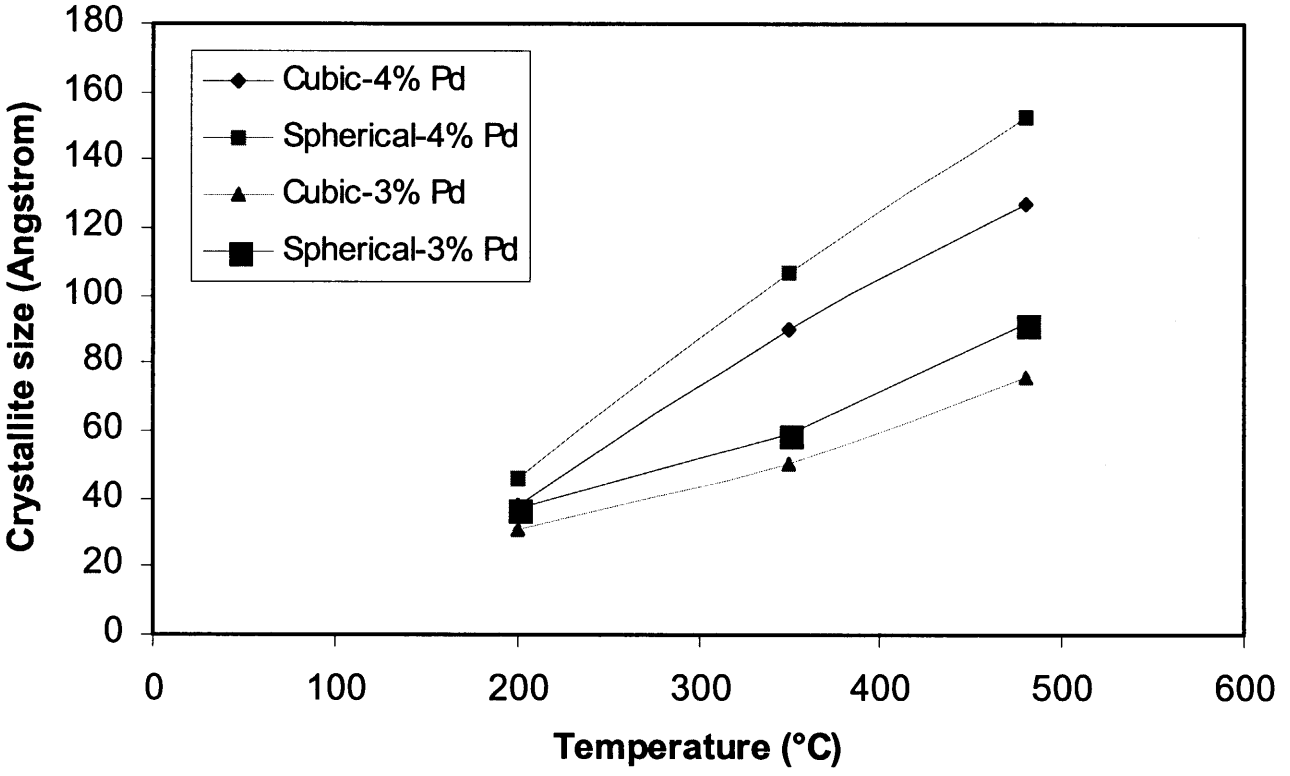

Figure 5.7 Effect of calcination temperature on Pd crystallite size.

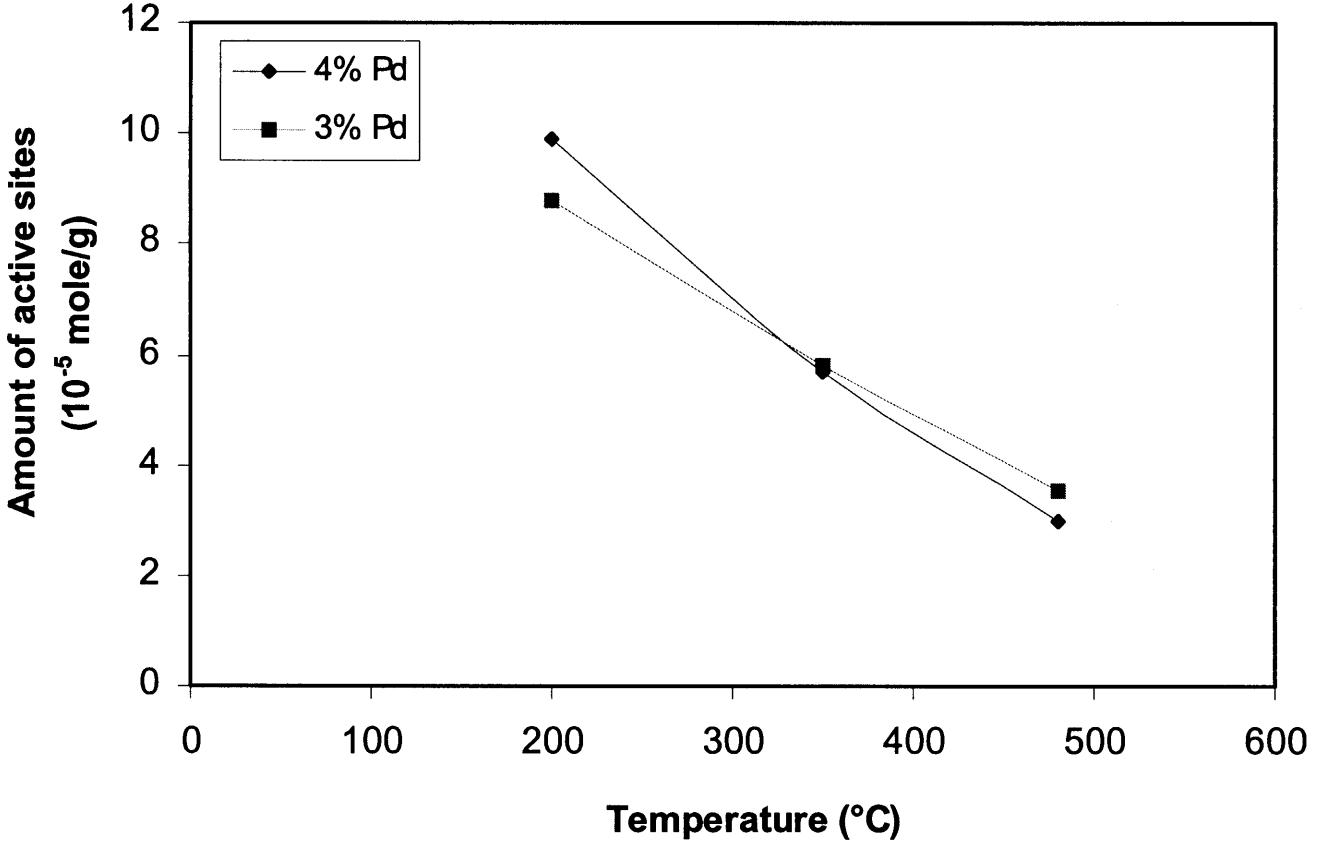

Figure 5.8 Effect of calcination temperature on moles of active sites.

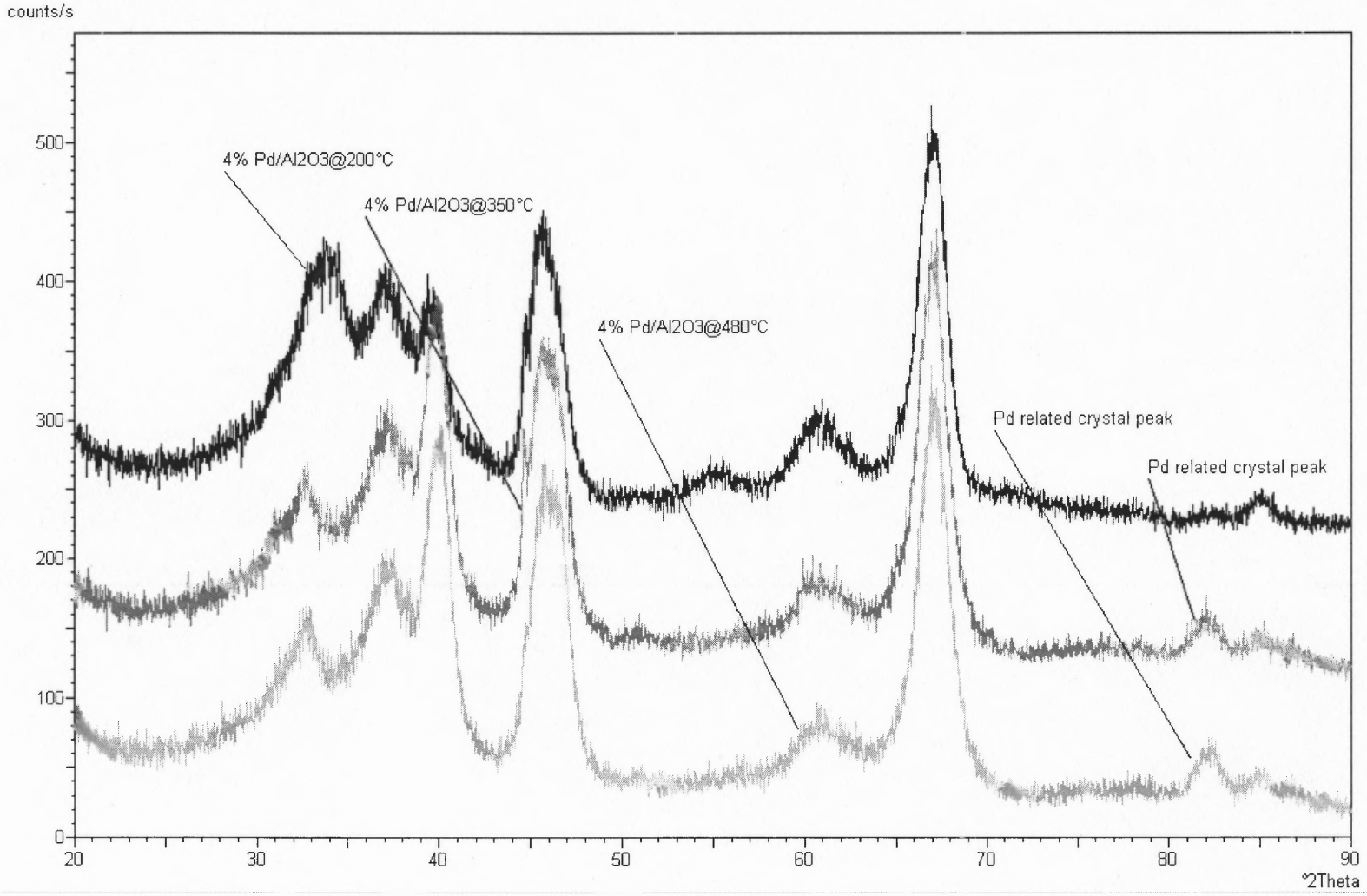

Figure 5.9 XRD pattern of 4% Pd/Al_2O_3 calcinated at different temperature.

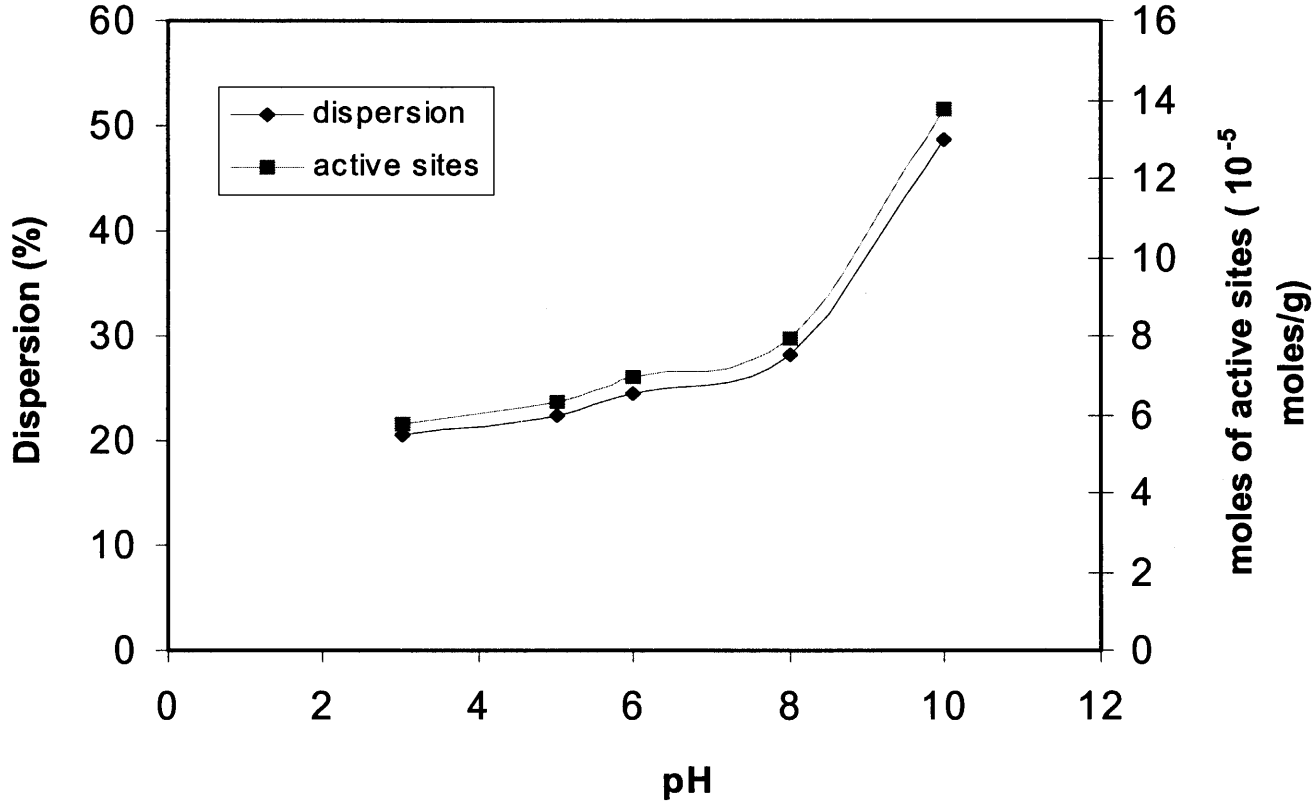

Figure 5.10 Effect of pH on 3% Pd dispersion & moles of active sites on 150 m^2/g γ Al_2O_3.

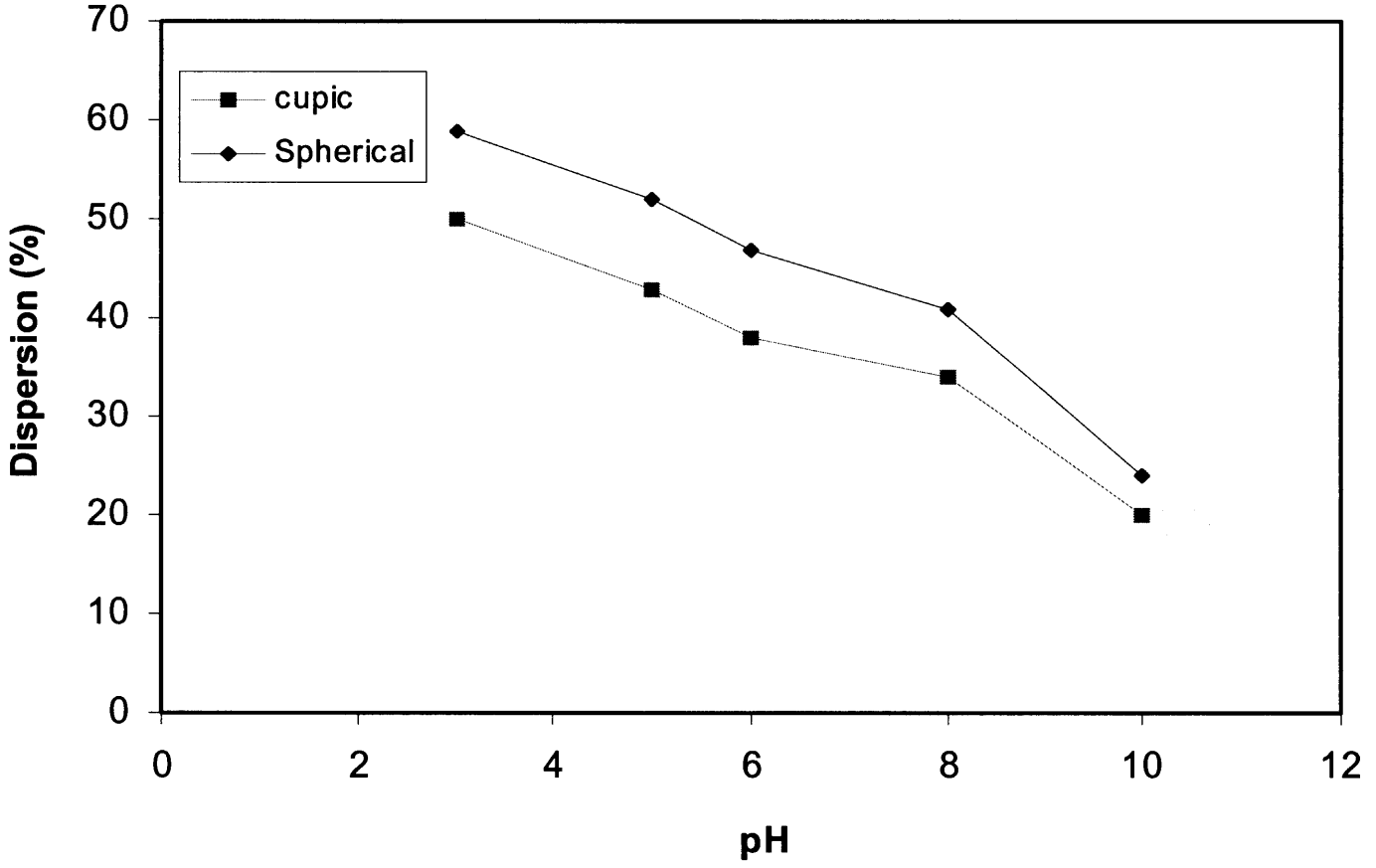

Figure 5.11 Effect of pH on Pd (3%) crystallite size on 150 m^2/g γ-Al_2O_3.

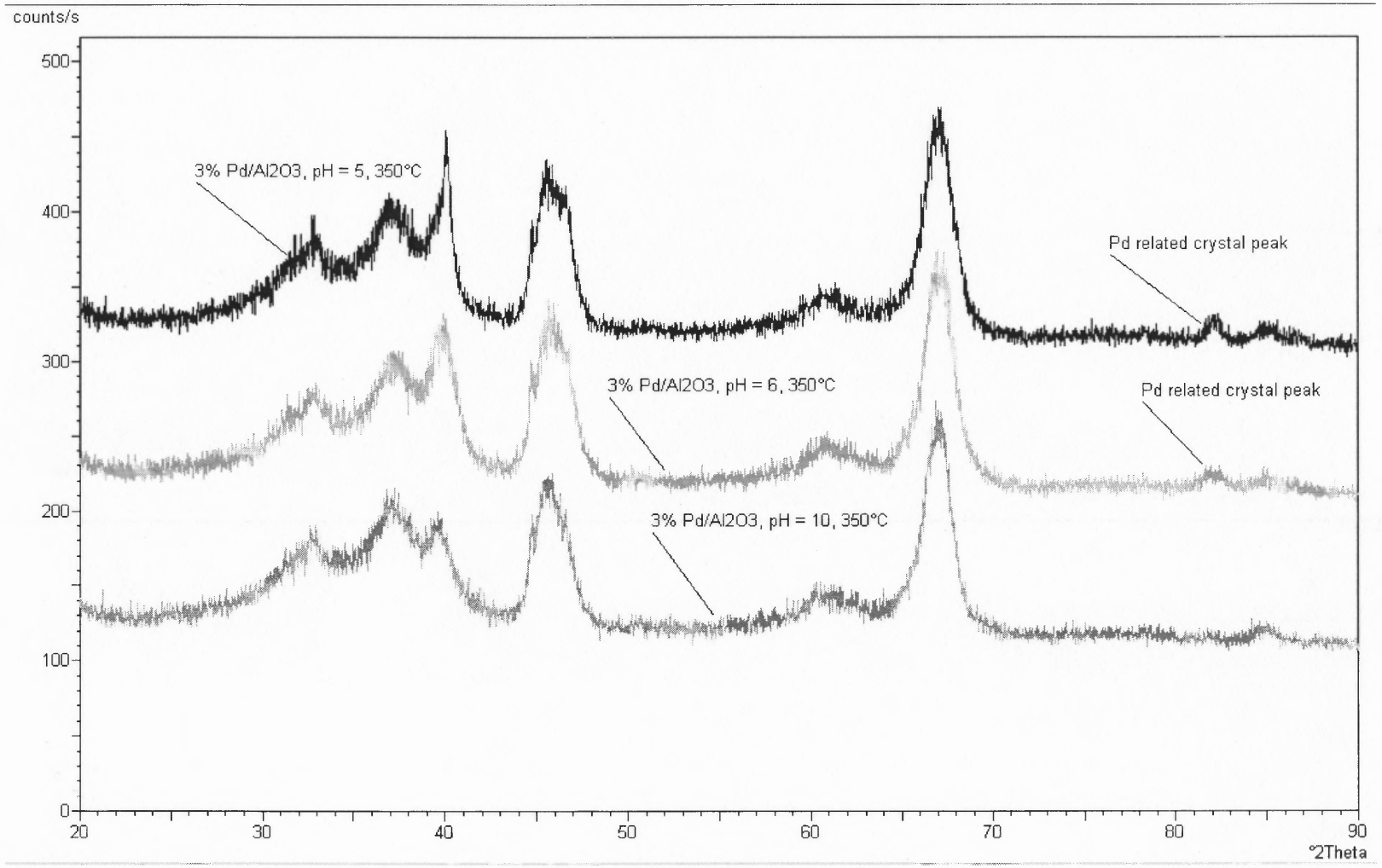

Figure 5.12 XRD pattern of 3% Pd/Al_2O_3 impregnation under different pH.

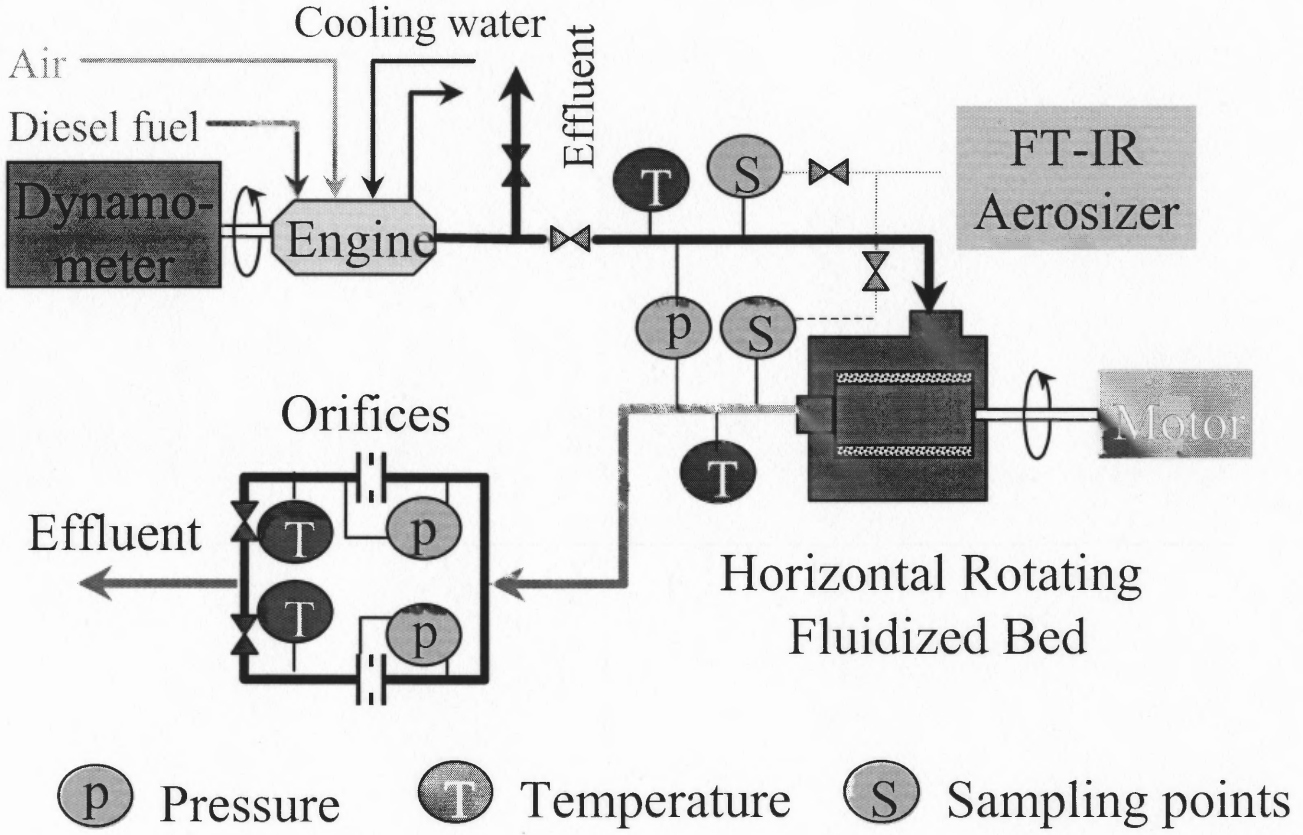

Figure 6.1 Schematic diagram of bench experimental set up.

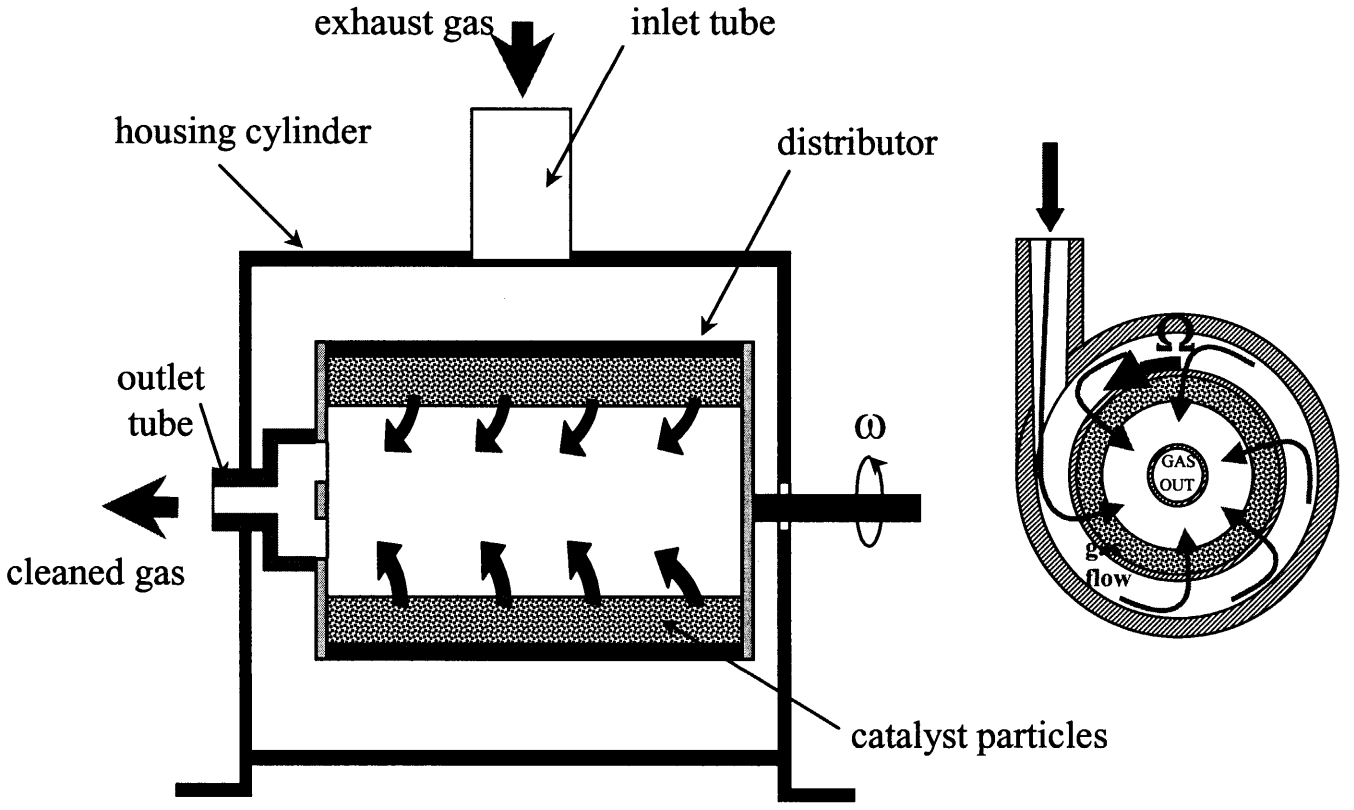

Figure 6.2 Rotating fluidized bed reactor.

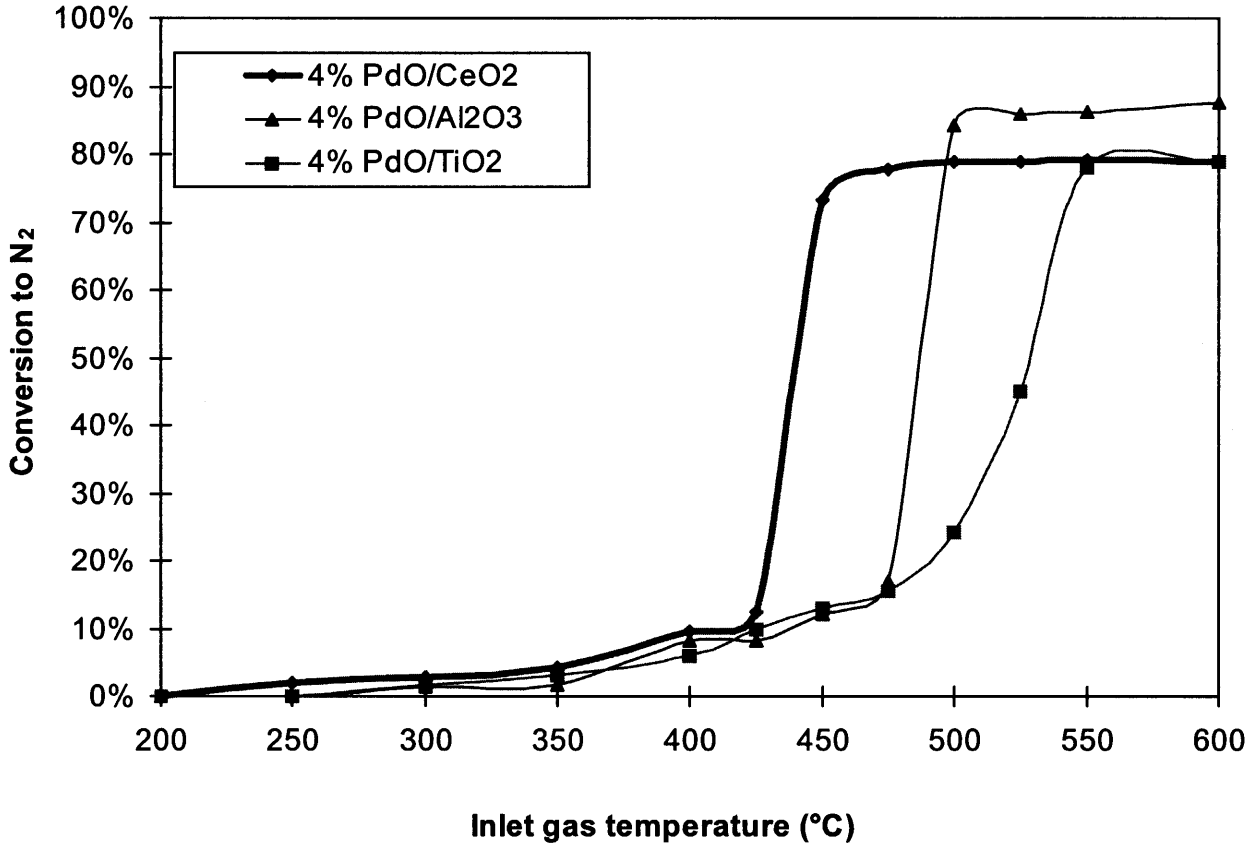

Figure 6.3 Catalytic activity of palladium catalysts under reaction condition: [NO] = 590 ppm, $[O_2]$ = 10%; GHSV = 50,000.

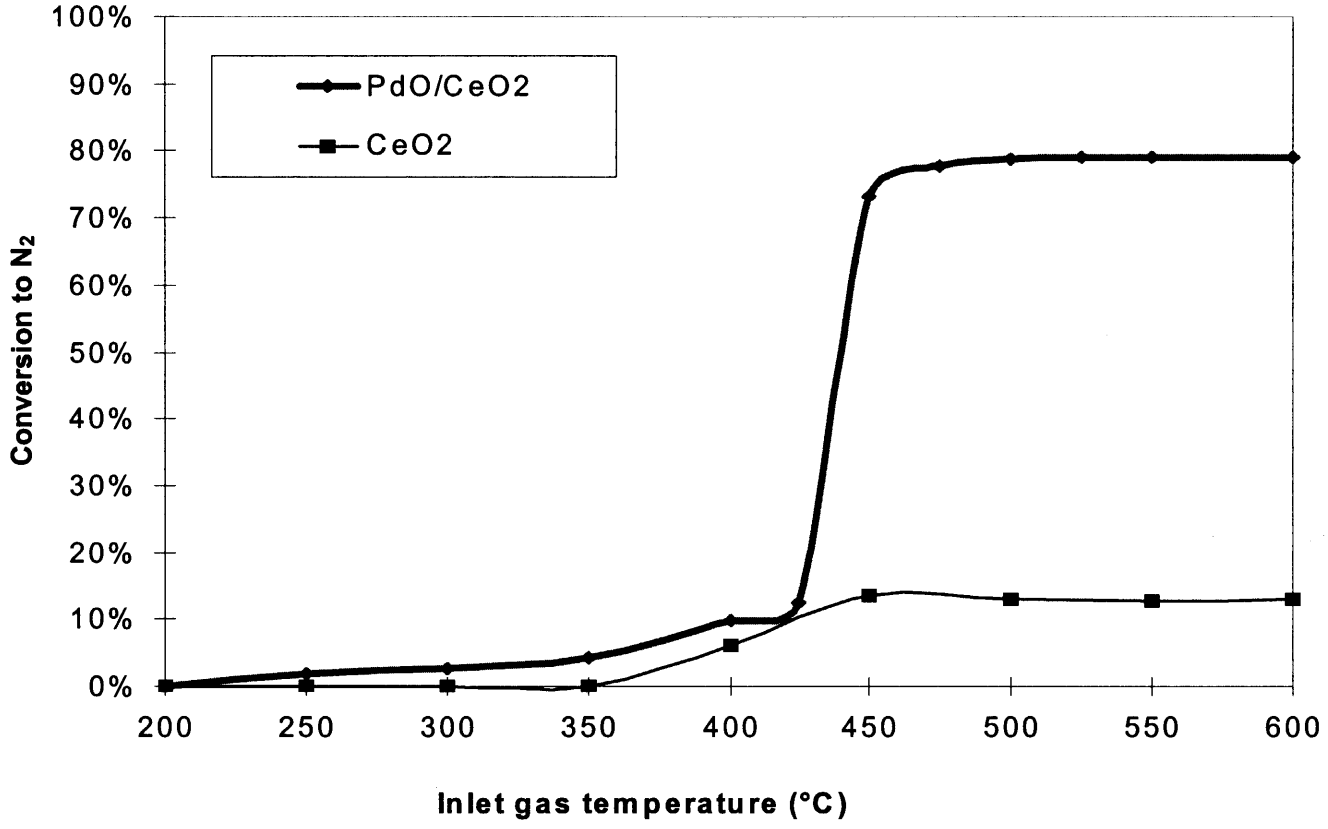

Figure 6.4 Comparing PdO/CeO_2 and CeO_2 activity on reaction NO + GAC under reaction condition: [NO] = 590 ppm, $[O_2]$ = 10%; GHSV = 50,000.

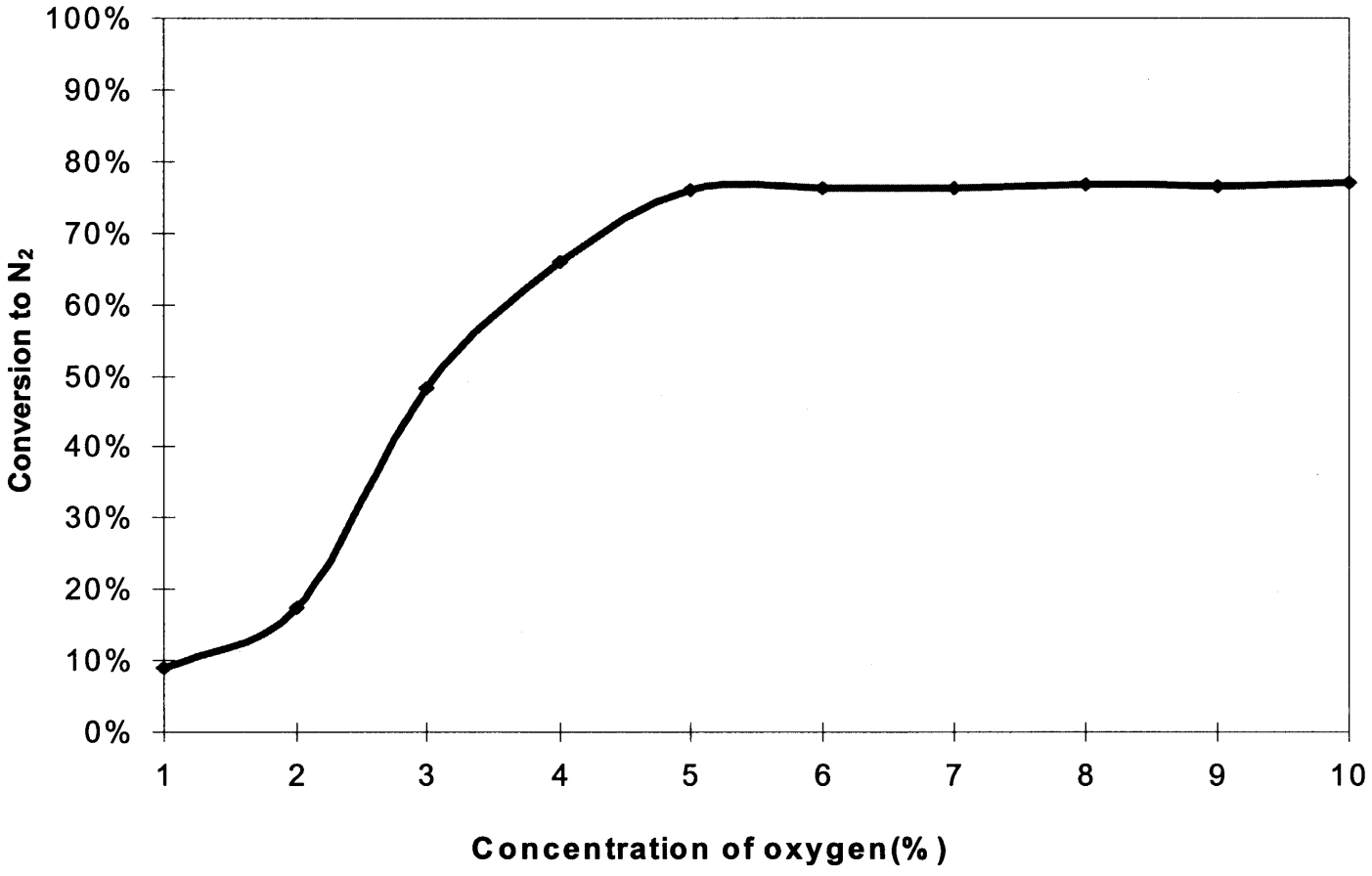

Figure 6.5 Effect of oxygen concentration on NO reduction to N_2 over PdO/CeO_2 under reaction condition: [NO] = 590 ppm, GHSV = 50,000, inlet gas temperature 500°C.

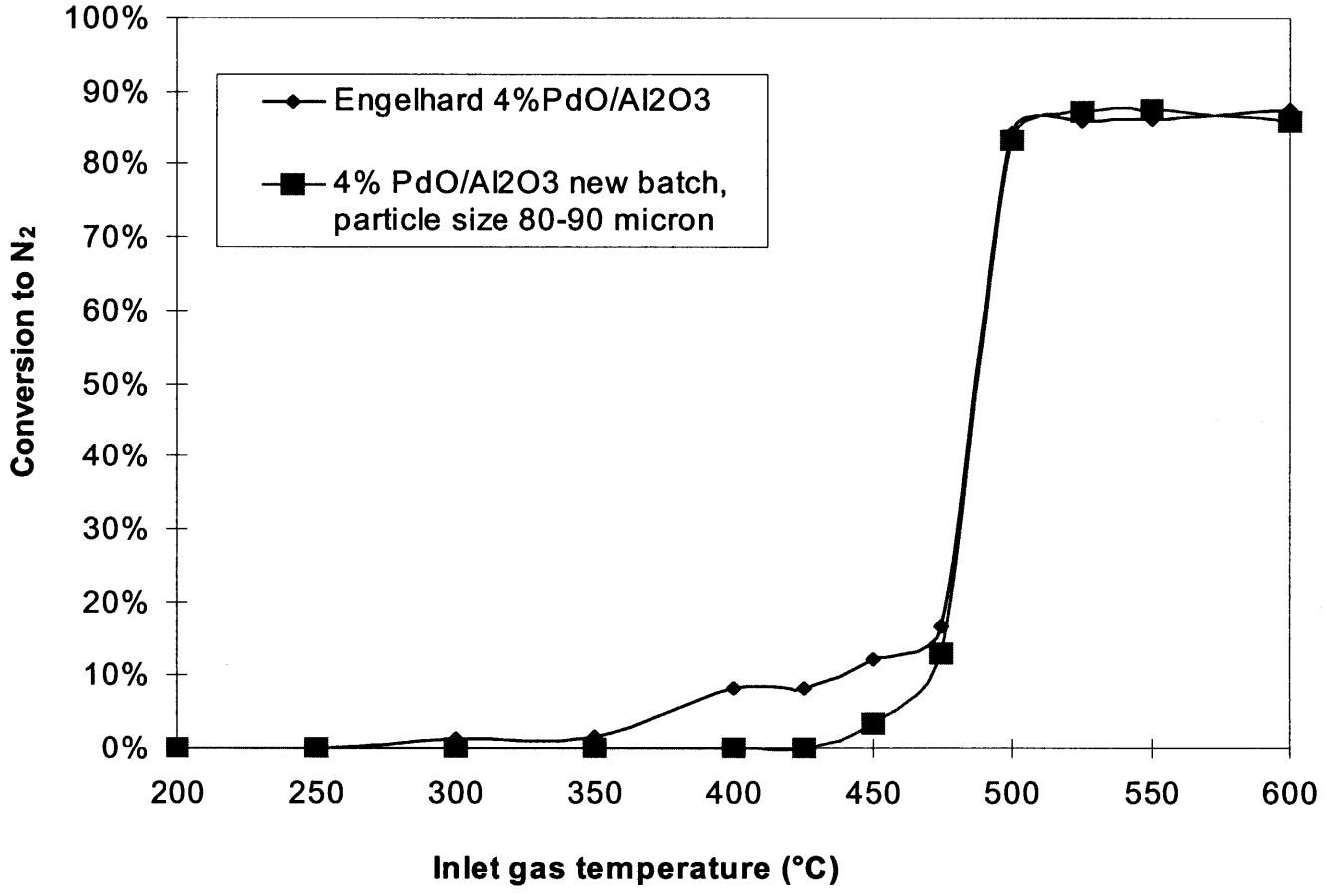

Figure 6.6 Effect of catalyst particle size on NO reduction to N_2 under reaction conditions: [NO] = 590 ppm; [O_2] = 10%; GHSV = 50,000.

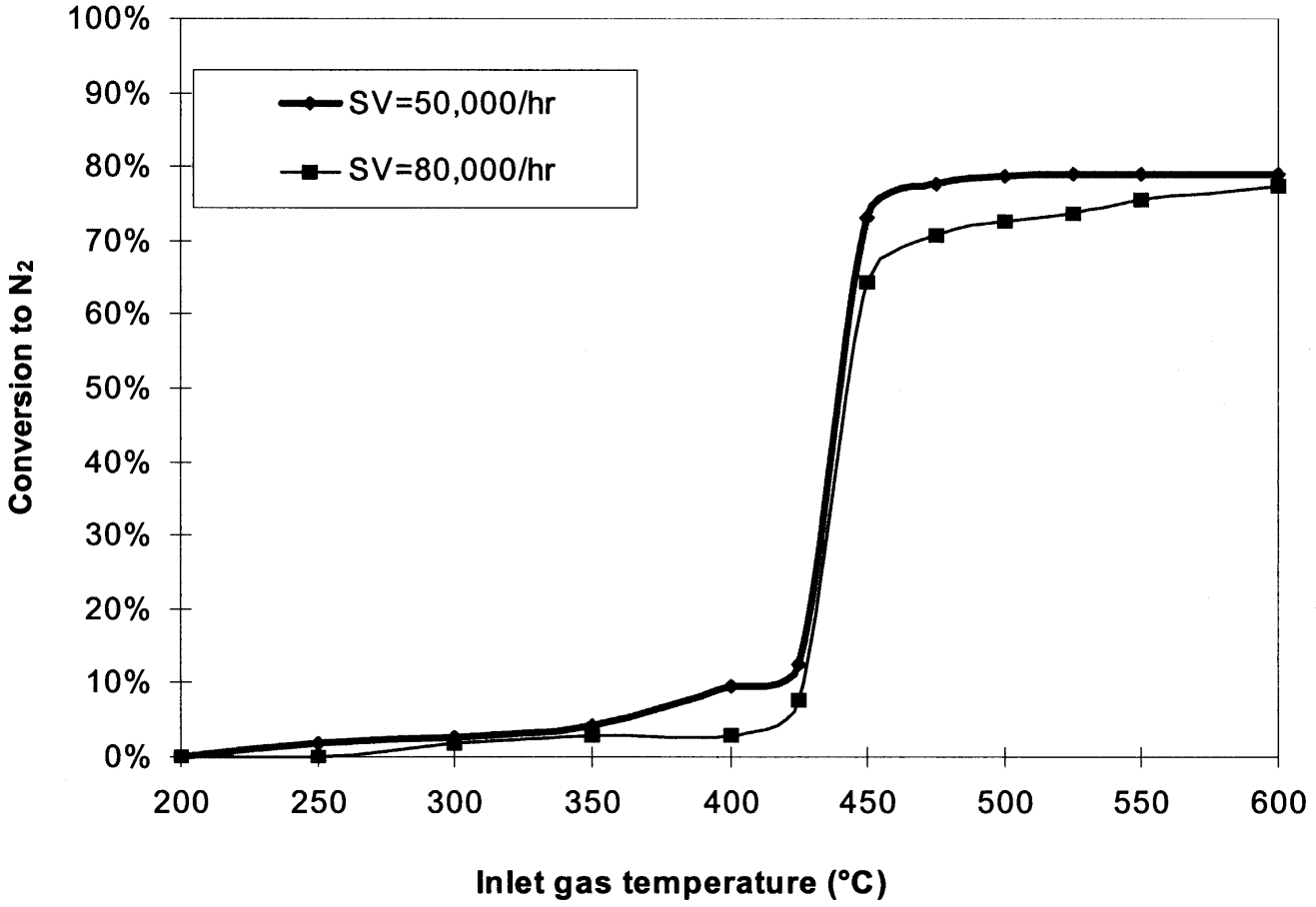

Figure 6.7 Effect of space velocity on NO reduction to N_2 over PdO/CeO_2 under reaction condition: [NO] = 590 ppm; [O_2] = 10%.

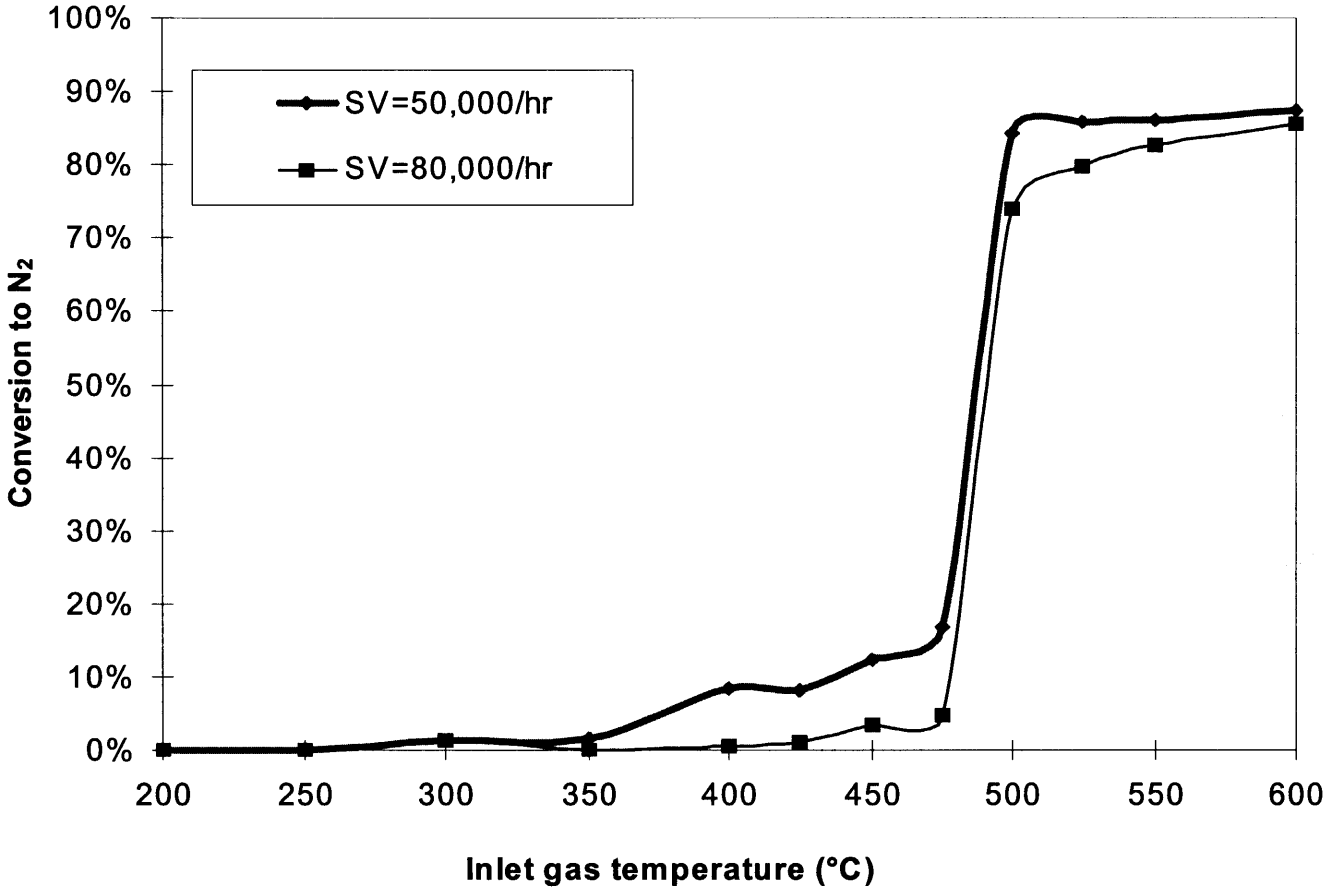

Figure 6.8 Effect of space velocity on NO reduction to N_2 over PdO/Al_2O_3under reaction condition: [NO] = 590 ppm; [O_2] = 10%.

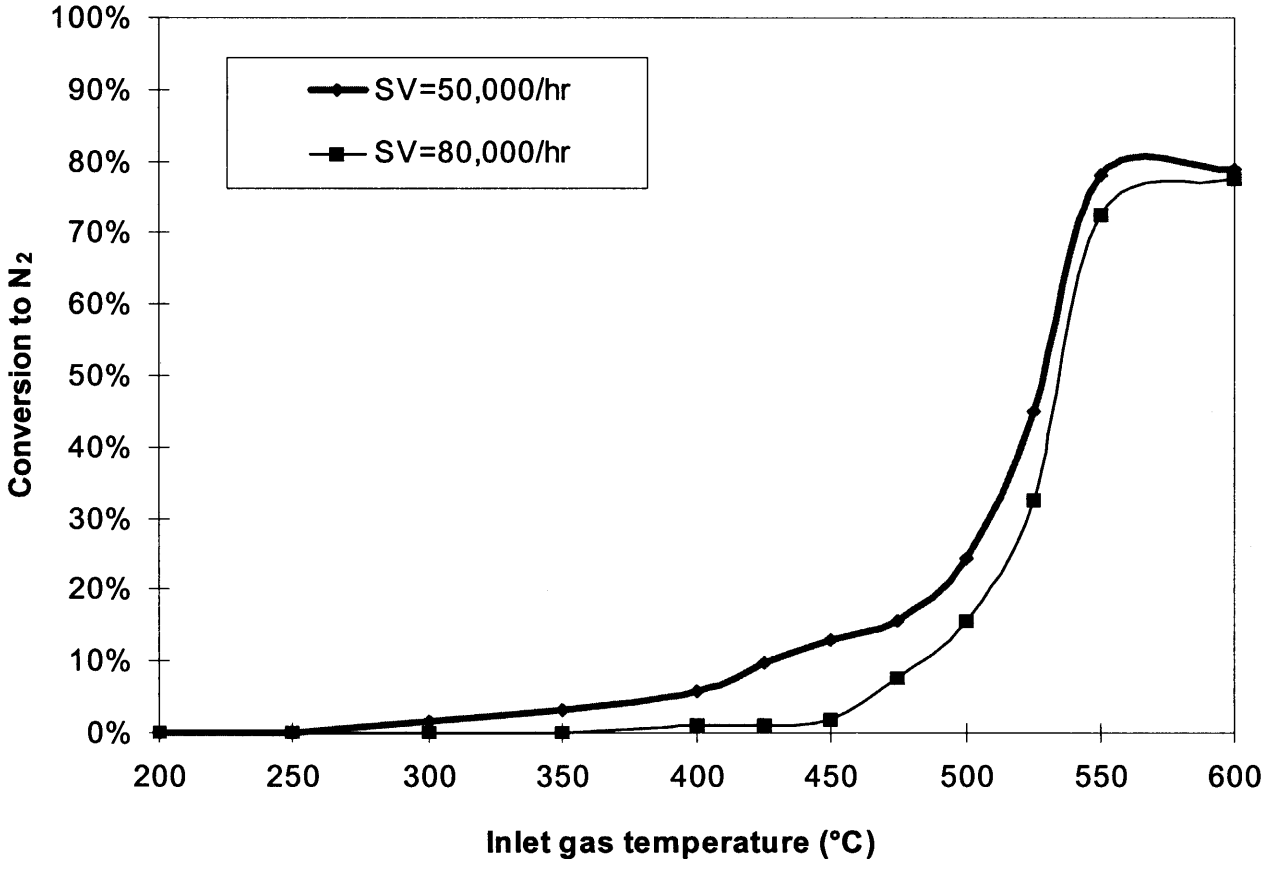

Figure 6.9 Effect of space velocity on NO reduction to N_2 over PdO/TiO_2 under reaction condition: [NO] = 590 ppm, $[O_2]$ = 10%.

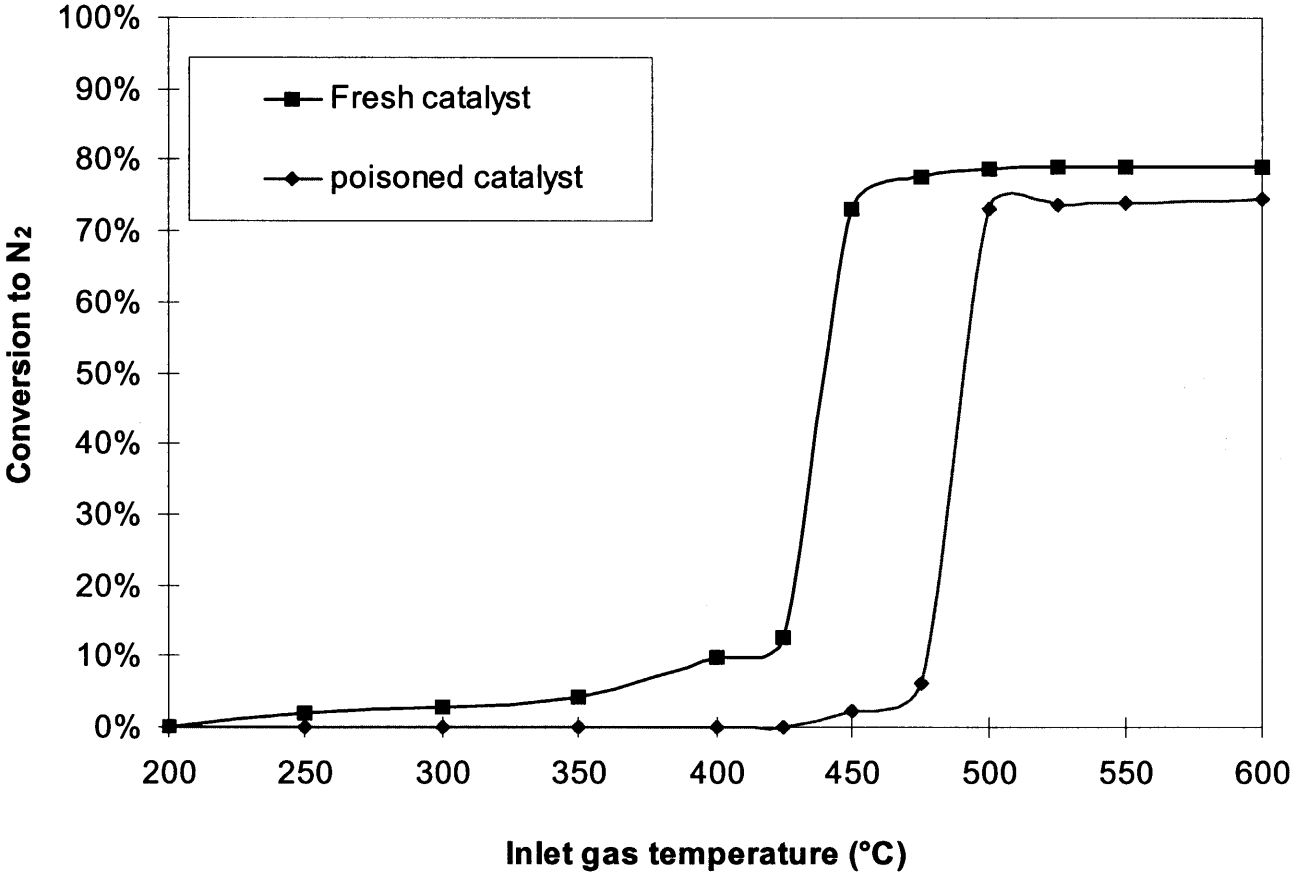

Figure 6.10 Effect of SO_2 and water on reduction of NO to N_2 over PdO/CeO_2 under reaction condition: [NO] = 590 ppm, [O_2] = 10%, [SO_2] = 20ppm, [H_2O] = 10%, 15 hr, GHSV = 50,000.

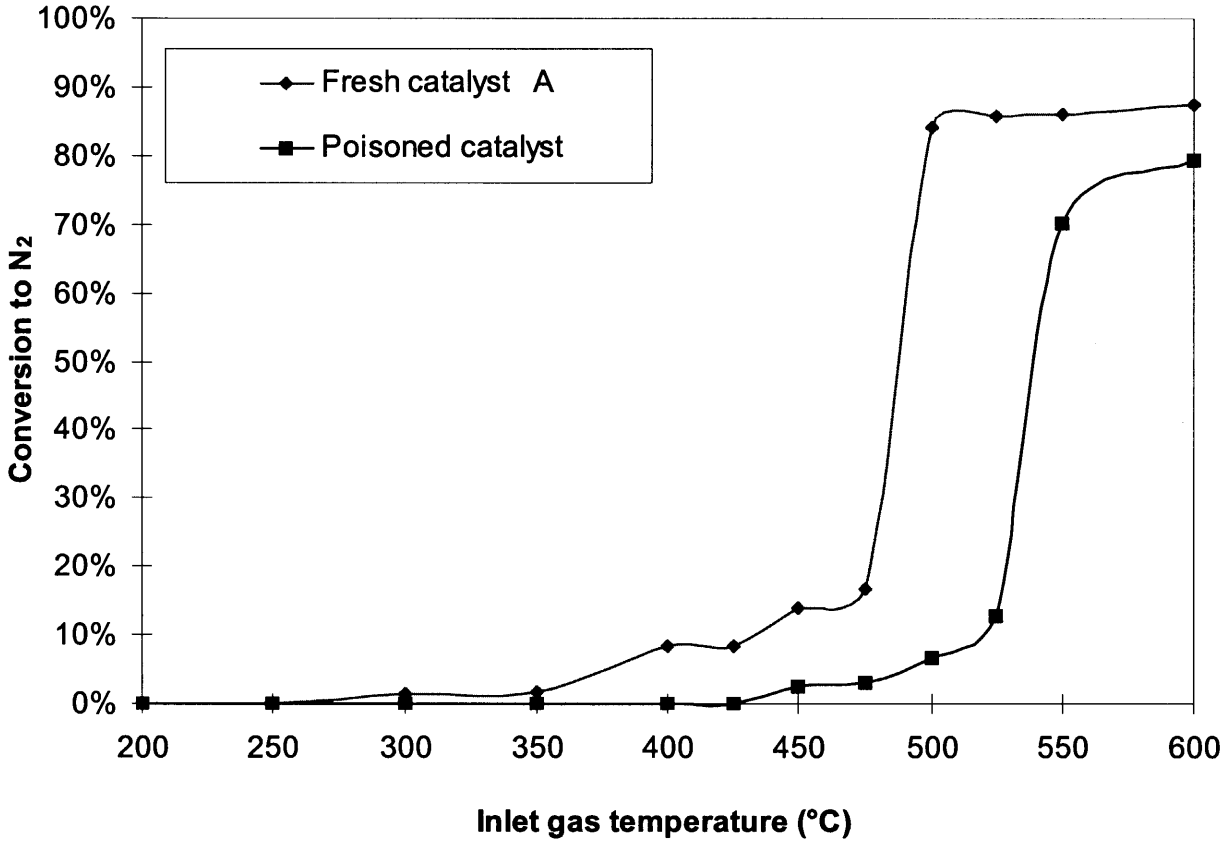

Figure 6.11 Effect of SO_2 and water on reduction of NO to N_2 over PdO/Al_2O_3 under reaction condition: [NO] = 590 ppm, $[O_2]$ = 10%, $[SO_2]$ = 20ppm, $[H_2O]$ = 10%, 15 hr, GHSV = 50,000.

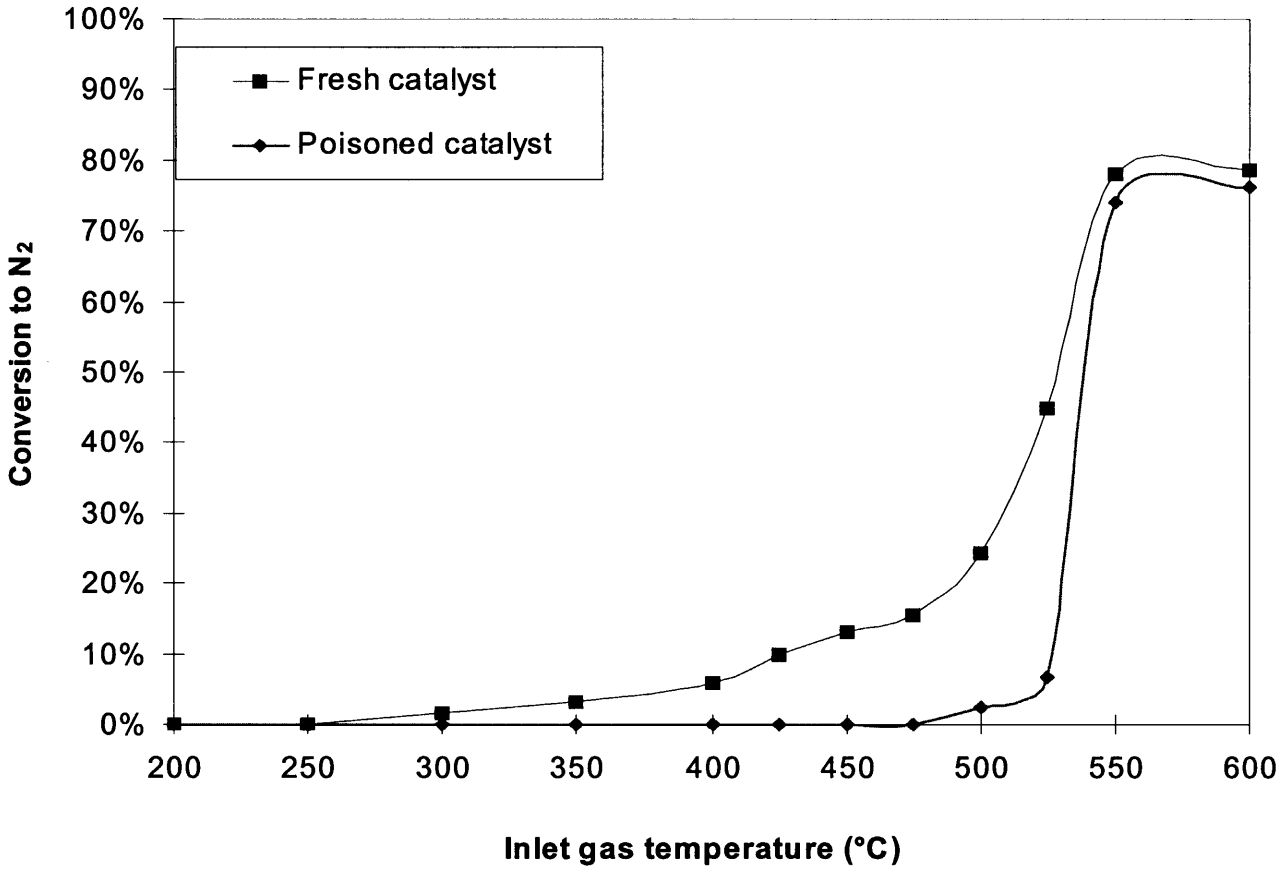

Figure 6.12 Effect of SO_2 and water on reduction of NO to N_2 over PdO/TiO_2 under reaction condition: [NO] = 590 ppm, [O_2] = 10%, [SO_2] = 20ppm, [H_2O] = 10%, 15 hr, GHSV = 50,000.

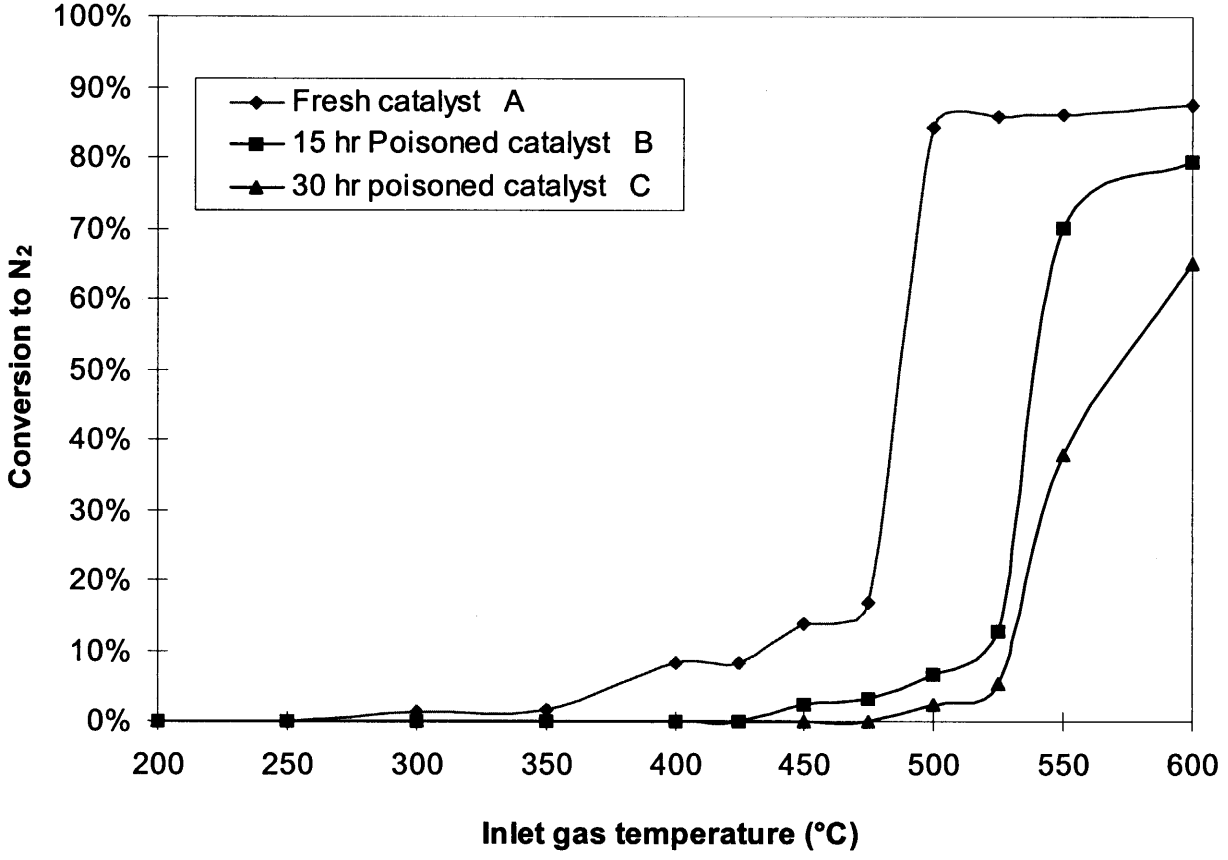

Figure 6.13 Effect of SO_2 and water on reduction of NO to N_2 over PdO/Al_2O_3 under reaction condition: [NO] = 590 ppm, [O_2] = 10%, [SO_2] = 20 ppm, [H_2O] = 10%, GHSV = 50,000.

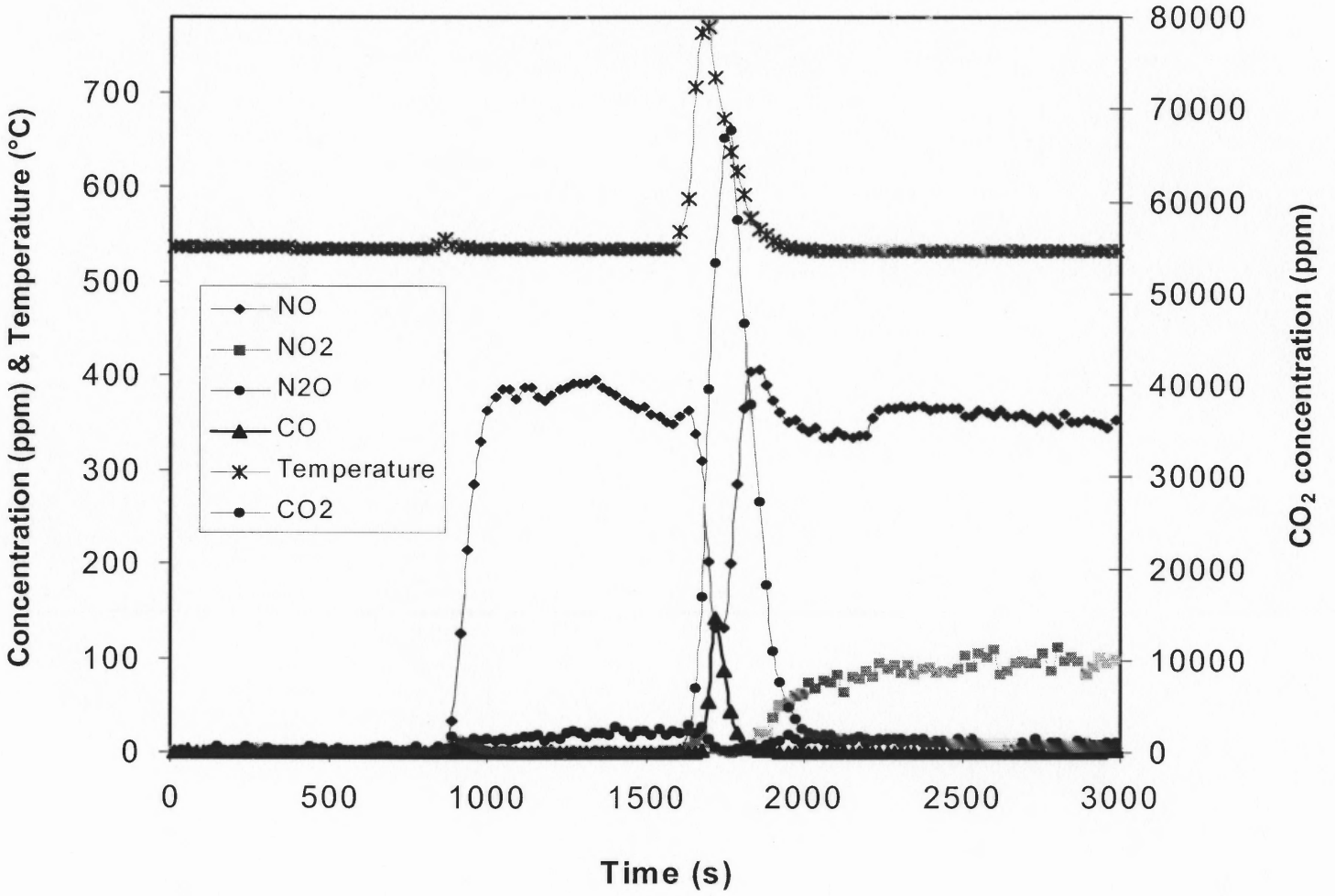

Figure 6.14 NO + O_2 over 0.0646g GAC + 0.5297g 3% PdO/Al_2O_3 (v/v=1), GSHV=50,000, [NO]=515 ppm, $[O_2]$=10%, $T_{furnace}$=490°C.

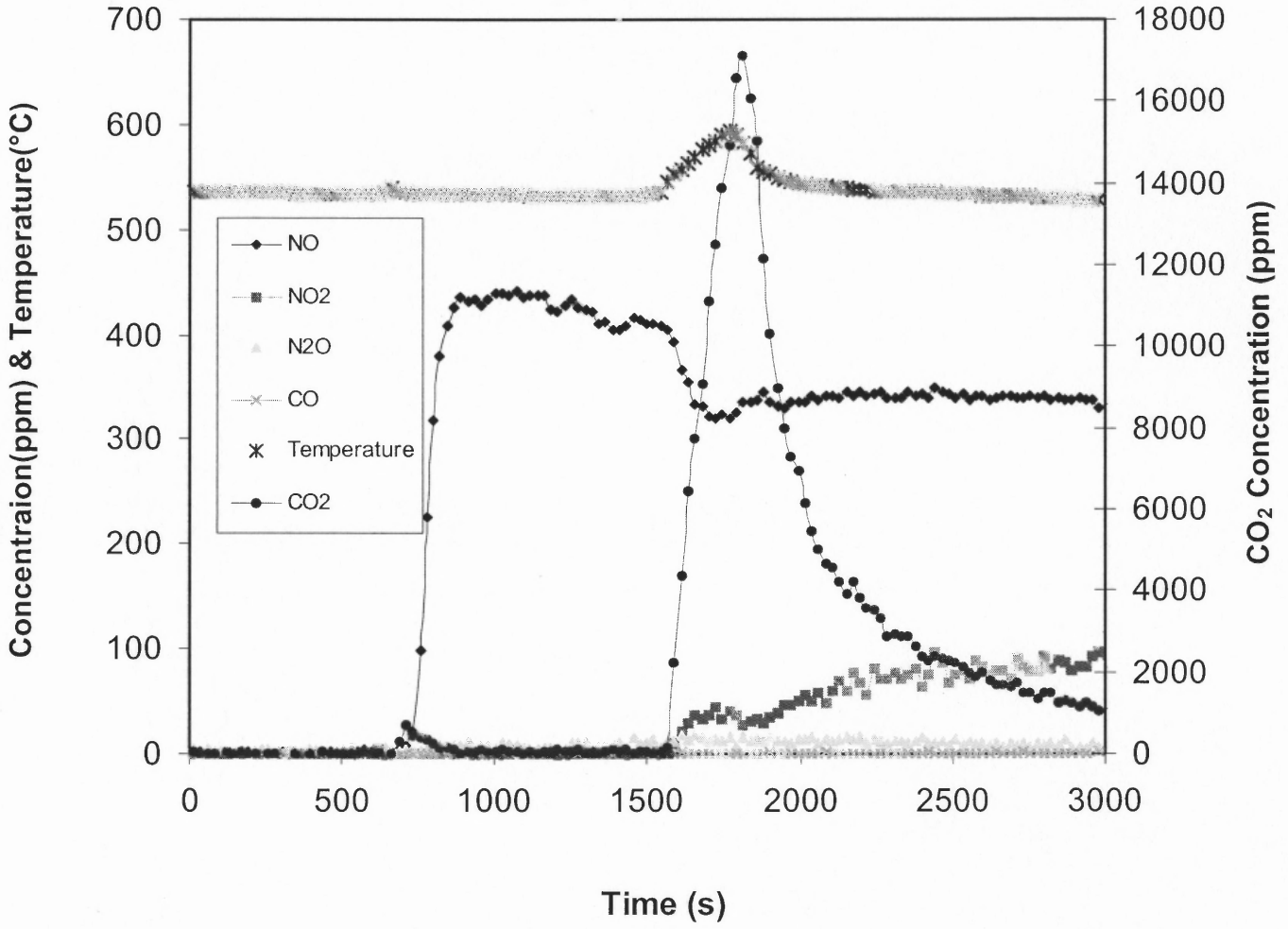

Figure 6.15 NO + O_2 over 0.7092g 3% PdO/Al_2O_3 + 0.0427 g GAC (v/v=2), GSHV=50,000, [NO]=520 ppm, $[O_2]$=10%, $T_{furnace}$=490°C.

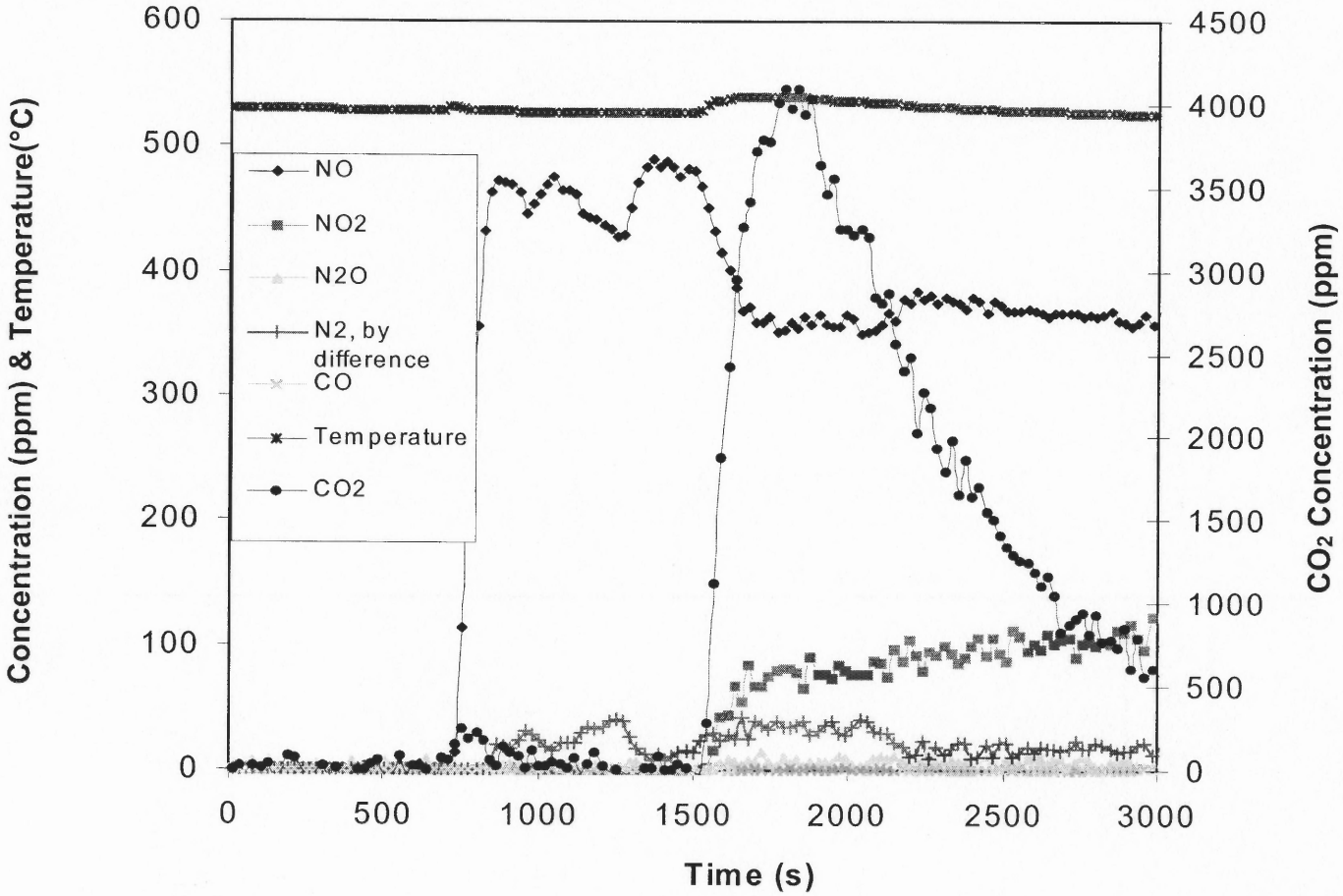

Figure 6.16 NO + O_2 over 3% 0.8634g PdO/Al_2O_3 + 0.0267g GAC (v/v=5), GSHV=50,000, [NO]=510 ppm, $[O_2]$=10%, $T_{furnace}$=490°C.

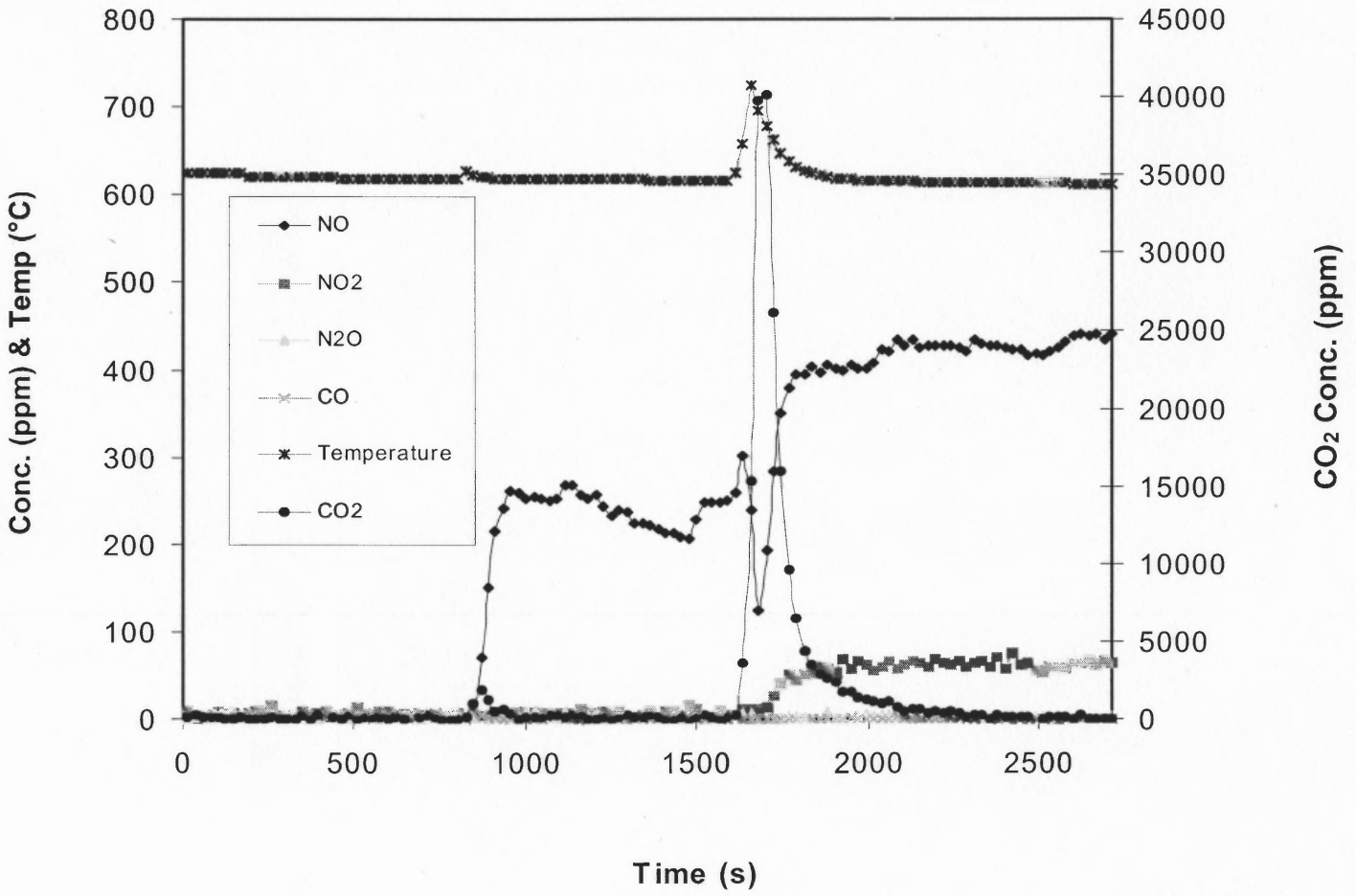

Figure 6.17 NO + O_2 over 1.25ml (0.8828g) PdO/Al_2O_3 + 0.25ml (0.0213g)GAC, GHSV = 50,000, [NO] = 500 ppm, [O_2] = 10%, $T_{furnace}$ = 580°C.

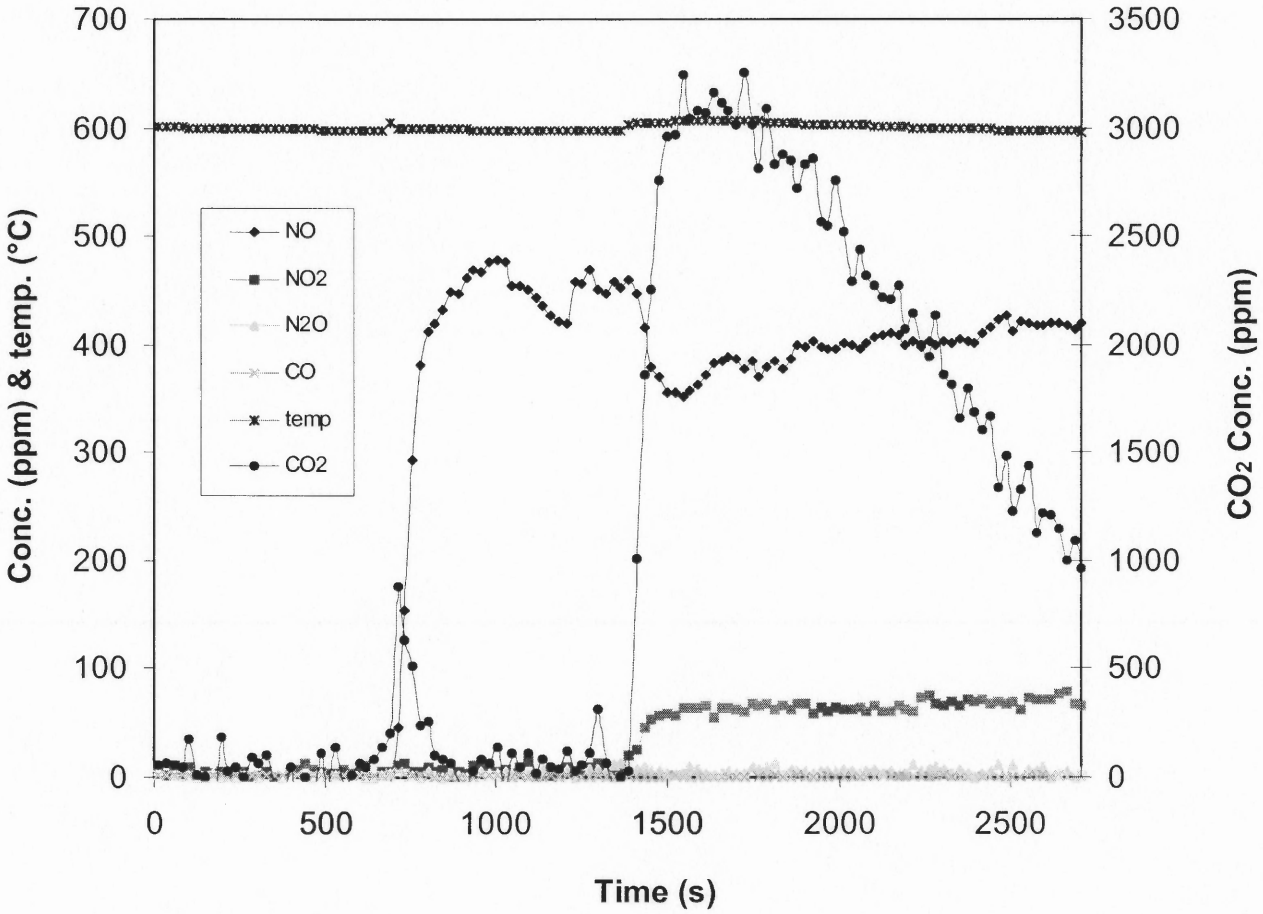

Figure 6.18 NO + O_2 over 0.25 ml GAC + 1.25 ml alumina, GHSV = 50,000, [NO] = 500 ppm, $[O_2]$=10%, $T_{furnace}$ = 560°C.

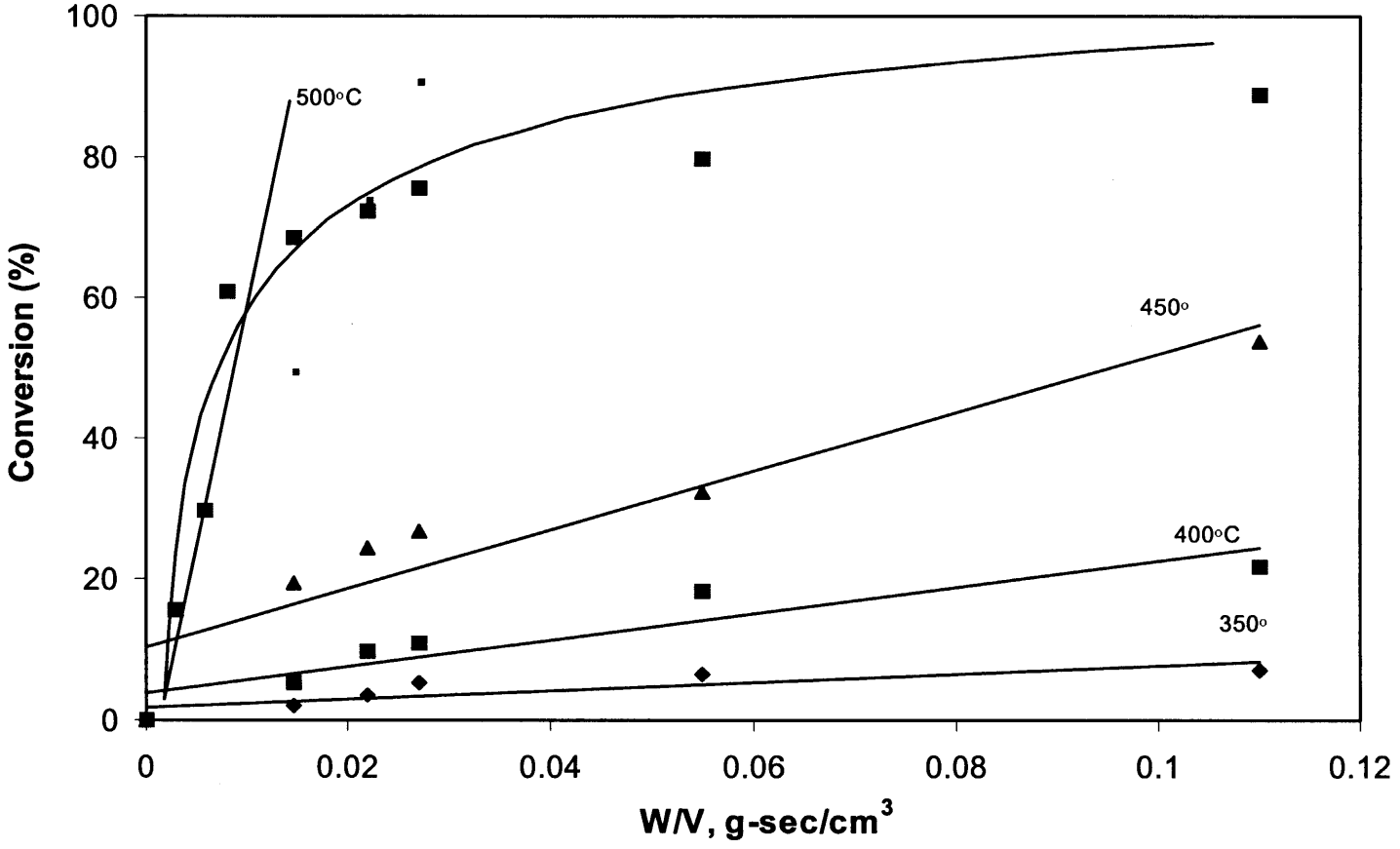

Figure 6.19 Initial slope for kinetic calculation for the NO-O_2-GAC reactions at 350, 400, 450, 500°C.

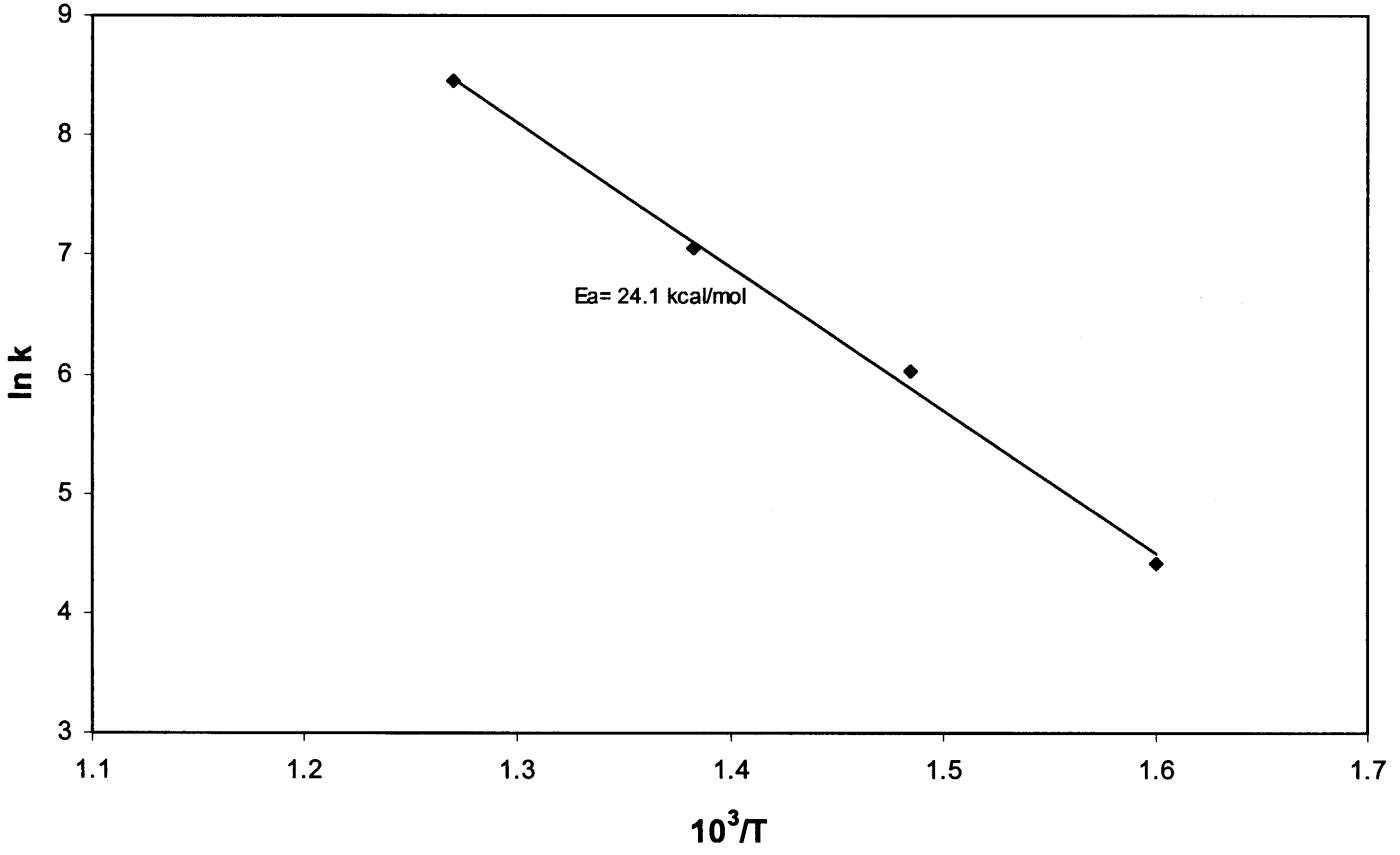

Figure 6.20 Arrhenuis Plot of NO_x Reduction with GAC over PdO/Al_2O_3 Catalyst.

APPENDIX B

TABLES OF EXPERIMENT RESULTS

Tables of the experiment results for Chapter 3 to Chapter 6.

Table 2.1 Example of Experimental Data Statistics

	Maximum Conversion to N_2 in each Space Velocity (%)				
Experiment	2,000/hr	20,000/hr	40,000/hr	50,000/hr	80,000/hr
1	56.78	38.53	14.79	9.63	7.82
2	55.43	36.02	16.03	10.46	8.46
3	58.16	35.46	14.66	9.56	8.42
4	59.03	35.71	16.08	9.26	7.55
5	57.21	37.77	15.65	10.08	7.91
Average	57.32	36.71	15.44	9.80	8.03
% RSD	2.39	3.69	4.38	4.82	4.92

%RSD is calculated as: $\%RSD = (\Sigma(Xi - X_a)^2/n\text{-}1)^{1/2}/X_a * 100$, X_a: average value.

Table 3.1 Carbon/Copper Mole Ratios for the Catalysts Used

Catalyst	Cu-GAC			GAC/Cu-ZSM-5	
				5% / 95%	50% / 50%
wt% Cu	1% Cu	10% Cu	20% Cu	1.1%	0.6%
Mole C / Mole Cu	524	48	21	23	441

Table 3.2 Catalyst Components

Catalyst	Volume (cm^3)	Mass (g)	Particle size (μm)
1% Cu-GAC	1.5 ± 0.05	0.48 ± 0.02	<20
GAC	1.5 ± 0.05	0.42 ± 0.02	<20
95% wt Cu-ZSM-5 + 5% wt GAC	Cu-ZSM-5: 1.25 ± 0.05 GAC: 0.15 ± 0.05	Cu-ZSM-5: 1.10 ± 0.02 GAC: 0.055 ± 0.003	Cu-ZSM-5: 60 ~ 80 GAC: <20
50% wt Cu-ZSM-5 + 50% wt GAC	Cu-ZSM-5: 0.43 ± 0.05 GAC: 1.0 ± 0.05	Cu-ZSM-5: 0.38 ± 0.02 GAC: 0.38 ± 0.03	Cu-ZSM-5: 60 ~ 80 GAC: <20

Table 3.3 Cu-GAC Isothermal Reactions

Ratio* (V/V)	Weight % of Cu-GAC In the bed	Peak temperature (°C)	Conversion to N_2(%) at Peak temperature	CO conc. at peak temperature (ppm)
1/0	100	763	60.5	11,200
1/2	12	690	47.9	1,850
1/4	7	674	43.5	1,435
1/5	5	627	29.6	211

*Volume ratio of Cu-GAC to α-Al_2O_3.
All experiments have been carried out at 500°C inlet gas temperature, GSHV of 50,000, [NO]=500 ppm, and [O_2]=10%.

Table 4.1 NO reduction with Cu-GAC[a]

Ratio[b] (v/v)	Wt.%[c] (%)	PT[d] (°C)	Conversion[e] at PT (%)	CO at PT (ppm)	Maximum Conversion[f] (%)	Maximum CO at PT (ppm)
1/0	100	763	60.5	11200	94.2	32280
½	12	690	47.9	1850	60.0	6791
¼	7	674	43.5	1435	45.3	4471
1/5	5	627	29.6	211	39.0	2077

[a] All experiments were carried out at 500°C preset bed temperature, GHSV of 50,000, [NO] =500 ppm, $[O_2]$ = 10%.
[b] Volume ratio of Cu-GAC to α-Al_2O_3.
[c] Weight percentage of Cu-GAC in the bed.
[d] Peak temperature.
[e] Conversion to N_2.
[f] Maximum conversion to N_2.

Table 6.1 Catalyst Properties

Catalyst	Metal loading(wt%)	source	BET surface area(m^2/g)	Preparation method
CeO_2	0.0	Engelhard	121.0 ± 1.8	
PdO/CeO_2	4.0	Engelhard	123.6 ± 1.9	Impregnation
PdO/Al_2O_3	4.0	Engelhard	132.6 ± 2.1	Impregnation
PdO/TiO_2	4.0	Engelhard	42.6 ± 1.7	Impregnation
PdO/Al_2O_3	4.0	the study	174.6 ± 1.7(80 μm)	Impregnation

Table 6.2 Catalyst Particle Size Distribution

wt% under particle size	PdO/Al_2O_3(μm) Engelhard	PdO/Al_2O_3 (μm) the study	PdO/CeO_2 (μm) Engelhard	PdO/TiO_2(μm) Engelhard
5%	5	48	3	12
25%	15	67	5	25
55%	10	83	8	41
85%	21	104	13	58
95%	24	113	16	68

Table 6.3 Catalyst BET Surface Area Change

Catalyst	PdO/CeO_2	PdO/Al_2O_3	PdO/TiO_2
Fresh catalyst BET surface area (m^2/g)	123.6 ± 1.9	132.6 ± 2.1	42.6 ± 1.7
Poison catalyst BET surface area(m^2/g)	119.0 ± 1.9	135.7 ± 1.8	41.3 ± 1.9

Table 6.4 Isothermal Reduction of NO[a]

Ratio[b](v/v)	PdO/Al_2O_3(g)	GAC (g)	Al_2O_3 (g)	initial T (°C)	Peak T (°C)
1/1	0.5297	0.1646	N/A	500	770
2/1	0.7092	0.1230	N/A	500	600
5/1	0.8865	0.0615	N/A	500	540
5/1	0.8693	0.0679	N/A	600	730
5/1	N/A	0.0656	0.7639	600	606

[a] All experiments were carried out at GHSV of 50,000, [NO] =500 ppm, $[O_2]$ = 10%.
[b] Volume ratio of PdO/Al_2O_3 or Al_2O_3 to GAC, total volume of mixture is 1.5 ml.

Table 6.5 The Specification and The Operation Conditions of The Diesel Engine

The specification of the diesel engine	
Type	4 Cycle, 3 cylinder
Displacement (liter)	2.60
Maximum power (kw/rpm)	45/2600
The operation conditions of the diesel engine	
Engine load (lb)	48 - 50
Engine speed (rpm)	1450 – 1750

Table 6.6 Rotating Fluidized Bed Reactor at Diesel Engine Bench Experiments (FTIR Results)

Measurements	Plain Al_2O_3	CuO/Al_2O_3	PdO/Al_2O_3
RFB speed (rpm)	1200	1100	1100
Engine load (lb)	49	51	50.3
Engine speed (rpm)	1619	1445	1685
Inlet gas temperature (°C)	531	531	626
Outlet gas temperature (°C)	331	317	337
Bed GHSV (vv/vv)	50,000	50,000	50,000
Inlet measuring time (min)	25	25	30
Outlet measuring time (min)	30	35	35
Inlet NO conc. (ppm)	120, 150	150, 160	120, 140
Outlet NO conc. (ppm)	120, 150	136, 145	90, 112
Inlet NO_2 conc. (ppm)	19, 20	19, 19	19, 19
Outlet NO_2 conc. (ppm)	19, 20	19, 19	19, 19
Inlet N2O conc. (ppm)	2, 2	2, 2	2, 2
Outlet N2O conc. (ppm)	2, 2	2, 2	2, 2
Inlet CO conc. (ppm)	220, 300	280, 300	320, 250
Outlet CO conc. (ppm)	220, 300	225, 225	50, 35
Inlet CO2 conc. (%)	5.0, 6.0	5.5, 5.5	4.2, 4.5
Outlet CO2 conc. (%)	5.0, 6.0	4.9, 5.0	4.2, 4.3

Table 6.7 Aerosizer Results for Diesel Engine Bench Experiments

Measurements	plain Al_2O_3	CuO/Al_2O_3	3% PdO/Al_2O_3
Particle size range (micron)			
Inlet gas	0.1 - 1	0.1 - 1	0.1 - 1
Outlet gas	0.1 - 20	0.1 - 20	0.1 - 20
Main particle size (micron)			
Inlet gas	<1	<1	<1
Outlet gas	10	10	10

REFERENCES

[1] R. Russell-Jones, 1987, "The health effects of vehicle emissions", Imech Conference on Vehicle emissions and their impact on European air quality, paper C355/87, 55-59.

[2] R.M. Heck, and R. J. Farrauto, 1995, *Catalytic Air Pollution Control: Commercial Technology*, Van Nostrand Reinhold, International Thomson Publishing Inc.

[3] L. Burgler, P. L. Herzog and P. Zelenka, 1992, "Strategies to Meet US 1994/95 Diesel Engine Federal Emission Legislation for HSDI Diesel Engine Powered Vehicles", *Proc. Instn. Mech. Engrs, Part D: Journal of Automobile Engineering*, 206: 47-54.

[4] J.R. Needham, S. A. Faulkner and D. M. Doyle, 1991, "Developing The Truck Engine for Ultra Low Emissions", *Proceedings of the Institution of Mechanical Engineers, Part D: Journal of Automobile Engineering*, 205: 149-159.

[5] R.J. Farrauto, R. M. Heck and B. K. Speronello, 1992, "Environmental Catalysts", *Chemical and Engineering News*, 70 (36): 34 – 44.

[6] M. Murtagh, D. Sherwood, L.S. Socha, 1994. Development of a New Diesel Particulate Filter Composition and its Effect on Durability and Performance. SAE 940235. Warrendale, Pa.: SAE International.

[7] F. C. Liu, *Basic Toxicology*, Hemisphere Publishing Corp. 1996.

[8] T. Suzuki, T. Kyotani and A. Tomita, Industrial Engineering, Chem. Res., 33 (1994) 2840.

[9] A. Tsutsumi, M. Sato, Y. Shibuya, M. Kikuchi and K. Yoshida, AIChE Symp. Ser., 90(301) (1996) 152.

[10] A. Tsutsumi, W. Ju and K. Yoshida, AIChE Symp. Ser., 92(313) (1994) 86.

[11] M. Iwamoto, H. Yahiro, Y. Mine and S. Kagawa, Chemistry Letters, (1989) 213.

[12] M. Iwamoto, H. Yahiro, K. Tanda, N. Mizuno, Y. Mine and S. Kagawa, Journal of Physical Chemistry, 95 (1991) 3727.

[13] S. Sato, Y. Yu, H. Yahiro, N. Mizuno and M. Iwamoto, Applied Catalysis, 70 (1991) L1.

[14] Y.P. Zhang, T. Sun, A.F. Sarofim and M. Flytzsni-Stephanopoulos, Symposium on NO_x Reduction, American Chemical Society, San Diego, California, (1994) 171.

[15] W. Held, A. Konig, T. Richter and L. Puppe, SAE paper 900496 (1990) 209.

[16] H. Yamashita, H. Yamada and A. Tomita, Applied Catalysis, 78 (1991) L1.

[17] H. Yamashita and A. Tomita, Energy & Fuels, 7 (1993) 85.

[18] A.P. Walker, Catalysis Today, 26 (1995) 107.

[19] H.W. Zeller, T.E. Westphal, NTIS Report (1992), (BUMINES-RI-9438; Order No. PB93-131985).

[20] V. D. N. Rao, H. A Cikanek, R. W. Horrocks, Soc. Automot. Eng., Special Publication (1994), SP-1020.

[21] G.D Harvey, K.J. Baumgard, J.H. Johnson, L.D Gratz, S.T. Bagley, D.G Leddy, Soc. Automot. Eng., Special Publication (1994), SP-1053.

[22] H. Shaw, Journal of Engineering for Power, Trans. ASME, Series A, 95, 301 (1973).

[23] S J. Jelles, R.R Krul, M. Makkee, J.A. Moulijn, Catal. Today (1999), 53(4), 623.

[24] J.L. D'Itri and W.M.H. Sachtler, Catalysis Letters, 15 (1992) 289.

[25] K. Ma, Master's Thesis in Applied Chemistry, New Jersey Institute of Technology (1998).

[26] D.R. Rainer, M. Koranne, S.M. Vesecky, and D.W. Goodman, Journal of Physical Chemistry, B, 101 (1997) 10769.

[27] K.C. Taylor, Catalysis-Science and Technology, J.R. Anderson, M. Boudart (Eds). Vol. 5, Springer, Berlin, (1984) 121.

[28] B. Harrison, M. Wyatt, K.G. Gough, Specialist periodical reports-catalysis, R. Soc. Chem. London 5(1982) 127.

[29] H. Hosose, H. Yahiro, N. Mizuno, M. Iwamoto, Chem. Lett. 1859 (1991).

[30] G. Centi, S. Perathoner, Appl. Catal. A 132 (1995) 179.

[31] J.A. Anderson, C. Marquez Alvarez, I. Rodriguez Ramos, Appl. Catal. B 14 (1997) 189.

[32] M. Iwamoto, H. Yahiro, K. Mizuno, Y. Mine, S. Kagawa, J. Phys. Chem. 95 (1991) 3727.

[33] S. Sato, Y. Yu-u, H. Yahiro, M. Iwamoto, Appl. Catal. 70 (1991) L1.

[34] J. Valyon, W.K. Hall, J. Phys. Chem. 97 (1991) 1204.

[35] R.H.H. Smits, Y. Iwasawa, Appl. Catal. B 6 (1995) L201.

[36] N.W. Hayes, R.W. Joyner, E.S. Shapiro, Appl. Catal. B 8 (1996) 343.

[37] N. Takahashi, H. Shinjoh, T. Iijma, T. Suzuki, K. Yamazaki, K. Yokota, H. Suzuki, N. Miyoshi, S. Mastsumoto, T. Tanizawa, T. Tanaka, Cata. Today 27 (1996) 63.

[38] S. Matsumoto Catal. Surveys Jpn. 1 (1997) 111.

[39] M.V. Twigg, Plat. Metals Rev. 41 (1997) 76.

[40] L.K. Chan, A.F. Sarofim, J.M. Beer, Combust. Flame 52 (1983) 37.

[41] L. Mochida, M. Ogaki, H. Fujitsu, Y. Komatsubara, S. Ida, Fuel 64 (1985) 1054.

[42] T. Furusawa, M, Tsunoda, M. Tsujimura, T. Adschiri, Fuel 64 (1985) 1306.

[43] H. Teng, E.M. Suuberg, J.M. Calo, Energy Fuels 6 (1992) 398.

[44] L. Singoredjo, J.A. Moulijn, H.P. Boehm, Carbon 31 (1993) 213.

[45] H. Yamashita, H. Yamada, T. Kyotani, A. Tomita, Energy Fuels 7 (1993) 85.

[46] S.N. Ahmed, R. Baldwin, B. McEnaney, J. Fuel 72 (1993) 287.

[47] S. Xiao, K. Ma, H. Shaw, R. Pfeffer, J.G. Stevens, Appl. Catal. B 32/1-2 (2001) 107.

[48] H. Yamashita, H. Yamada, A. Tomita, Appl. Catal. 78 (1991) L1.

[49] M. Komiyama, Catalysis reviews: Sci. Eng. 27(2): 342-372, 1985.

[50] A.H. Thomas, Brundrett, C.P., Chemical Engineering Progress 76(6): 41-45, 1980.

[51] J.H. Worsell, Chemical Engineering Progress 88(6): 33-39, 1992.

[52] A. Stiles, Catalyst manufacture: laboratory and commercial preparations. New York: Marcel Dekker, 1983.

[53] D. Trimm, Design of industrial catalysts. Amsterdam: Elsevier Scientific, 1980.

[54] R.W. Maatman, C.D. Prater, Ind. Eng. Chem., 49: 253, 1957.

[55] R.W. Maatman, Ind. Eng. Chem., 51:913, 1959.

[56] J.C. Summers, L.L Hegedus, J.Catal., 51:158, 1978.

[57] E.R. Becker, T.A. Nuttall, in: B, Delmon, P. Grange, P.A.Jacobs, G. Poncelet (Eds.), Preparation of Catalysts II, Amsterdam: Elsevier Scientific, 1978, p. 159.

[58] M. Komiyama, R.P. Merrill, H.F. Harnsberger, J. Catal., 63: 35, 1980.

[59] K. Kottor, L. Riekent, in: B, Delmon, P. Grange, P.A.Jacobs, G. Poncelet (Eds.), Preparation of Catalysts II, Amsterdam: Elsevier Scientific, 1978, p. 51.

[60] G.H. van den Berg, H.Th. Rijnten, in: B, Delmon, P. Grange, P.A.Jacobs, G. Poncelet (Eds.), Preparation of Catalysts II, Amsterdam: Elsevier Scientific, 1978, p. 256.

[61] L.L. Hegedus, T.S. Chou, J.C. Summers, N.M. Potler, in: B, Delmon, P. Grange, P.A.Jacobs, G. Poncelet (Eds.), Preparation of Catalysts II, Amsterdam: Elsevier Scientific, 1978, p. 171.

[62] H.C. Chen, R.B. Anderson, Ind. Eng. Chem. Prod. Res. Dev., 12: 122, 1973.

[63] R. Srinivansan, H.C. Liu, S.W. Weller, J. Catal., 57: 87, 1979.

[64] J.L.G. Fierro, P. Grange, B. Delmon, in: B, Delmon, P. Grange, P.A.Jacobs, G. Poncelet (Eds.), Preparation of Catalysts IV, Amsterdam: Elsevier Scientific, 1987, p. 591.

[65] M.A. Goula, Ch. Kordulis, A. Lycourghiotis, J. Catal., 133: 486, 1992.

[66] J. Prasad, P.G. Menon, J. Catal. 44:314, 1976.

[67] C. Serrano, J.J. Carberry, Appl. Catal. 19:119, 1985.

[68] J. Prasad, K.R.Murthy, P.G. Menon, J. Catal. 52:515, 1978.

[69] Z. Schay, K. Matusek, L. Guczi, Appl. Catal. 10:173, 1984.

[70] D.J. O'Rear, D.G. Loffker, M. Boudart, J. Catal.121:131, 1990.

[71] X. Gao, S.R. Bare, J.L.G. Fierro, M.A. Banares, L.E. Waches, J. Phys. Chem. B 102:5653, 1998.

[72] A.S. Russell, J.J. Stokes Jr., Ind. Eng. Chem. 38:1071, 1946.

[73] Y.C. Xie, Y.Q. Tang, Adv. Catal.m37:1, 1990.

[74] E. Ruckenstein, J. Catal. 26:70, 1972.

[75] E. Ruckenstein, B. Pulvermacher, J. Catal. 29:224, 1973.

[76] E. Ruckenstein, B. Pulvermacher, J. Catal. 35:115, 1974.

[77] E. Ruckenstein, B. Pulvermacher, J. Catal. 37:416, 1975.

[78] E. Ruckenstein, D.R. Dadyburjor, J. Catal. 48:73,1977.

[79] P.C. Flynn, S.E. Wanke, J. Catal. 34:390, 1974.

[80] P.C. Flynn, S.E. Wanke, J. Catal. 34:400, 1974.

[81] S.E. Wanke, J. Catal. 44:234, 1977.

[82] A.G. Grahams, S.E. Wanke, J. Catal. 68:1, 1981.

[83] U.S. EPA, "Control of Emissions of Air Pollution from 2004 and Later Model Year Heavy-duty Highway Engines and Vehicles; Revision of Light-Duty On-board Diagnostic Requirements" 40 CFR Parts 85 and 86, 65 FR 59896 (Oct. 6, 2000).

[84] U.S. EPA, "Control of Air Pollution from New Motor Vehicles: Heavy-Duty Engines and Vehicle Standards and Highway Diesel Sulfur Control Requirements," 40 CFR Parts 69, 80, and 86 (Dec. 21, 2000).

[85] M.Iwamoto, H. Yahiro, S. Shundo, Y. Yu, N. Mizuno, Appl. Catal. 69: L15, 1991.

[86] H. Hamada, Y. Kintaichi, M. Sasaki, T. Ito, M. Tabata, Appl. Catal. 70:L15, 1991.

[87] T. Inui, S. Iwamoto, S. Kojo, T. Yoshida, Catal. Lett. 13:87, 1992.

[88] T. Nakatsuji, R. Yasukawa, K. Tabata, K. Ueda, M. Niwa, Appl. Catal 17:333, 1998.

[89] G.P. Ansell, P.S. Benett, J.P. Cox, J.C. Frost, P.G. Gray, A.M. Jones, P.R. Rajaram, A.P. Walker, M. Litorell, Appl. Catal. B 10:183, 1996.

[90] J. Jochheim, D. Hesse, T. Duesterdiek, W. Engeler, D. Neyer, J.P. Warren, A.J.J. Wikkins, M.V. Twigg, SAE Paper, 962042, 1996.

[91] M. Iwamoto, H. Yahiro, Y. Yuu, S. Shundo, N. Mizuno, Appl. Catal. 32:430, 1990.

[92] T. Miyadera, Appl. Catal B 2:199, 1993.

[93] R. J. Farrauto, K. E. Voss, R. M. Heck, U.S. Patent 5,462,907, 1995.

[94] S. Xiao, K. Ma, H. Shaw, R. Pfeffer, J. G. Stevens, Appl. Catal. 32/1-2:107, 2001.

[95] R. M. Heck, R. J. Farrauto, Catalytic Air Pollution Control. Van Nostrand Reinhold, 1995.

[96] G. H. Qian, I. Bagyi, R. Pfeffer, H. Shaw, J.G. Stevens, AIChE J.,45/7:1401, 1999.

[97] G.H. Qian, Ph.D. dissertation, New Jersey Institute of Technology, May, 2000.

[98] G. H. Qian, I. Bagyi, R. Pfeffer, H. Shaw, J.G. Stevens, AIChE J. 47/5:1022, 2001.

[99] G. H. Qian, I. Bagyi, R. Pfeffer, H. Shaw, J.G. Stevens, AIChE J. 50/:3018, 2002

[100] Y. Teraoka and S. Kagawa, Catalysis Surveys from Japan 2:155-164, 1998.

[101] J. R. Pels, M. A. Wojtowicz, J. A. Moulijn, Energy & Fuel 9, 743-752, 1995.

[102] T. Furusawa, M. Tsunoda, M. Tsujimura, T. Adschiri, Fuel 64, 1306-1309, 1985.

[103] R. N. Smith, D. Lesnini, J. Moor, J. Phys. Chem. 61, 81-86, 1959.

[104] L. K. Chan, A. F. Sarofim, J. M. Beer, Combust. Flame 52, 37-45, 1983.

[105] G. G. De Soete, 23rd Symposium on Combustion, 1257-1264, 1990.

[106] E. M. Suuberg, H. Teng, J. M. Calo, 23rd Symposium on Combustion, 1190-1205, 1990.

[107] H. Teng, E. M. Suuberg, J. M. Calo, Energy & Fuels 6, 398-406, 1992.

[108] H. Yamashita, H. Yamada, A. Tomita, T. Kyotani, L. R. Radovic, Energy & Fuels 7, 85-89, 1993.

[109] Y. A. Zarifyanz, V. F. Kiselev, N. Lezhnev, O. Nilitina, Carbon 5, 127-135, 1967.

[110] X. Chu, D. Schmidt, Ind. Engng Chem. Res. 32, 1359-1366, 1993.

[111] J.E. Johnsson, CHEC, Rep. No. 9003, March 1990.

[112] I. Mochida, M. Ogaki, H. Fujitsu, Fuel 64, 1054-1057, 1985.

[113] I. Mochida, Y. N. Sun, H. Fujitsu, S. Kisamori, S. Kawano, Nippon Kagaku Kaishi, 1991.

[114] H. Yamashita, H. Yamada, A. Tomita, Appl. Catal. 78, L1-L6, 1991.

[115] P. G. Gray, D. D. Do, Chem. Engng Commun, 125, 109-120, 1993.

[116] J. Rodriguez- Mirasol, A. C. Ooms, J. R. Pels, F. Kapteijn, J. A. Mouliji, Combust. Flame 99, 499-507, 1994.